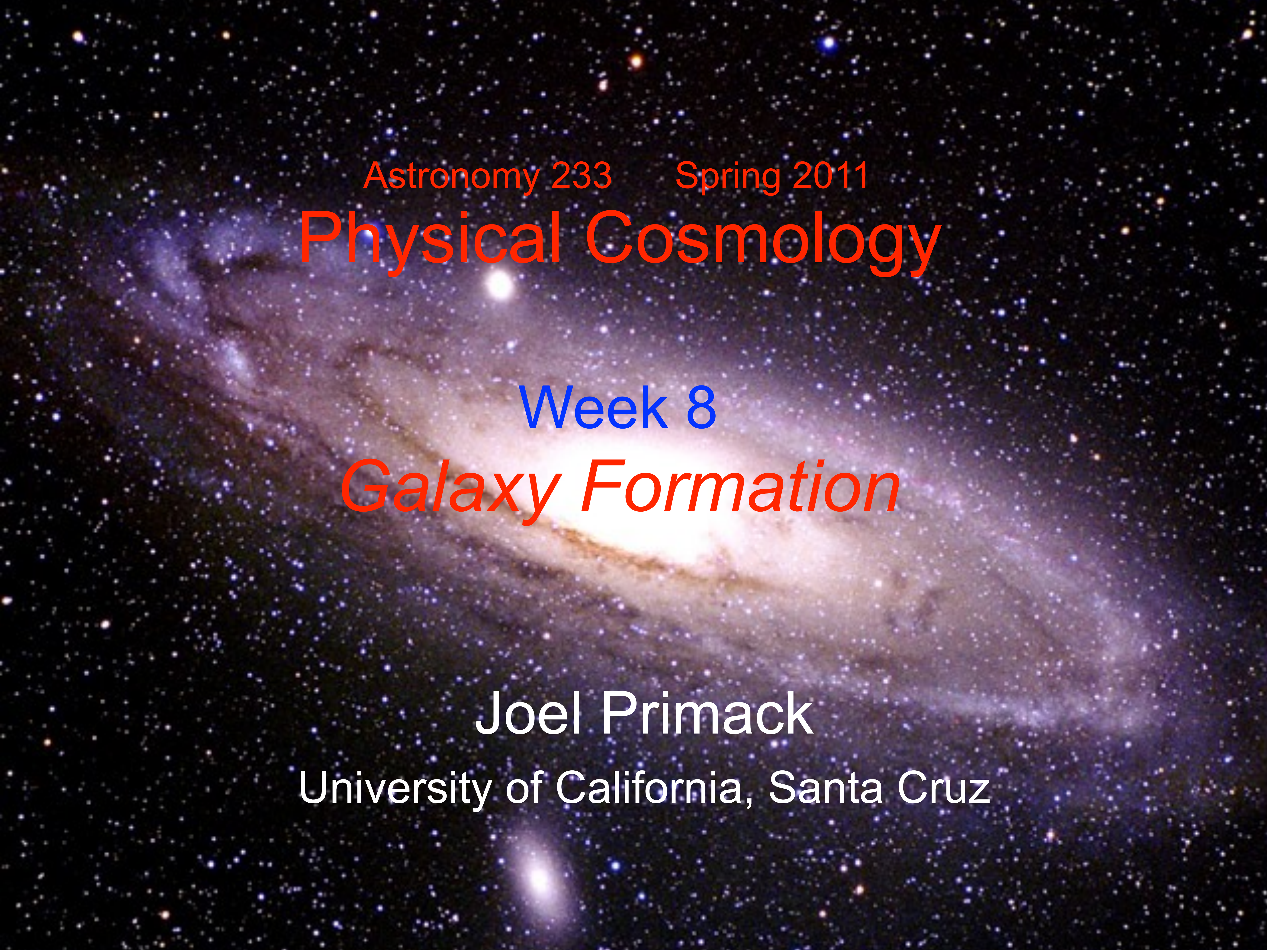

Astronomy 233 Spring 2011

Physical Cosmology

Week 8

Galaxy Formation

Joel Primack

University of California, Santa Cruz

Astro 233 - Spring 2011

Physical Cosmology

Week	Topics
1	Introduction
2	General Relativistic Cosmology
3	Big Bang Nucleosynthesis
4	Recombination, Dark Matter (DM)
5	DM Detection, Cosmic Microwave Background
6	Structure Formation
7	(Reminder: no lectures May 10 & 12)
8	Galaxy Formation
9	Galaxies; Cosmic Inflation, and Before
10	After Inflation: Baryogenesis, Strings, ...
11	Student Presentations of Term Projects

Cosmological Simulation Methods

Dissipationless Simulations

Particle-Particle (PP) - Aarseth NbodyN, N=1,...,6
Particle Mesh (PM) - see Klypin & Holtzman 1997
Adaptive PM (P3M) - Efstathiou et al.
Tree - Barnes & Hut 1986, PKDGRAV Stadel
TreePM - GADGET2, Springel 2005
Adaptive Mesh Refinement (AMR) - Klypin (ART)

Hydrodynamical Simulations

Fixed grid - Cen & Ostriker
Smooth Particle Hydrodynamics (SPH) - GADGET2, Springel 2005
- Gasoline, Wadsley, Stadel, & Quinn
Moving Mesh SPH - AREPO, Springel 2010-11
Adaptive grid - ART+hydro - Klypin & Kravtsov; ENZO - Norman et al.;
- RAMSES - Teyssier

Initial Conditions

Standard: Gaussian P(k) realized uniformly, Zel'dovich displacement
Multimass - put lower mass particles in a small part of sim volume
Constrained realization - small scale: simulate individual halos (NFW)
large scale: simulate particular region

Reviews

Bertschinger ARAA 1998; Klypin lectures 2002; U Washington website
http://www-hpcc.astro.washington.edu/

Aquarius Simulation: Formation of a Milky-Way-size Dark Matter Halo

Diameter of Milky Way Dark Matter Halo
1.6 million light years

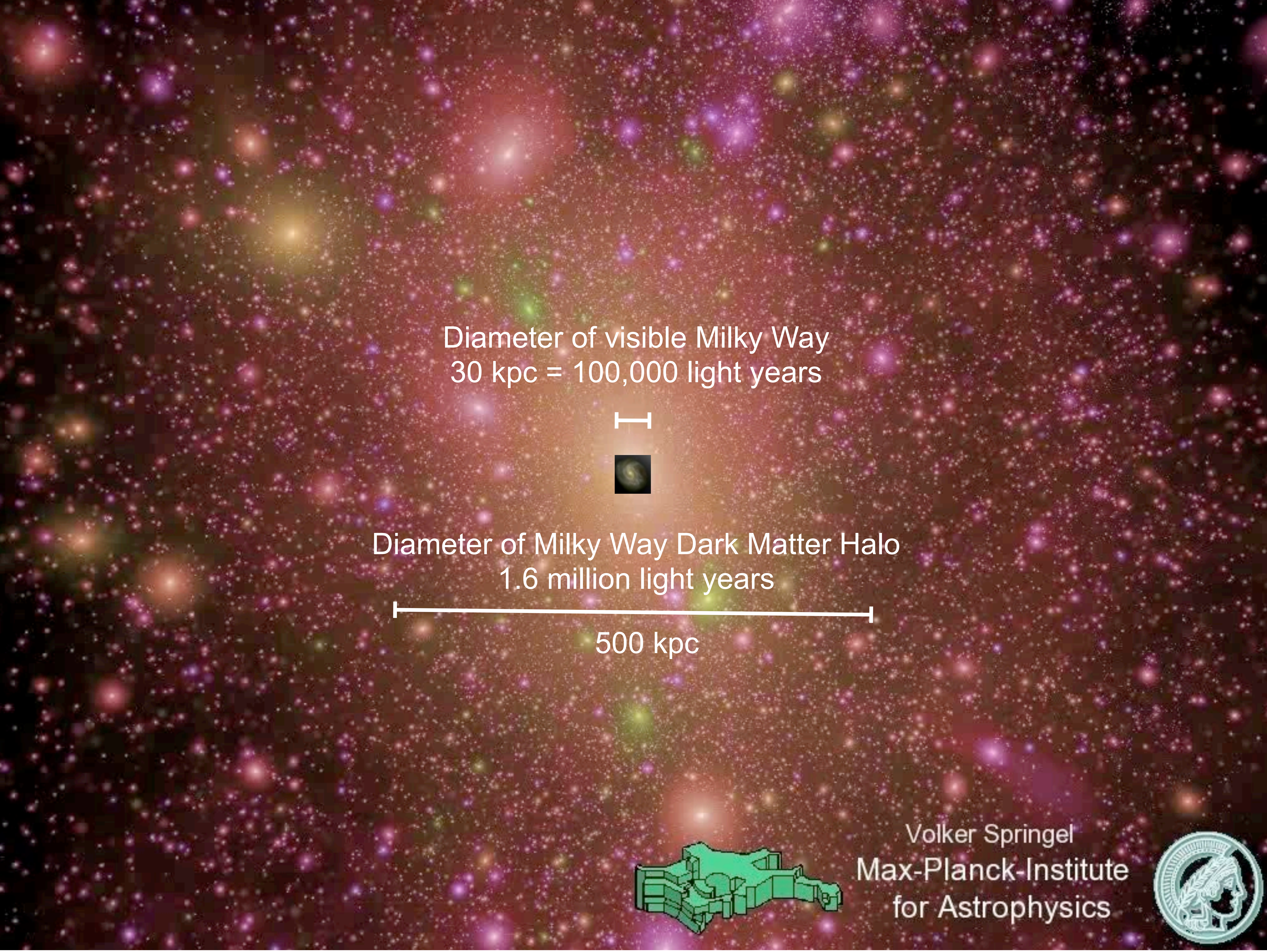
Diameter of visible Milky Way
30 kpc = 100,000 light years
Diameter of Milky Way Dark Matter Halo
1.6 million light years
500 kpc
Volker Springel
Max-Planck-Institute
for Astrophysics

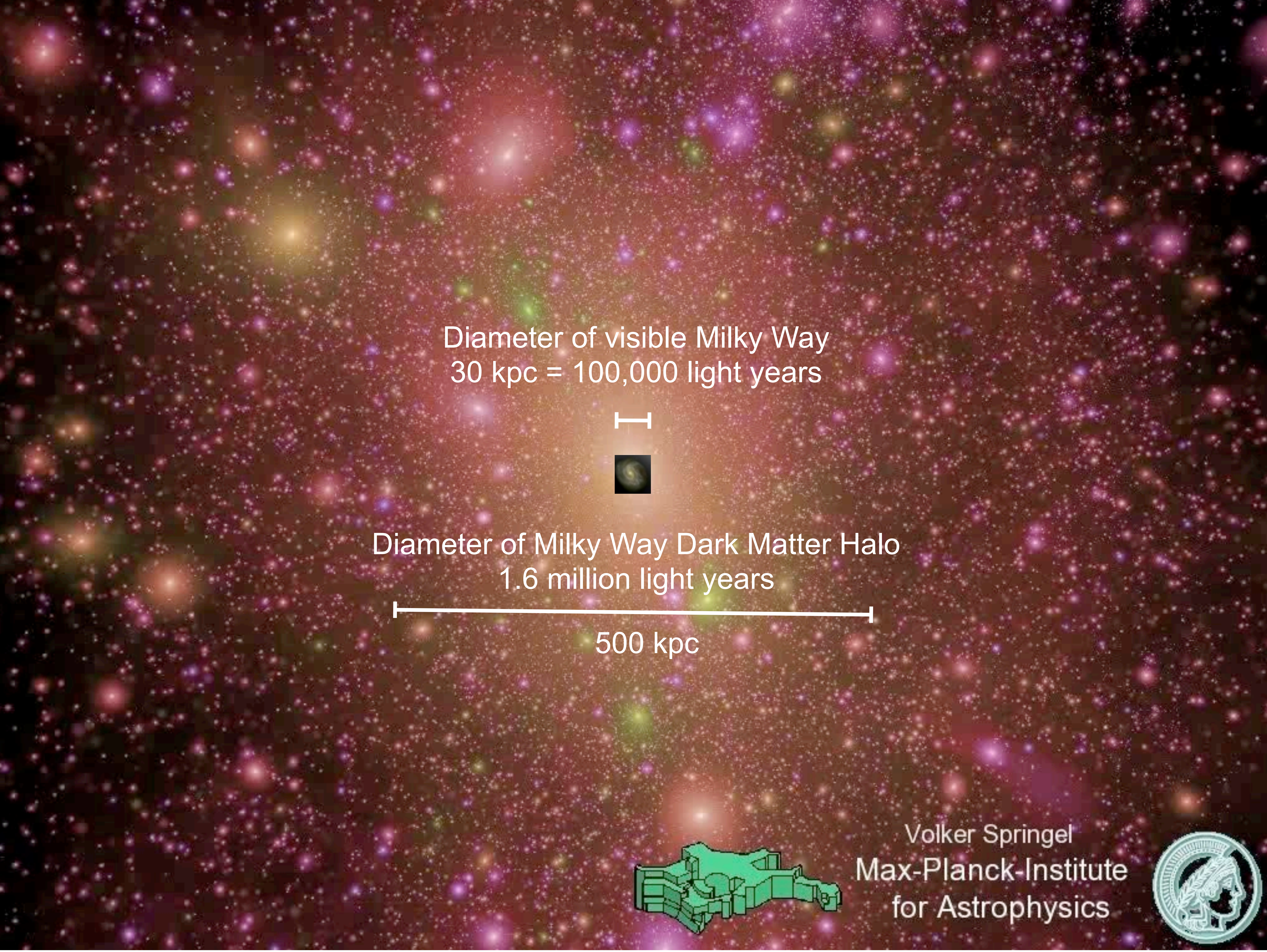
Diameter of visible Milky Way
30 kpc = 100,000 light years
Diameter of Milky Way Dark Matter Halo
1.6 million light years
500 kpc
Volker Springel
Max-Planck-Institute
for Astrophysics

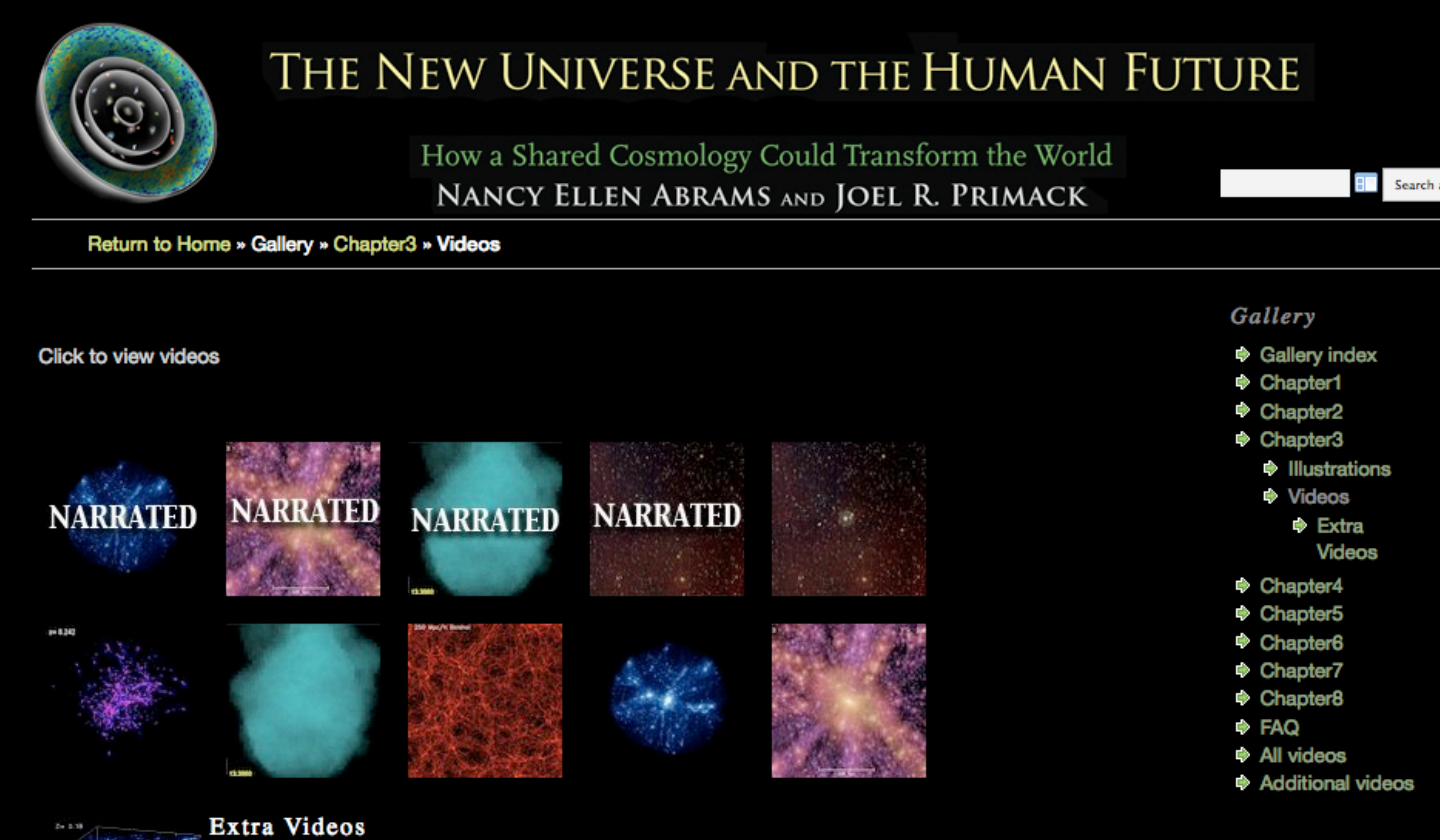

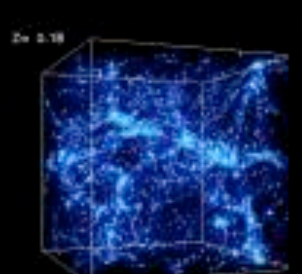

Many relevant videos can be found at this URL:

http://new-universe.org/zenphoto/Chapter3/Videos/

Particle number in cosmological N-body simulations vs. pub date

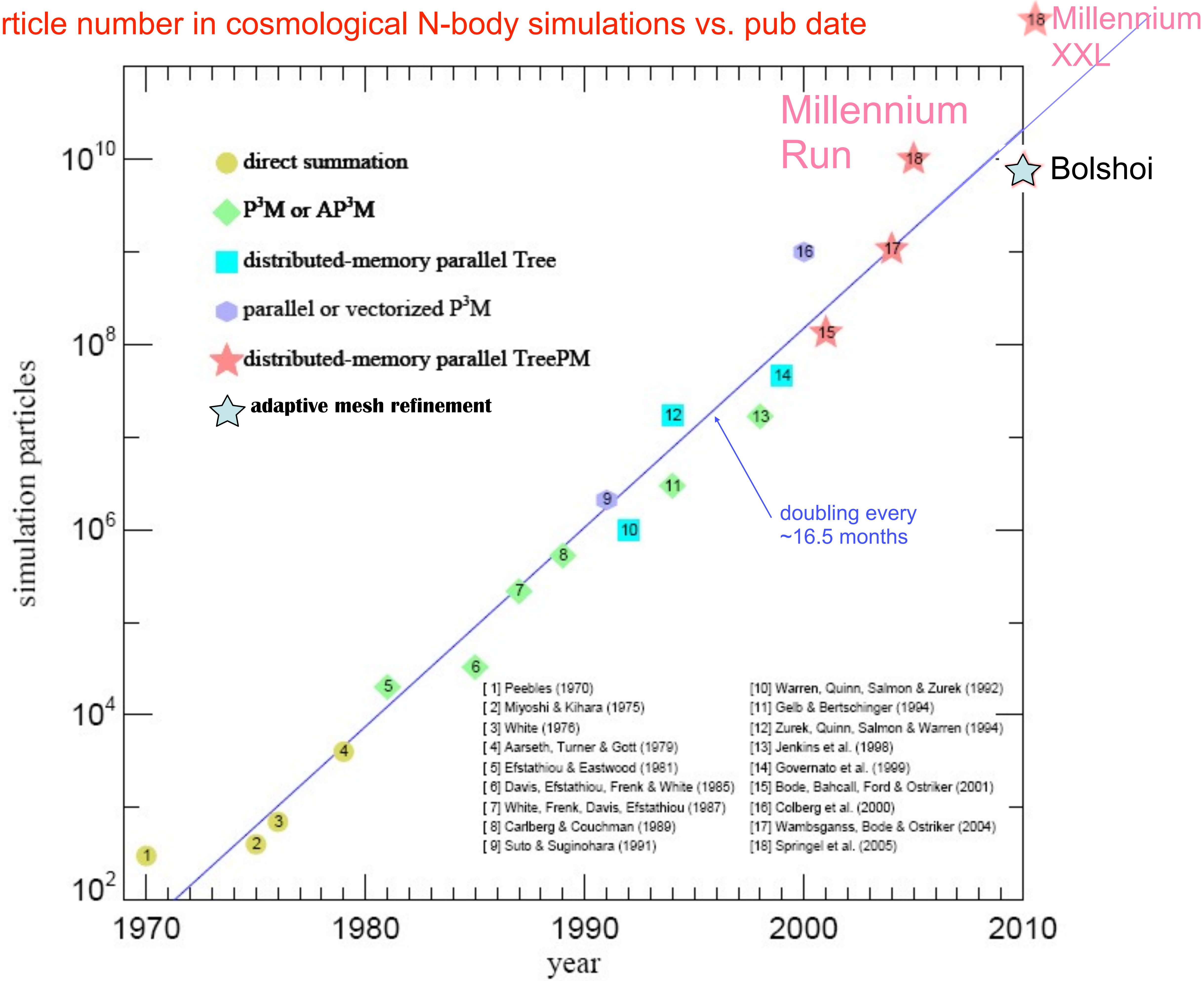

WMAP-only Determination of σ_8 and Ω_M

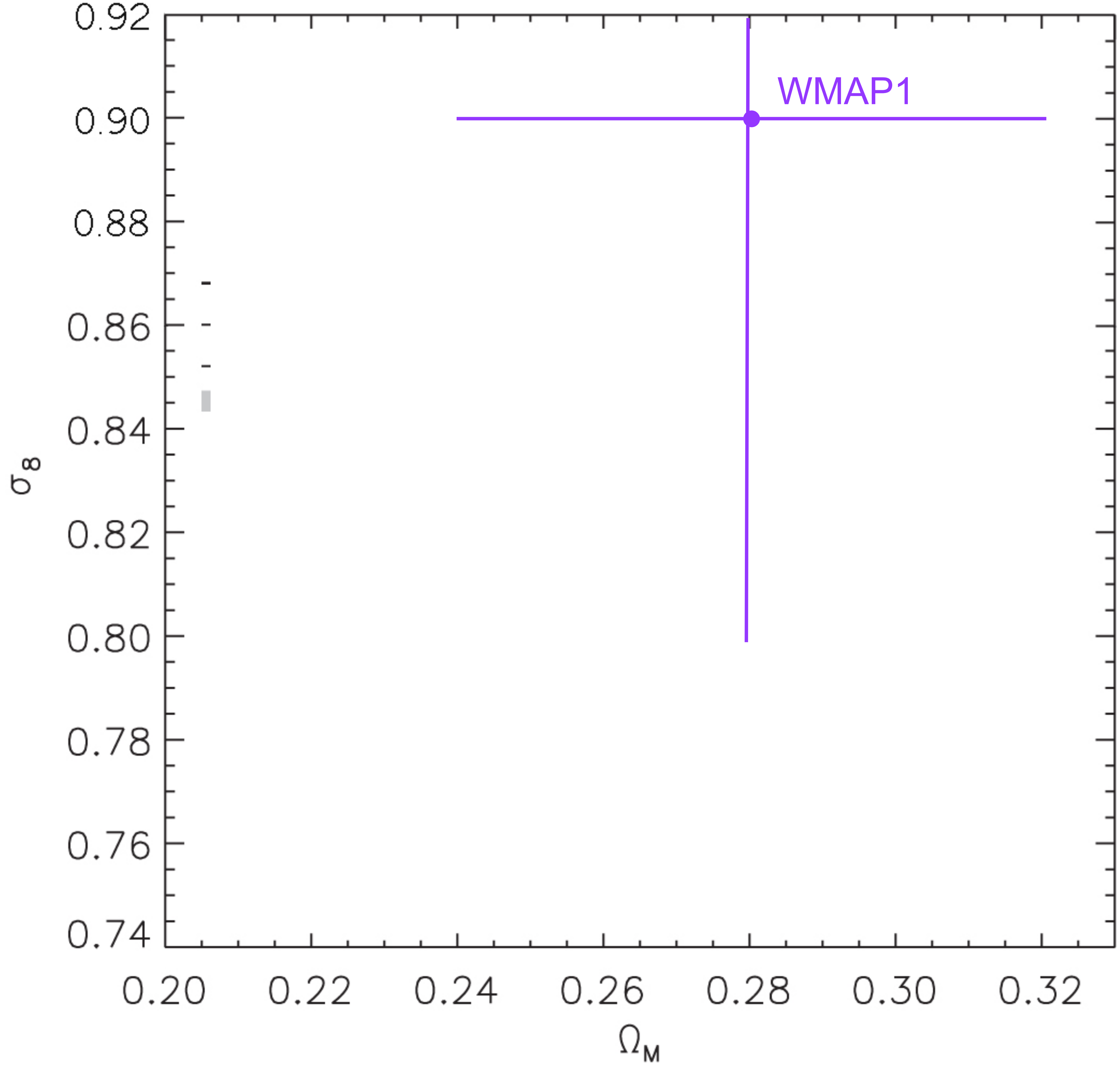

2003

The Millennium Run

- **properties of halos** (radial profile, concentration, shapes)
- **evolution of the number density of halos**, essential for normalization of Press-Schechter-type models
- **evolution of the distribution and clustering of halos** in real and redshift space, for comparison with observations
- **accretion history of halos**, assembly bias (variation of large-scale clustering with as- sembly history), and correlation with halo properties including angular momenta and shapes
- **halo statistics** including the mass and velocity functions, angular momentum and shapes, subhalo numbers and distribution, and correlation with environment

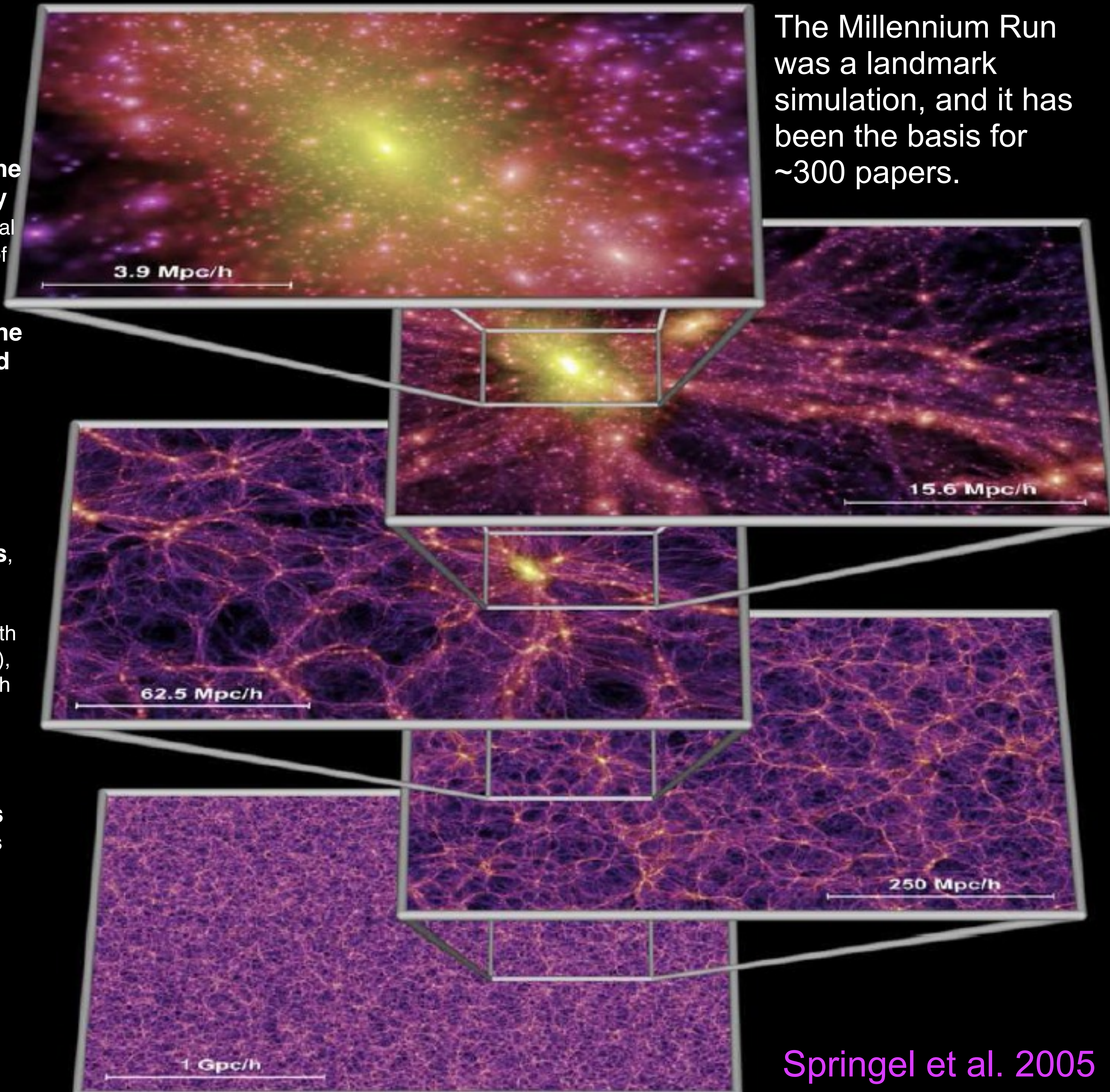

The Millennium Run was a landmark simulation, and it has been the basis for ~300 papers.

Springel et al. 2005

- **void statistics**, including sizes and shapes and their evolution, and the orientation of halo spins around voids
- quantitative descriptions of the evolving **cosmic web**, including applications to weak gravitational lensing
- preparation of **mock catalogs**, essential for analyzing SDSS and other survey data, and for preparing for new large surveys for dark energy etc.
- **merger trees**, essential for **semi-analytic modeling** of the evolving galaxy population, including models for the galaxy merger rate, the history of star formation and galaxy colors and morphology, the evolving AGN luminosity function, stellar and AGN feedback, recycling of gas and metals, etc.

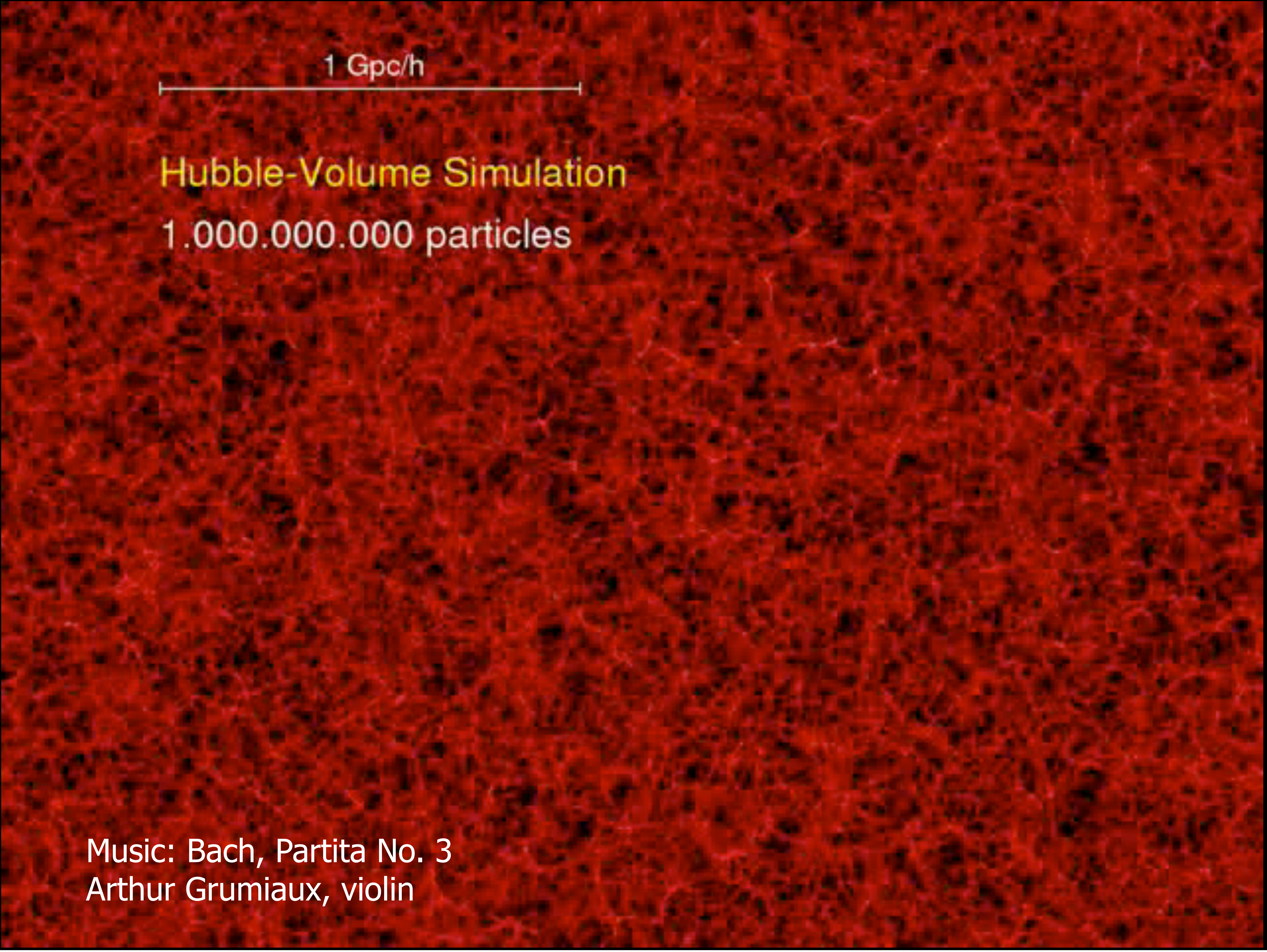

Music: Bach, Partita No. 3
Arthur Grumiaux, violin

Environment of a ‘first quasar candidate’ at high and low redshifts. The two panels on the left show the projected dark matter distribution in a cube of comoving sidelength $10h{-}1$Mpc, colourcoded according to density and local dark matter velocity dispersion. The panels on the right show the galaxies of the **semi-analytic model (SAM)** overlayed on a gray-scale image of the dark matter density.

The volume of the sphere representing each galaxy is proportional to its stellar mass, and the chosen colours encode the restframe stellar $B{-}V$ colour index. While at $z = 6.2$ (top) all galaxies appear blue due to ongoing star formation, many of the galaxies that have fallen into the rich cluster at $z = 0$ (bottom) have turned red.

Springel et al. 2005

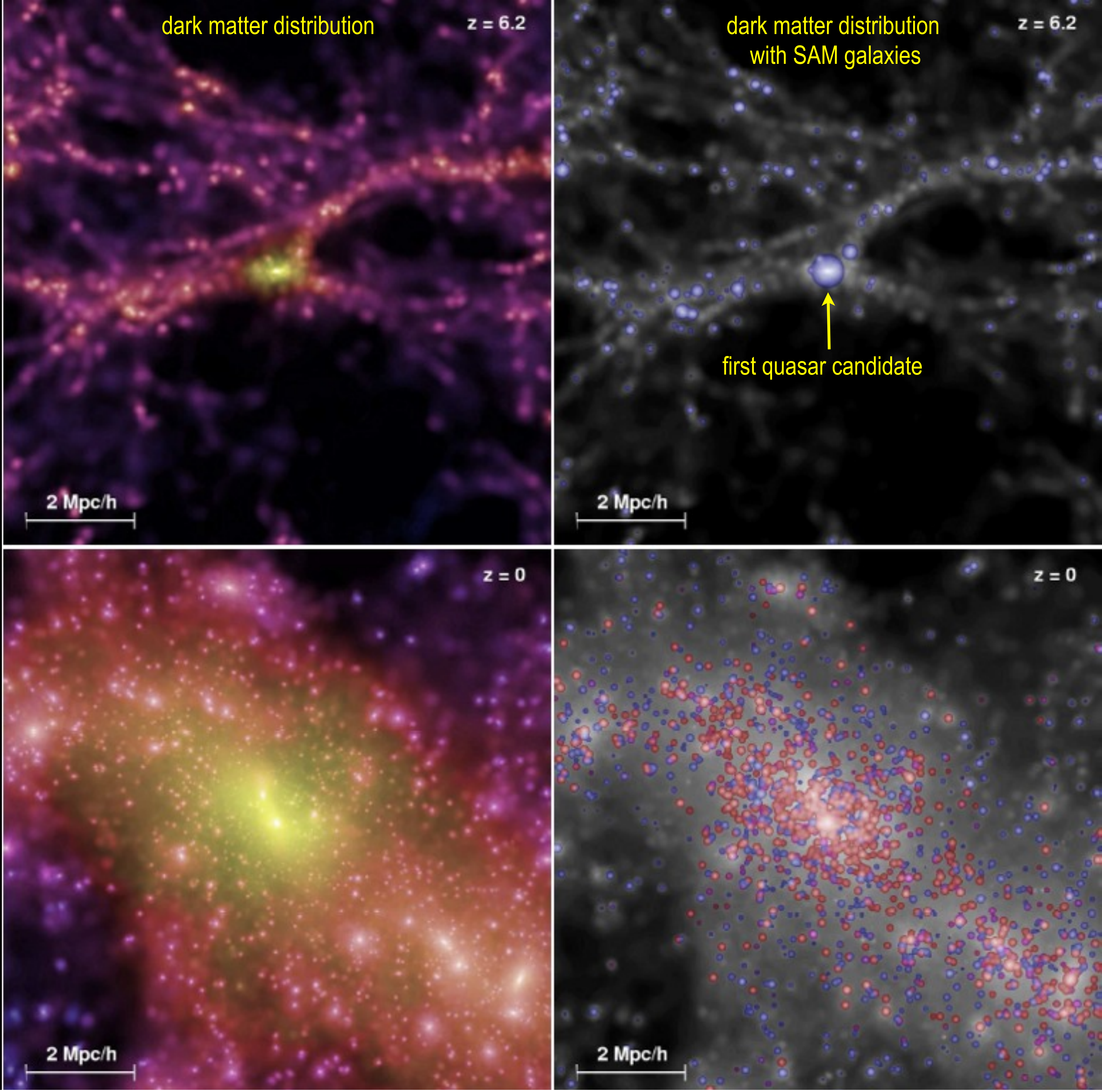

WMAP-only Determination of σ_8 and Ω_M

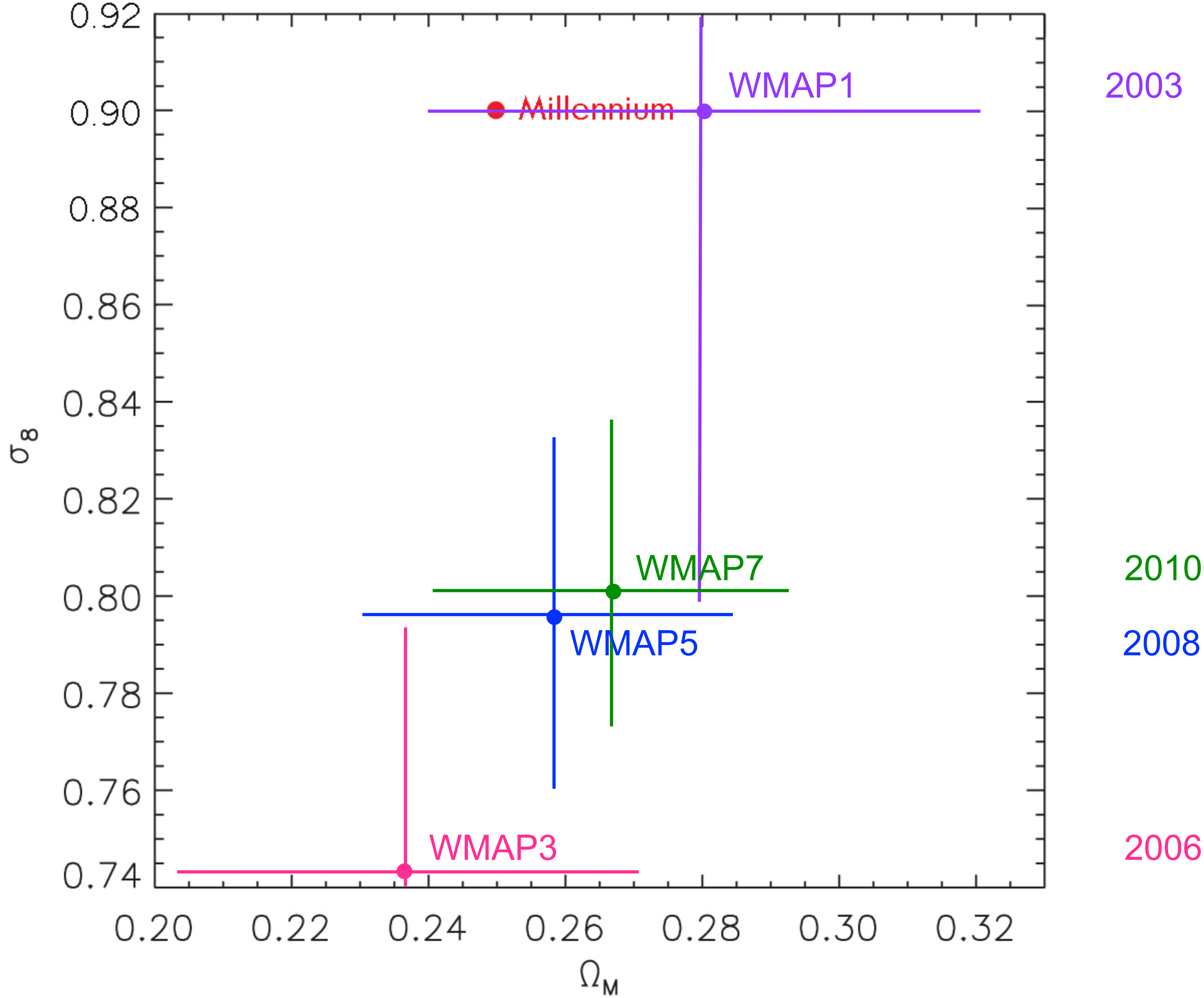

WMAP+SN+Clusters Determination of σ_8 and Ω_M

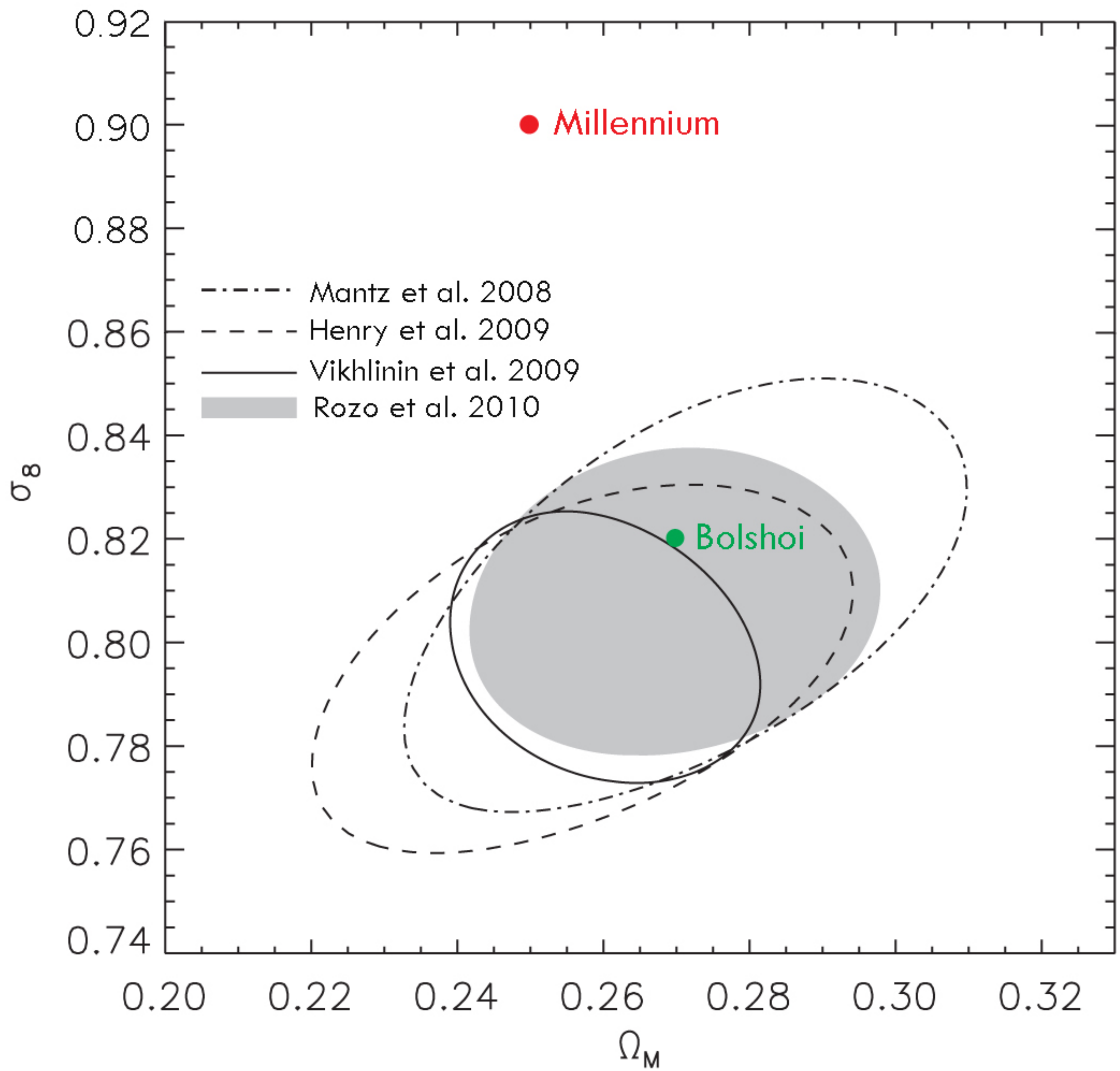

WMAP+SN+Clusters Determination of σ_8 and Ω_M

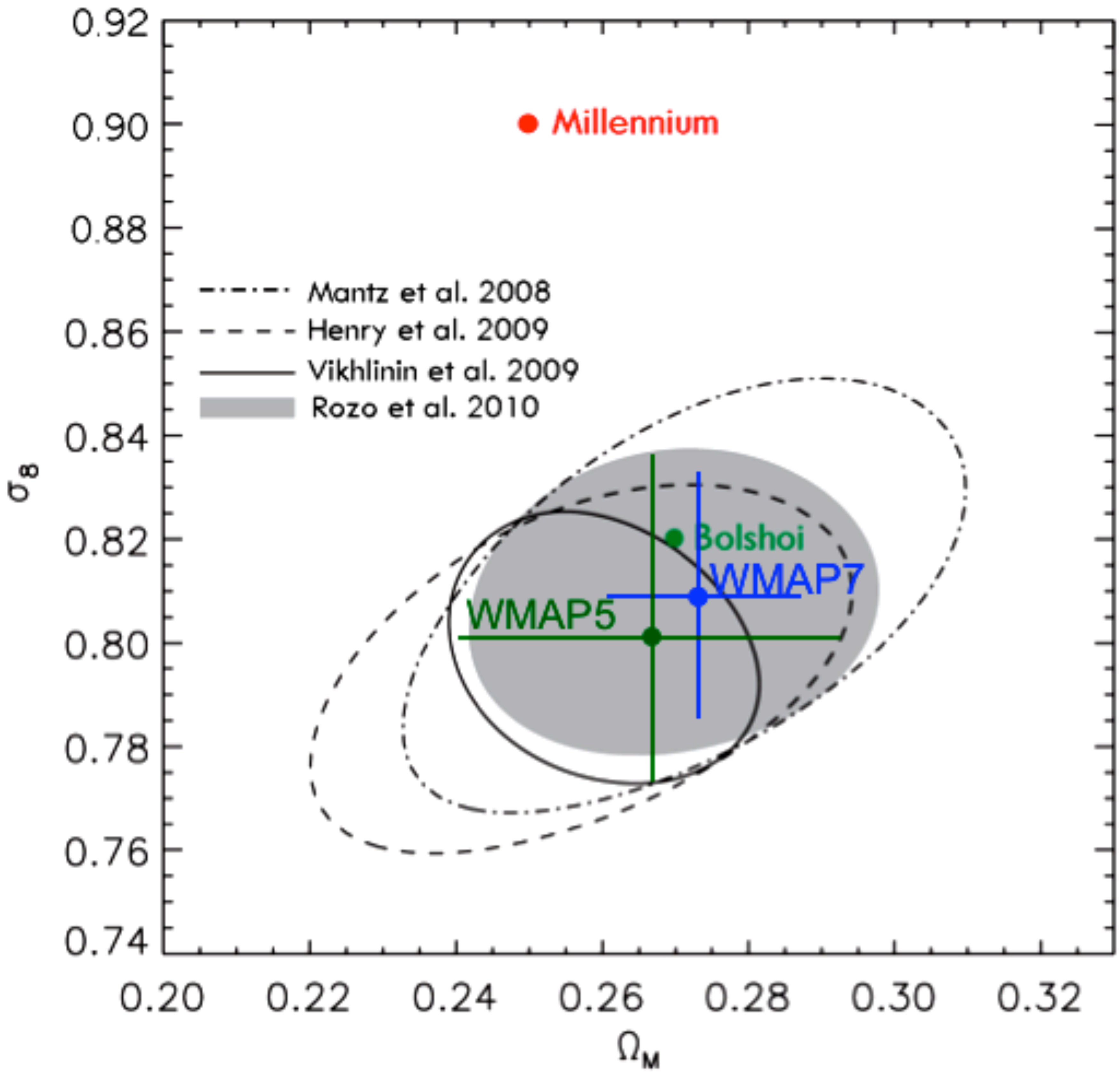

The Bolshoi simulation

ART code

250Mpc/h Box
LCDM
$\sigma_8 = 0.82$
$h = 0.73$
8G particles
1kpc/h force resolution
1e8 Msun/h mass res

dynamical range 262,000
time-steps = 400,000

NASA AMES
supercomputing center
Pleiades computer
13824 cores
12TB RAM
75TB disk storage
6M cpu hrs
18 days wall-clock time

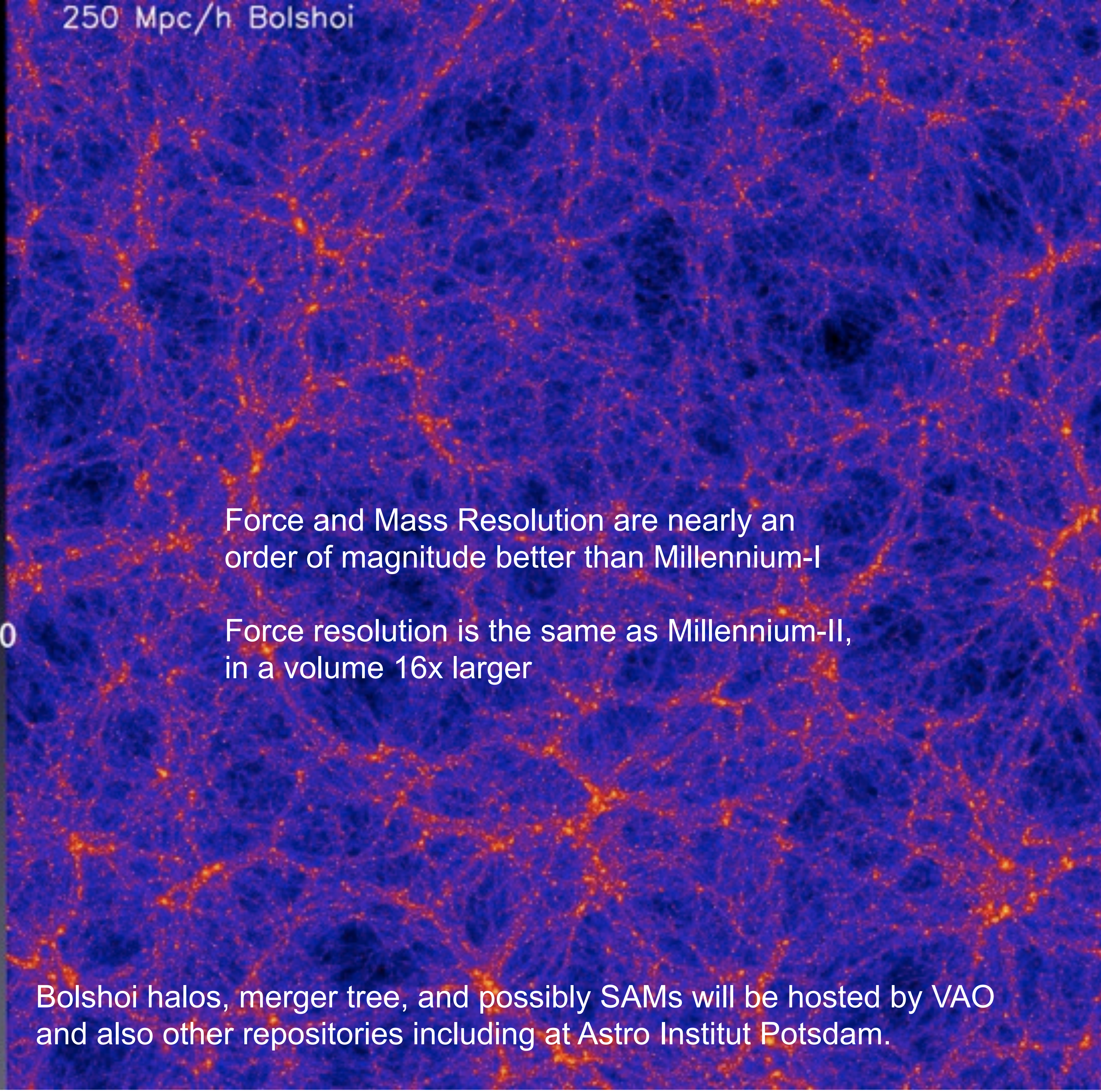

Force and Mass Resolution are nearly an order of magnitude better than Millennium-I

Force resolution is the same as Millennium-II, in a volume 16x larger

Bolshoi halos, merger tree, and possibly SAMs will be hosted by VAO and also other repositories including at Astro Institut Potsdam.

BOLSHOI SIMULATION ZOOM-IN

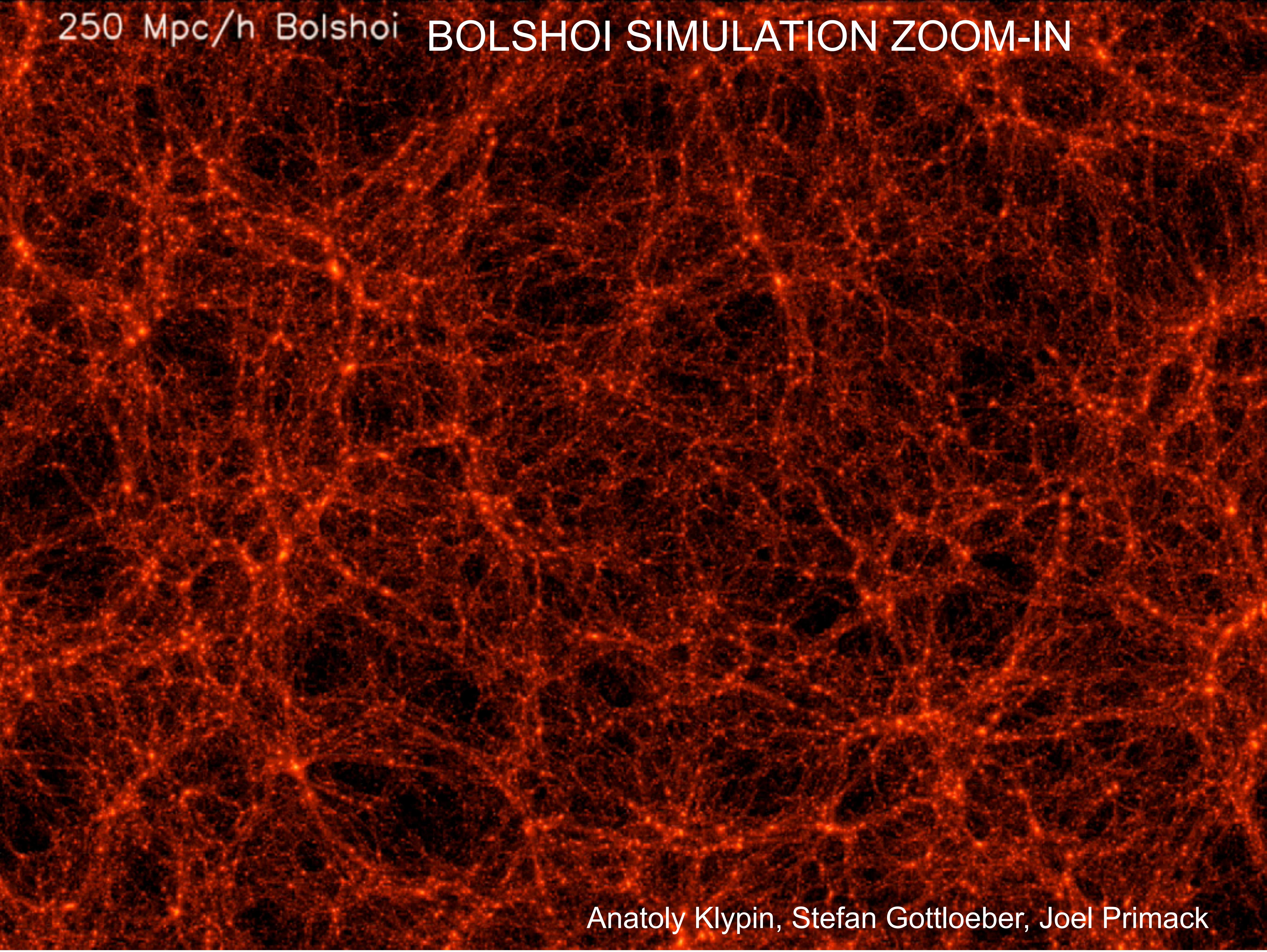

Anatoly Klypin, Stefan Gottloeber, Joel Primack

Halos and galaxies: results from the Bolshoi simulation

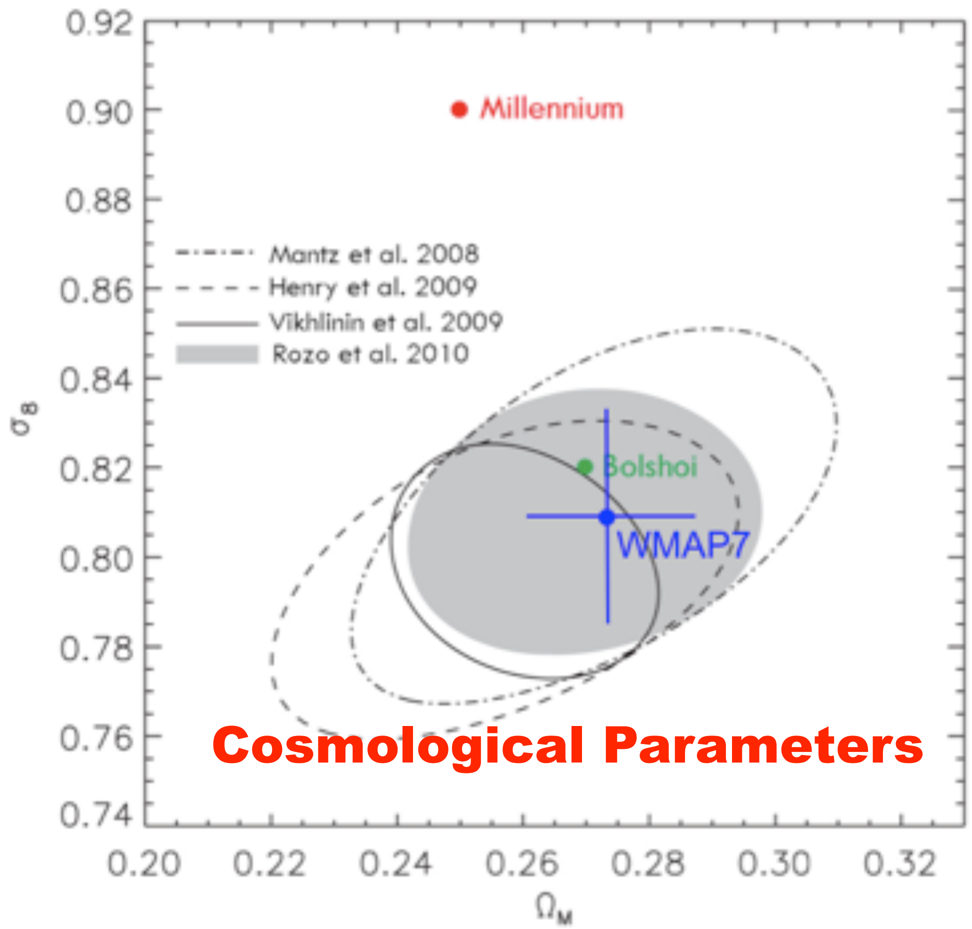

The Millennium Run (Springel+05) was a landmark simulation, and it has been the basis for ~300 papers. However, it and the new Millennium-II simulations were run using WMAP1 (2003) parameters, and the Millennium-I resolution was inadequate to see many subhalos. The new Bolshoi simulation (Klypin, Trujillo & Primack 2010) used the WMAP5 parameters (consistent with WMAP7) and has nearly an order of magnitude better mass and force resolution than Millennium-I. We have now found halos in all 180 stored timesteps, and we have complete merger trees based on Bolshoi.

Klypin, Trujillo-Gomez, & Primack, arXiv:1002.3660 ApJ in press

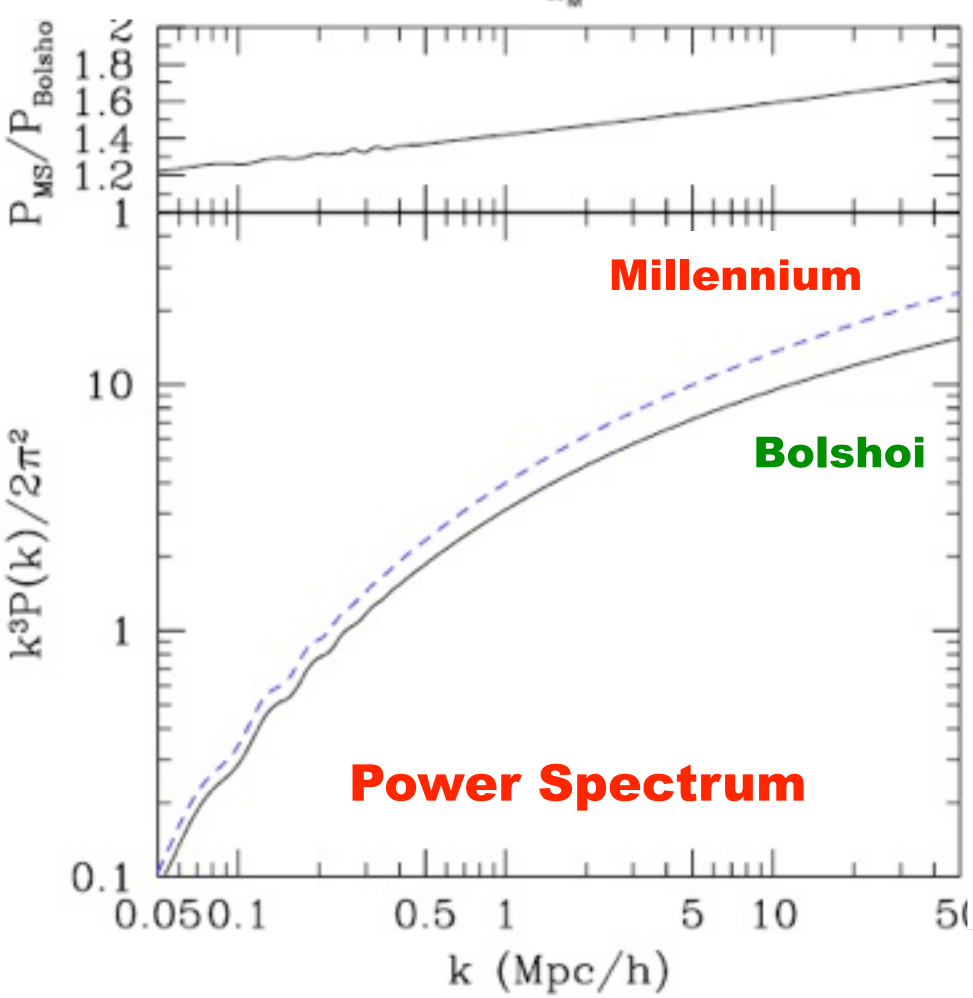

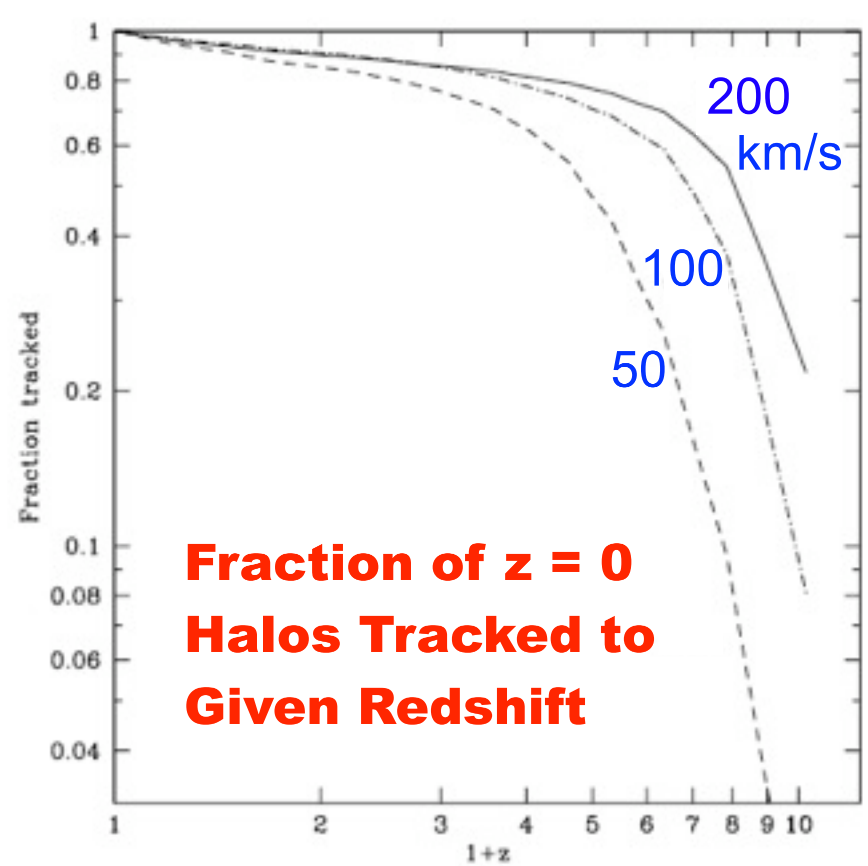

Subhalos follow the dark matter distribution

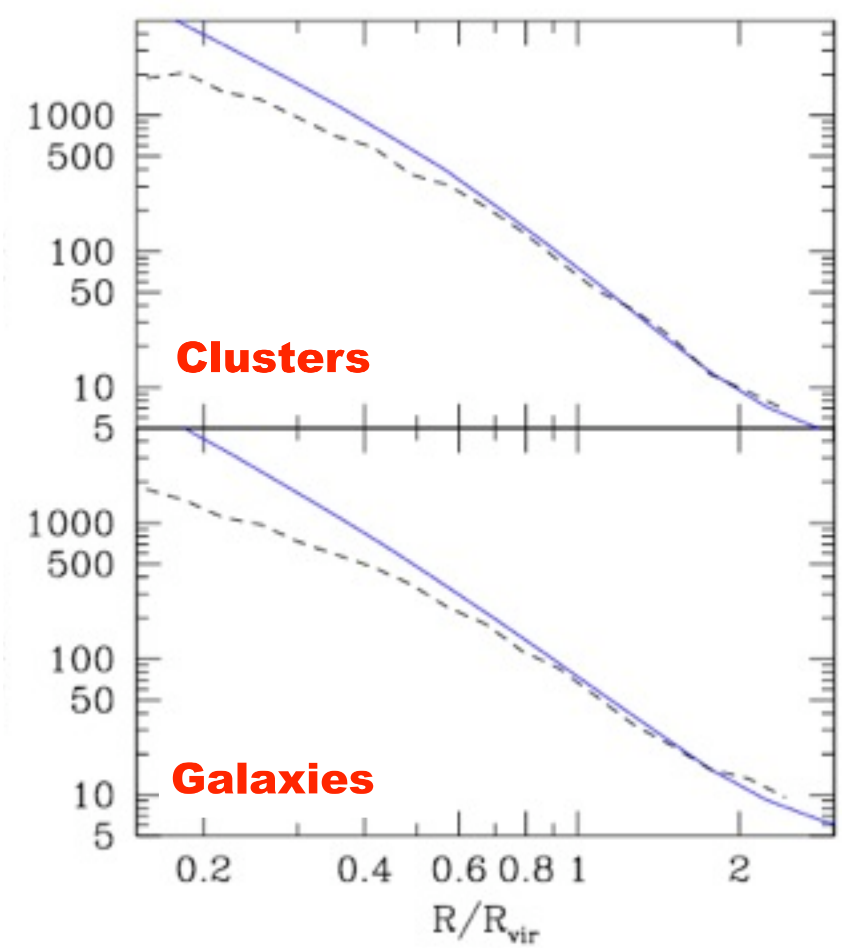

BOLSHOI SIMULATION FLY-THROUGH

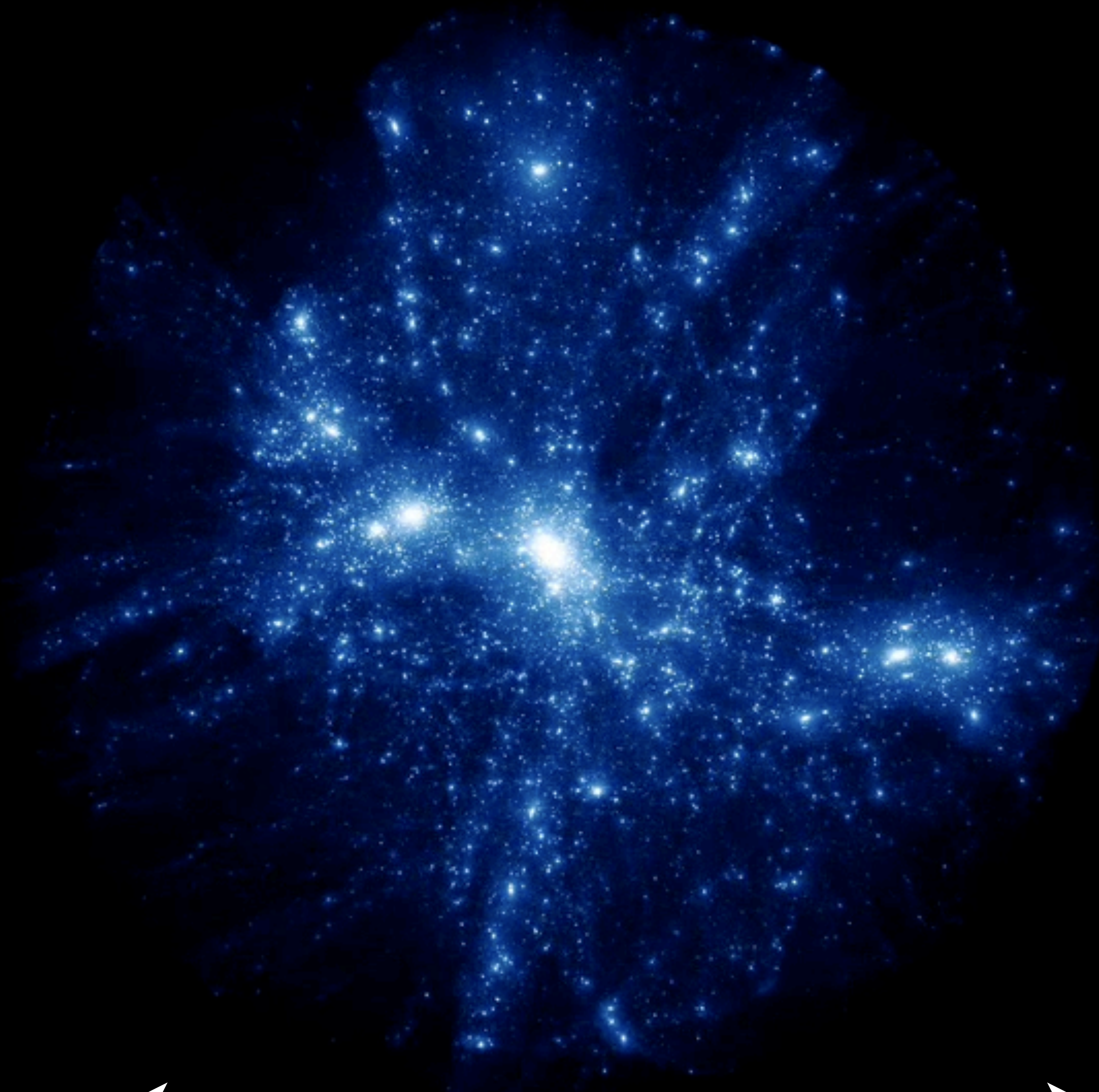

100 million light years

$<10^{-3}$ of the Bolshoi Simulation Volume

BOLSHOI SIMULATION FLY-THROUGH

$<10^{-3}$
of the
Bolshoi
Simulation
Volume

BOLSHOI
Merger Tree
Peter Behroozi, et al.

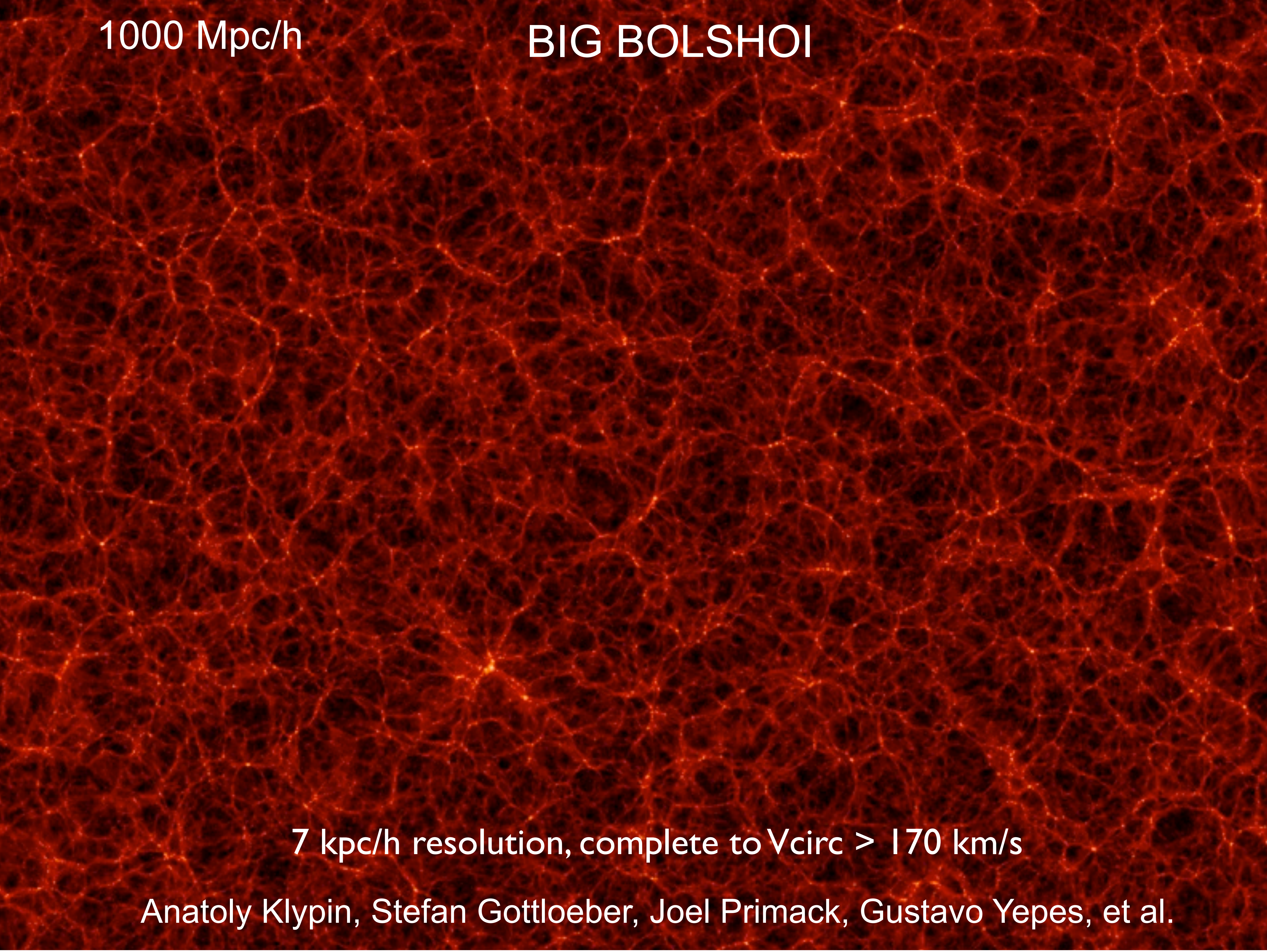
1000 Mpc/h
BIG BOLSHOI
7 kpc/h resolution, complete to Vcirc > 170 km/s
Anatoly Klypin, Stefan Gottloeber, Joel Primack, Gustavo Yepes, et al.

Zoom-in on the Largest Cluster in BIG BOLSHOI

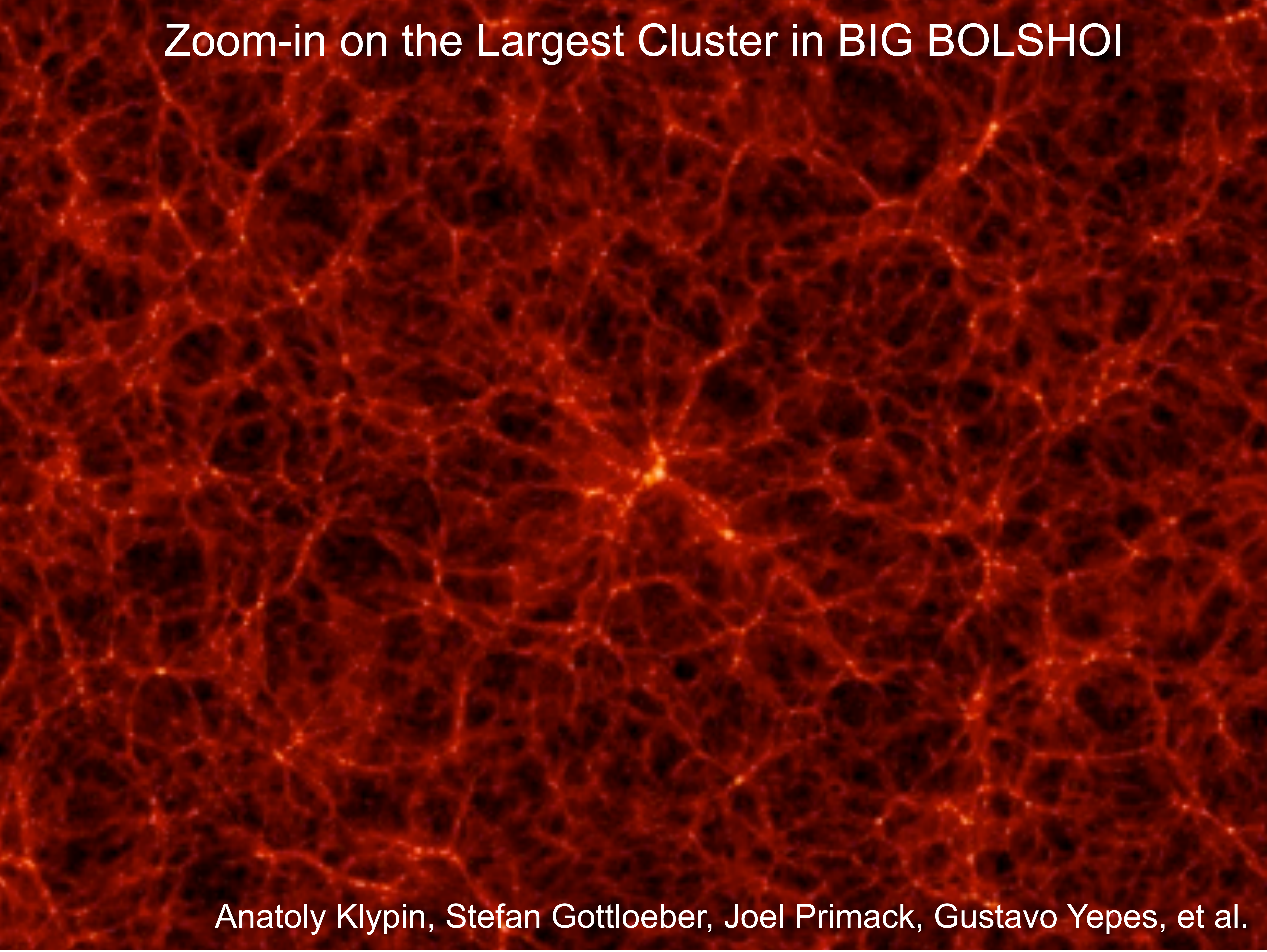

Anatoly Klypin, Stefan Gottloeber, Joel Primack, Gustavo Yepes, et al.

MultiDark Hydro Simulation of Largest Cluster in BIG BOLSHOI

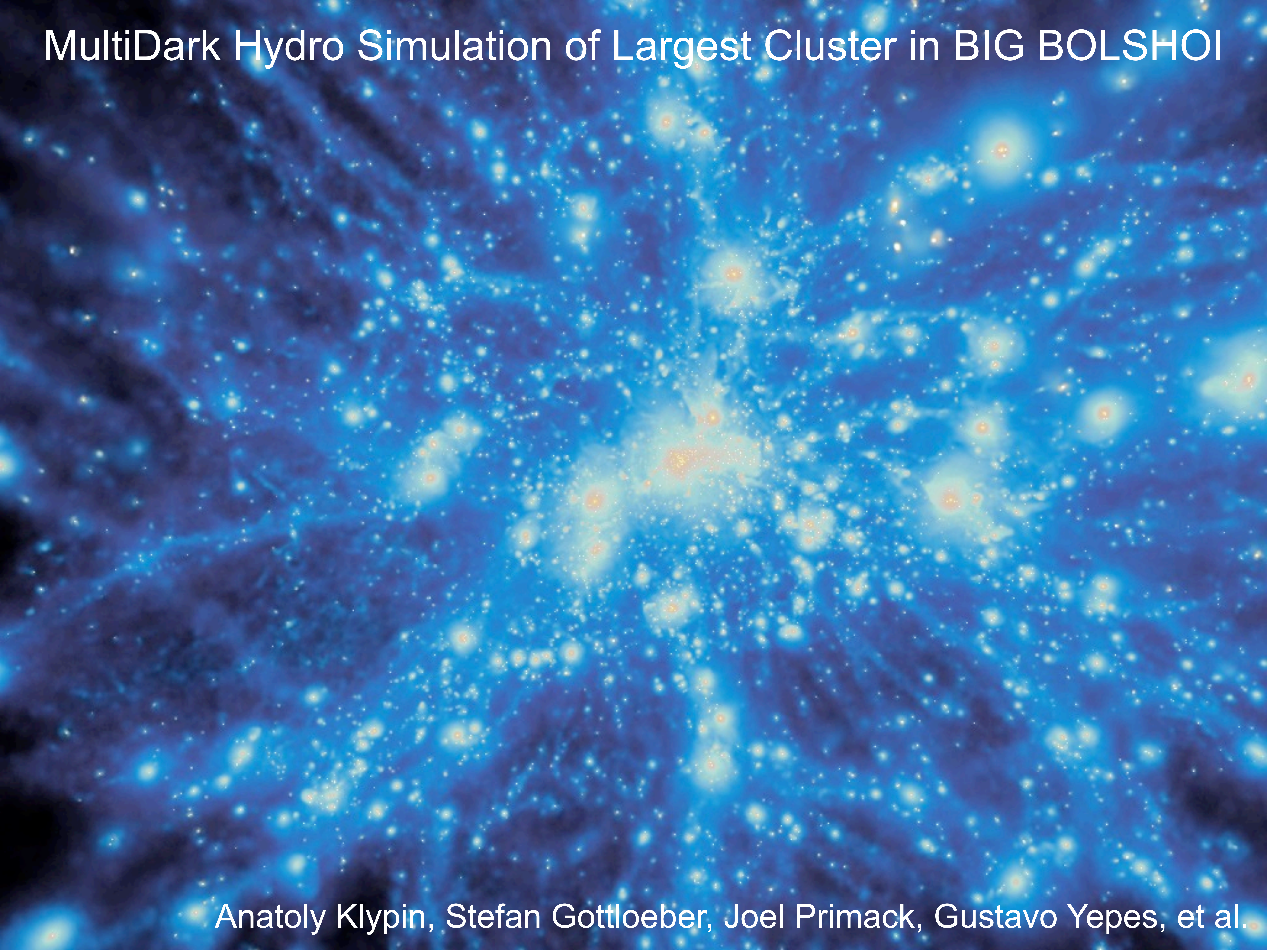

Anatoly Klypin, Stefan Gottloeber, Joel Primack, Gustavo Yepes, et al.

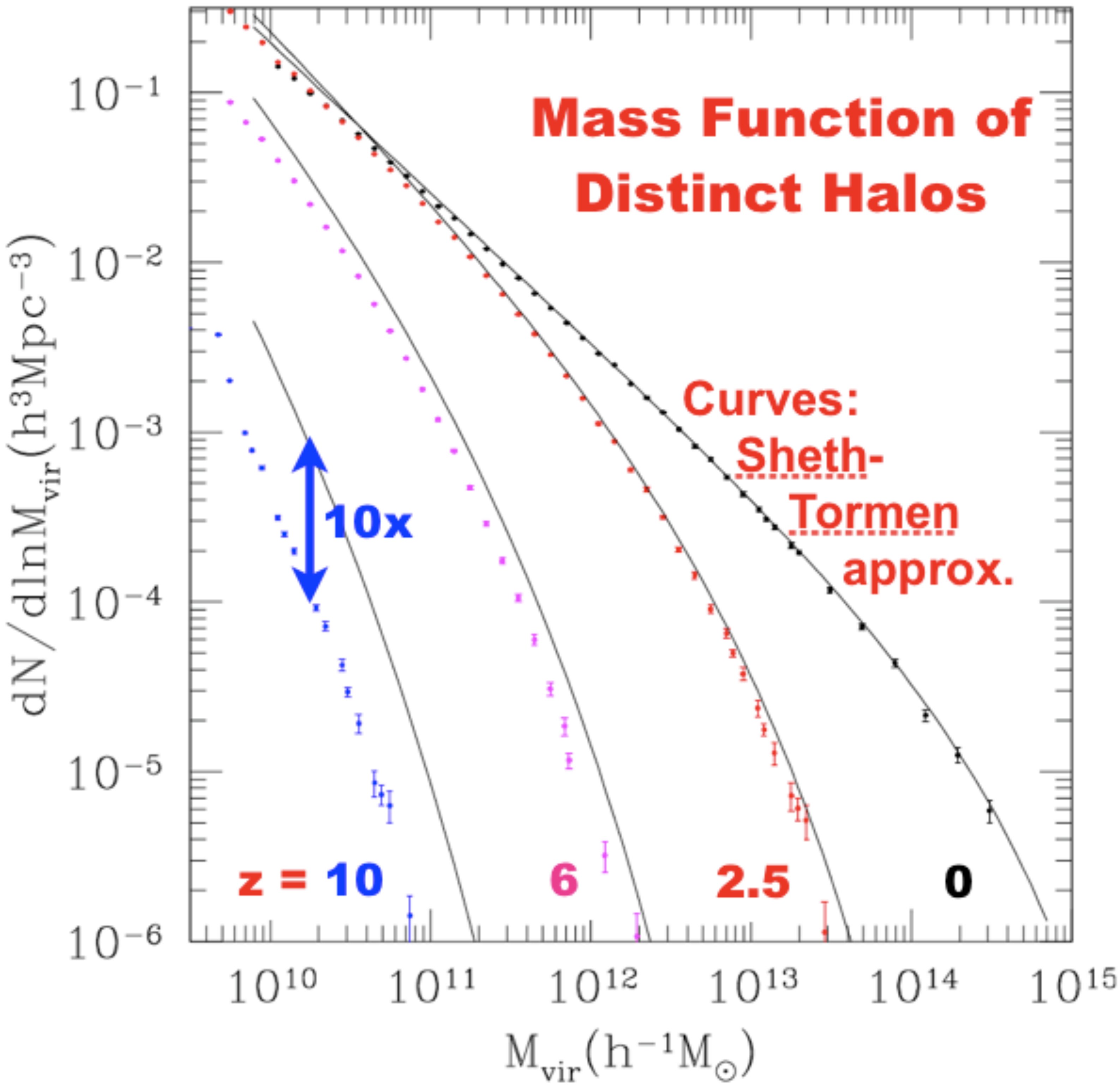

Sheth-Tormen Fails at High Redshifts

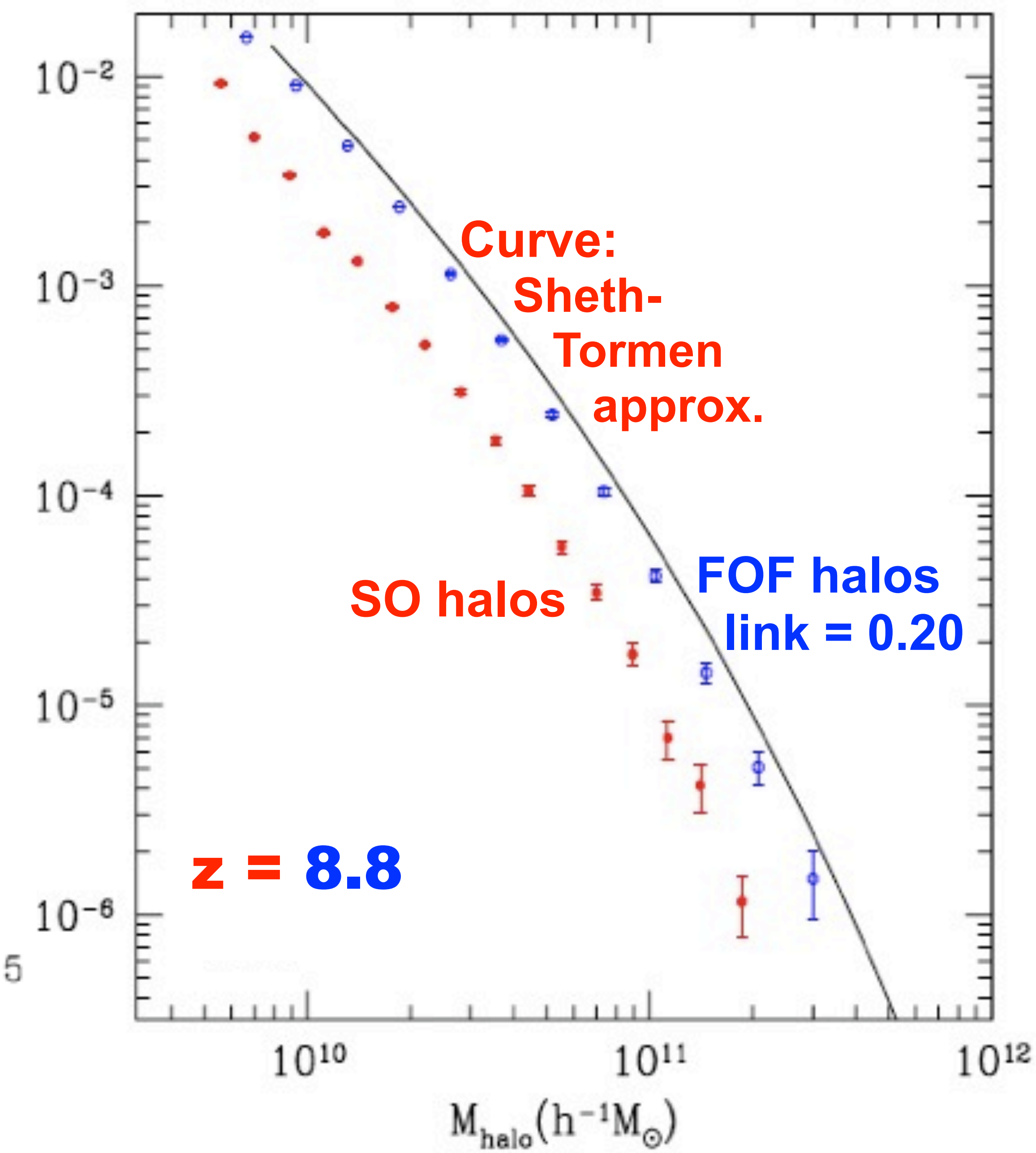

Sheth-Tormen approximation with the same WMAP5 parameters used for Bolshoi simulation very accurately agrees with abundance of halos at low redshifts, but increasingly overpredicts bound spherical overdensity halo abundance at higher redshifts.

Klypin, Trujillo, & Primack, arXiv: 1002.3660v3

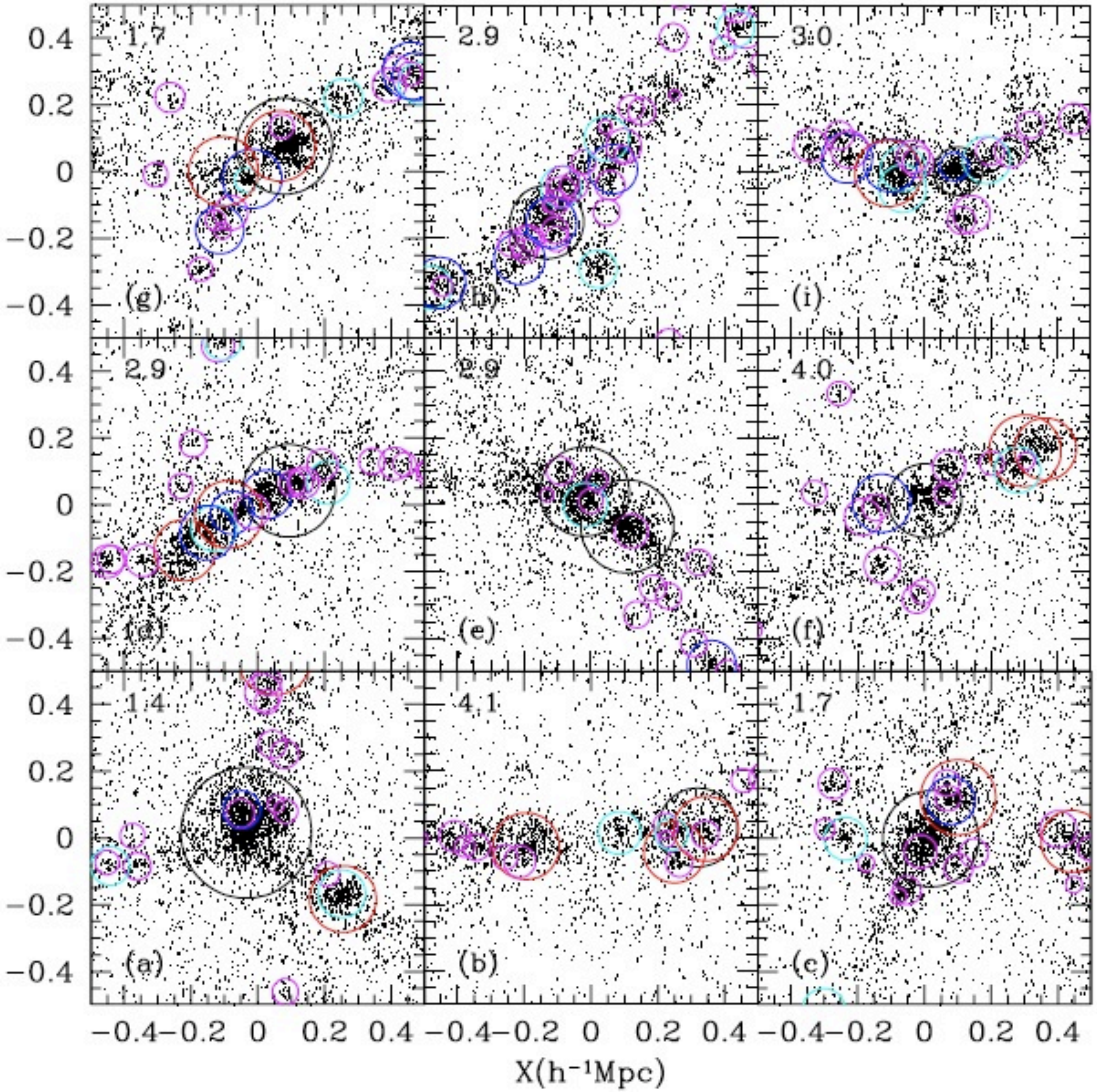

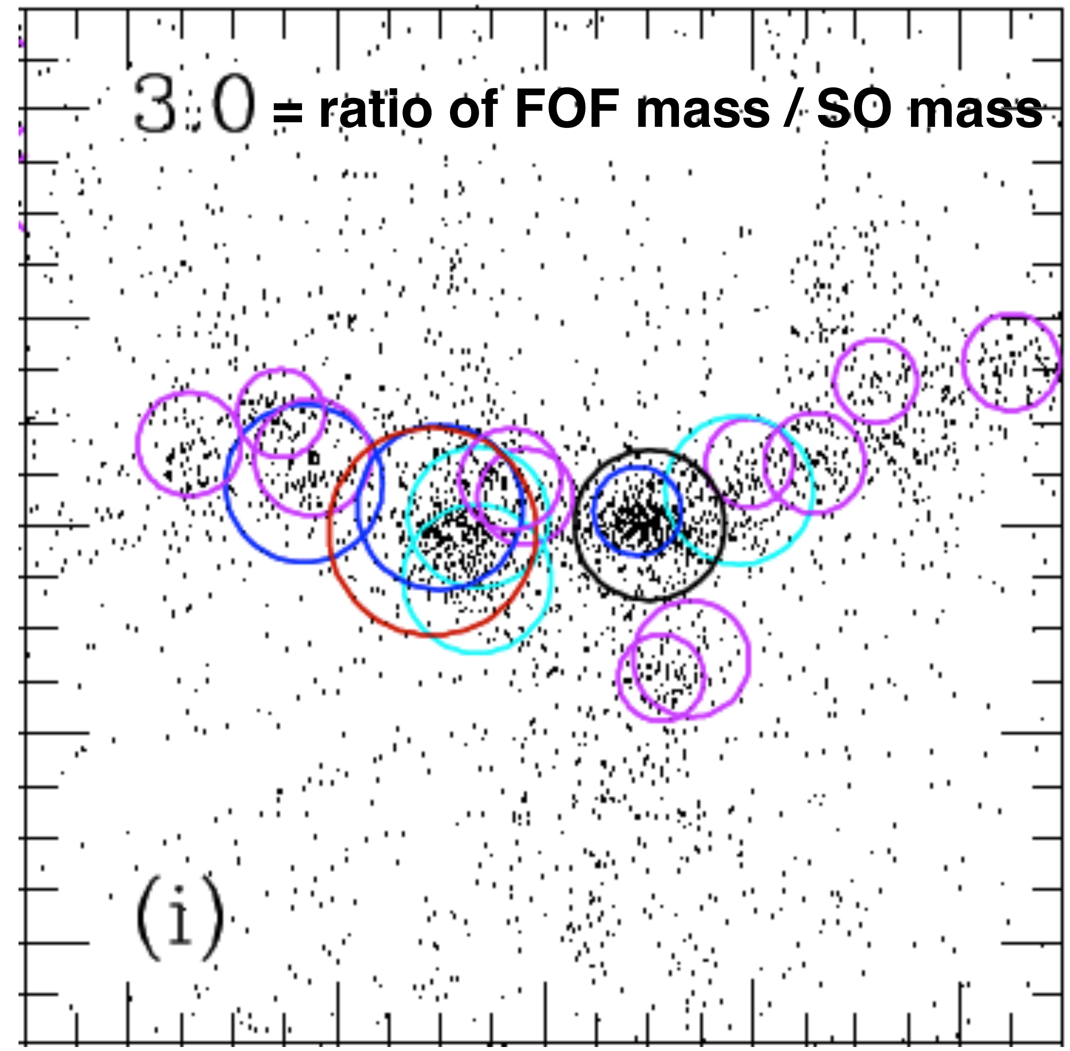

FOF linked together a chain of halos that formed in long and dense filaments (also in panels b, d, f, h; e = major merger)

Each panel shows 1/2 of the dark matter particles in cubes of 1h^{-1} Mpc size. The center of each cube is the exact position of the center of mass of the corresponding FOF halo. The effective radius of each FOF halo in the plots is 150 – 200 h^{-1} kpc. Circles indicate virial radii of distinct halos and subhalos identified by the spherical overdensity algorithm BDM.

Klypin, Trujillo-Gomez, & Primack, arXiv: 1002.3660 ApJ in press

UNDERSTANDING GALAXY CORRELATIONS

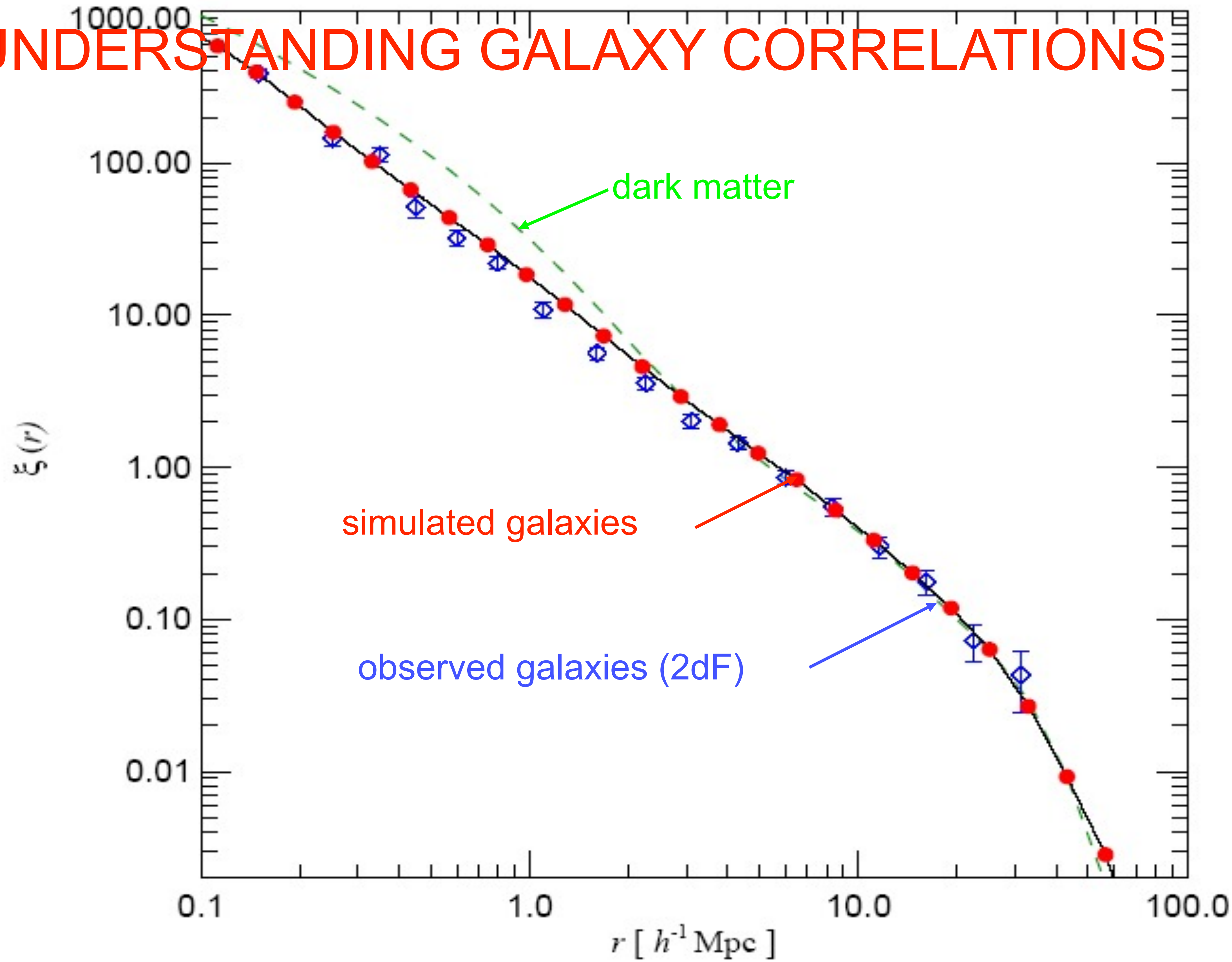

Galaxy 2-point correlation function at the present epoch.

Springel et al. 2005

ΛCDM PREDICTS EVOLUTION IN THE GALAXY CORRELATION FUNCTION

$\xi_{gg}(r)$

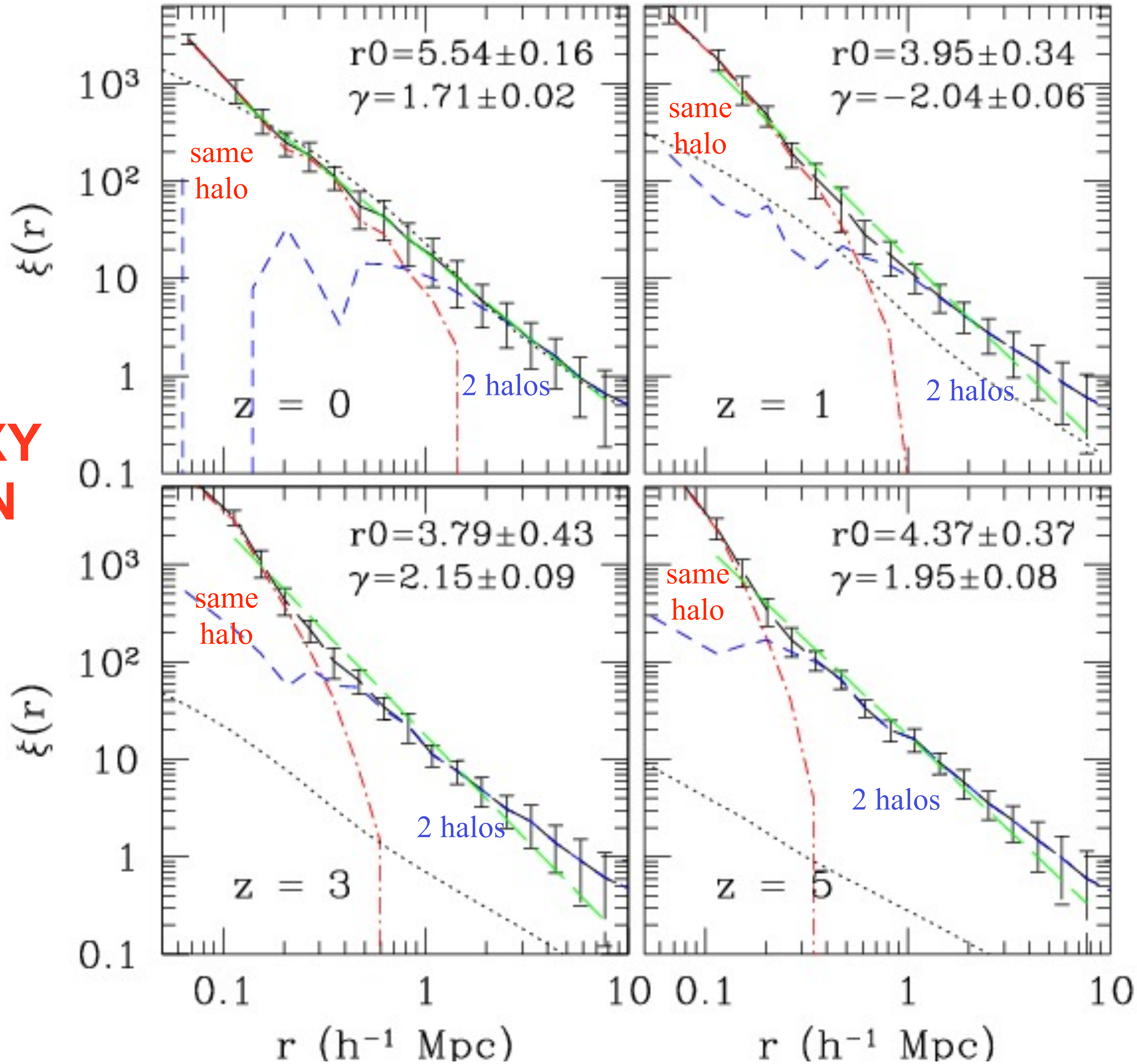

FIG. 8.— Evolution of the two-point correlation function in the $80h^{-1}$ Mpc simulation. The solid line with error bars shows the clustering of halos of the fixed number density $n = 5.89 \times 10^{-3} h^3$ Mpc^{-3} at each epoch. The error-bars indicate the "jack-knife" one sigma errors and are larger than the Poisson error at all scales. The dot-dashed and dashed lines show the corresponding one- and two-halo term contributions. The long-dashed lines show the power-law fit to the correlation functions in the range of $r = [0.1 - 8h^{-1}$ Mpc$]$. Although the correlation functions can be well fit by the power law at $r \gtrsim 0.3h^{-1}$ Mpc in each epoch, at $z > 0$ the correlation function steepens significantly at smaller scales due to the one-halo term.

Kravtsov, Berlind, Wechsler, Klypin, Gottloeber, Allgood, & Primack 2004

Galaxy clustering in SDSS at z~0 agrees with ΛCDM simulations

projected 2-point correlation function

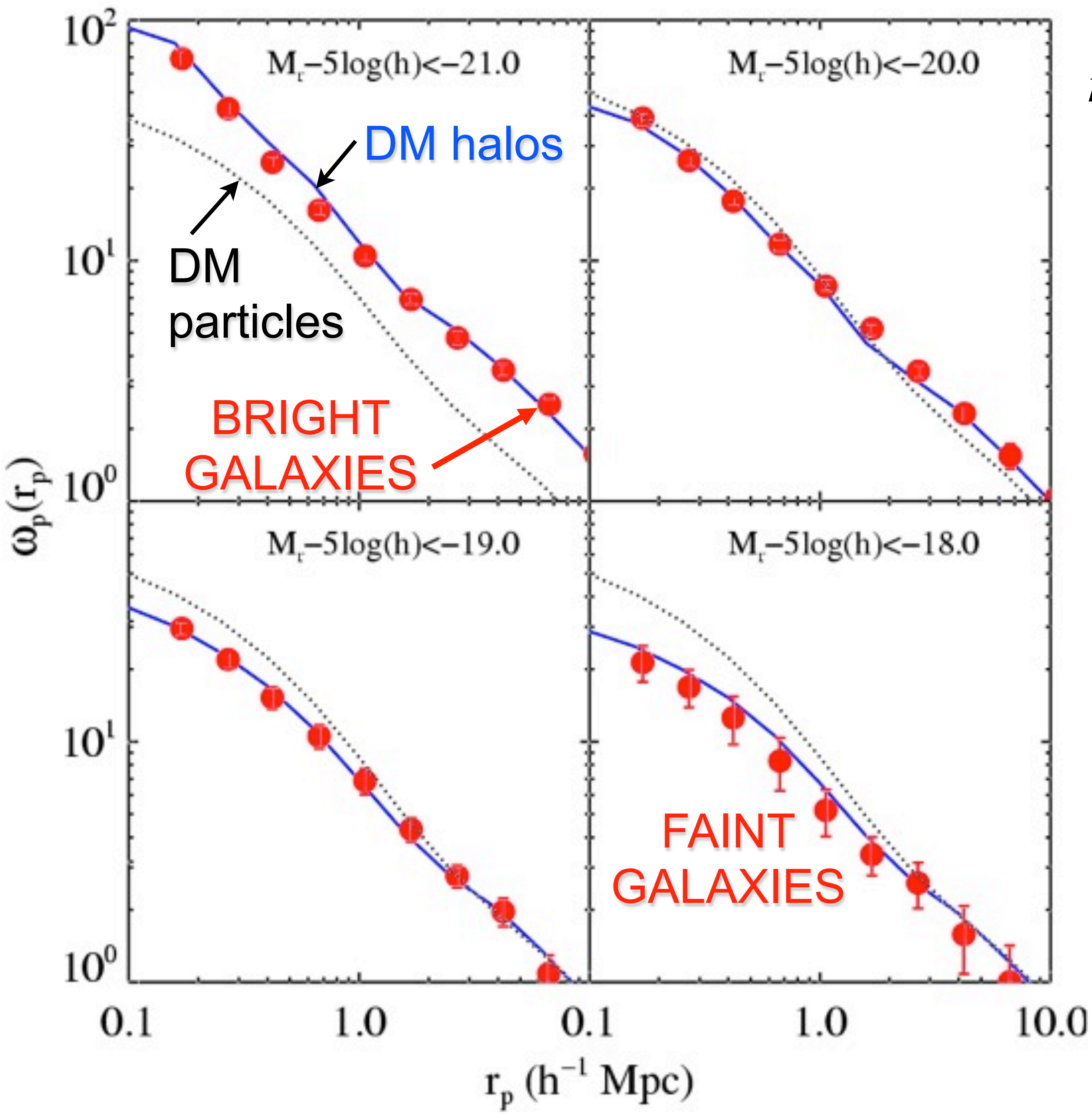

projected separation

$n(>V_{\mathrm{max,acc}}) = n(>L)$

Conroy, Wechsler & Kravtsov 2006, ApJ 647, 201

and at redshift z~1 (DEEP2)!

projected 2-point correlation function

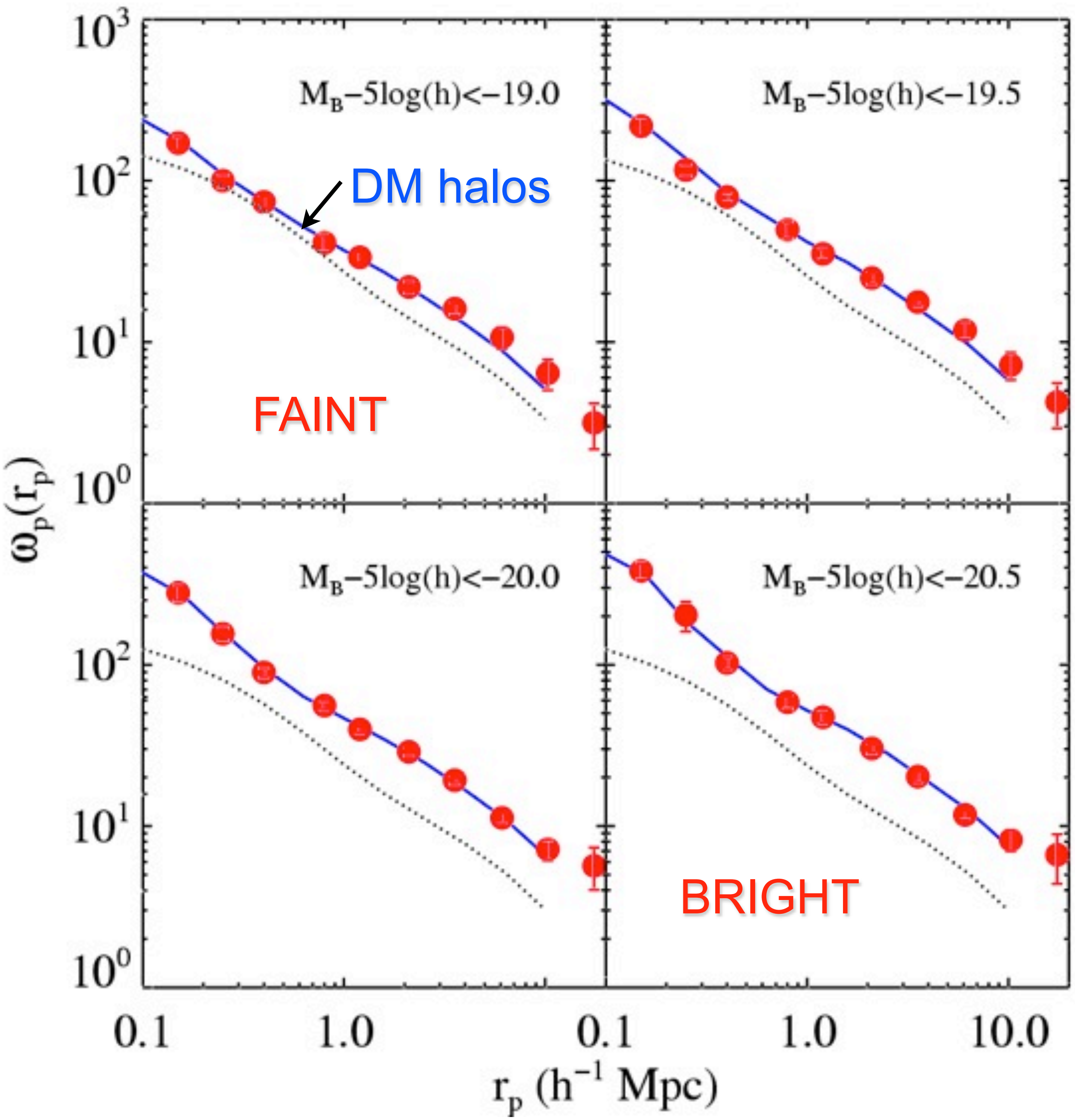

$n(>V_{\mathrm{max,acc}}) = n(>L)$

Conroy, Wechsler & Kravtsov 06

projected separation

and at z~4-5 (LBGs, Subaru)!!

angular 2-point correlation function

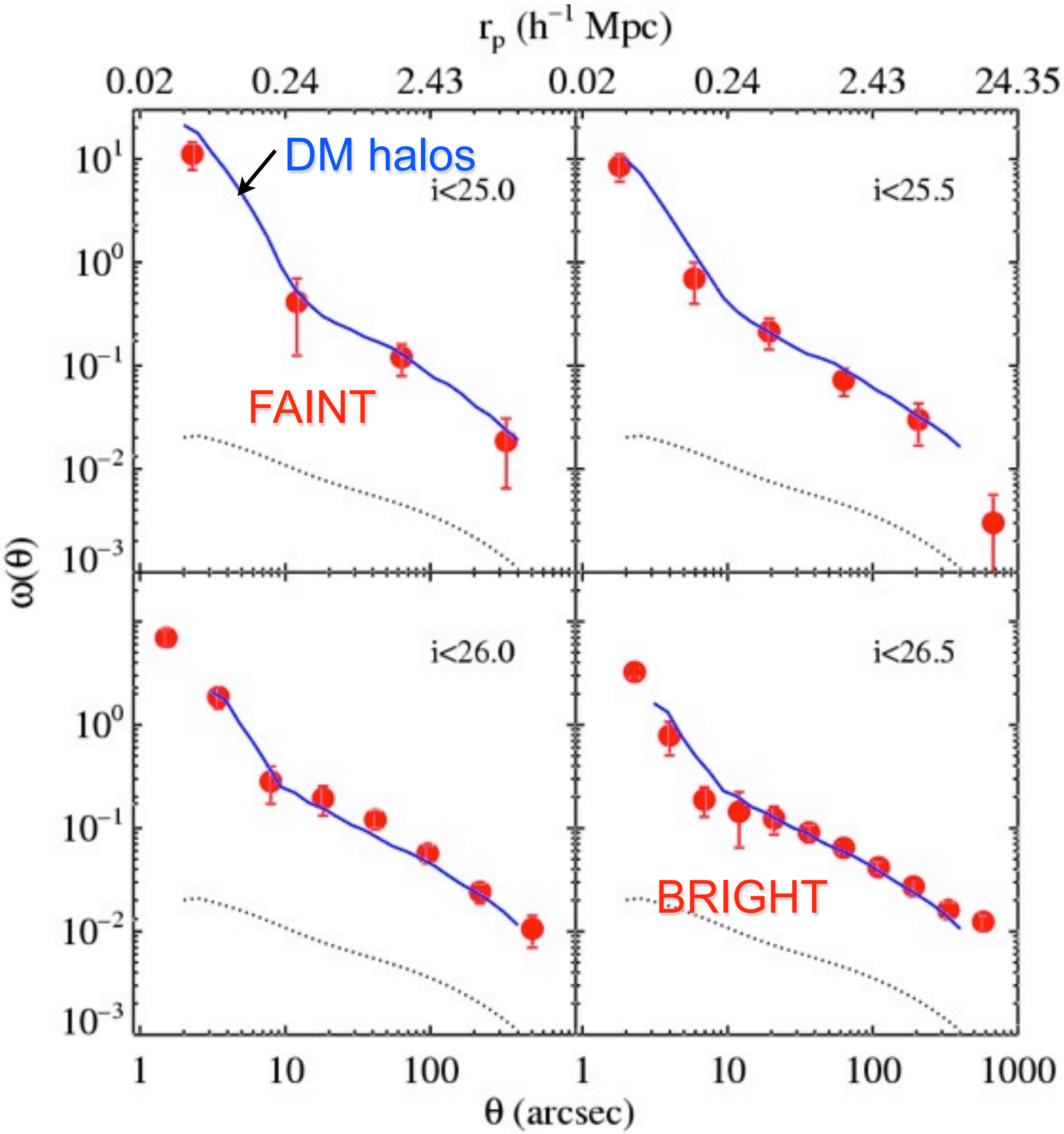

$n(>V_{\rm max,acc})=n(>L)$

projected separation

Conroy, Wechsler & Kravtsov 06

Halo Abundance Matching

To investigate the statistics of galaxies and their relation to host DM halos as predicted by the LCDM model, we predicted the properties of our model galaxies using the following Halo Abundance Matching (HAM) procedure:

1. Using the merger tree of each DM halo and subhalo, obtain V_{acc} = the peak value of the circular velocity over the history of the halo (this is typically the maximum circular velocity of the halo when the halo is first accreted). Perform abundance matching of the velocity function of the halos to the LF of galaxies to obtain the luminosity of each model galaxy.

2. Perform abundance matching of the velocity function to the stellar mass function of galaxies to obtain the stellar mass of each model galaxy.

3. Use the observed gas-to-stellar mass ratio as a function of stellar mass to assign cold gas masses to our model galaxies. The stellar mass added to the cold gas mass becomes the total baryonic mass.

4. Using the density profiles of the DM halos, obtain the circular velocity at 10 kpc (V_{10}) from the center of each halo. Multiply the DM mass, as it comes from simulations, by the factor $(1 - f_{bar})$, where f_{bar} is the cosmological fraction of baryons. This is the dark-matter-only contribution. Add the contribution to V_{10} of the baryon mass from step 3 assuming it is enclosed within a radius of 10 kpc.

5. Optionally implement the BFFP86 correction to V_{10} due to the adiabatic contraction of the DM halos from the infall of the baryon component to the center.

GRAVITATIONALLY CONSISTENT HALO CATALOGS AND MERGER TREES FOR PRECISION COSMOLOGY

PETER S. BEHROOZI, MICHAEL T. BUSHA, RISA H. WECHSLER
Physics Department, Stanford University; Department of Particle and Particle Astrophyiscs, SLAC National Accelerator Laboratory; Kavli Institute for Particle Astrophysics and Cosmology Stanford, CA 94305

ANATOLY KLYPIN
Astronomy Department, New Mexico State University, Las Cruces, NM, 88003

JOEL PRIMACK
Department of Physics, University of California at Santa Cruz, Santa Cruz, CA 95064

Preliminary

Draft version January 28, 2011

ABSTRACT

We present a new algorithm for generating merger trees and halo catalogs which explicitly ensures consistency of halo properties (mass, position, velocity, radius) across timesteps. We use this algorithm to generate merger trees for two large simulations (Bolshoi and Consuelo) and discuss the relative consistency of two halo finders (BDM and SUBFIND). Finally, we use the merger trees thus generated to examine the question of when satellite halos reached their peak mass. We find that the peak mass for infalling halos occurs at roughly 3 $R_{\rm vir}$ of the final host halo, which suggests that dark matter stripping occurs even before halos cross the virial radius of a larger halo.

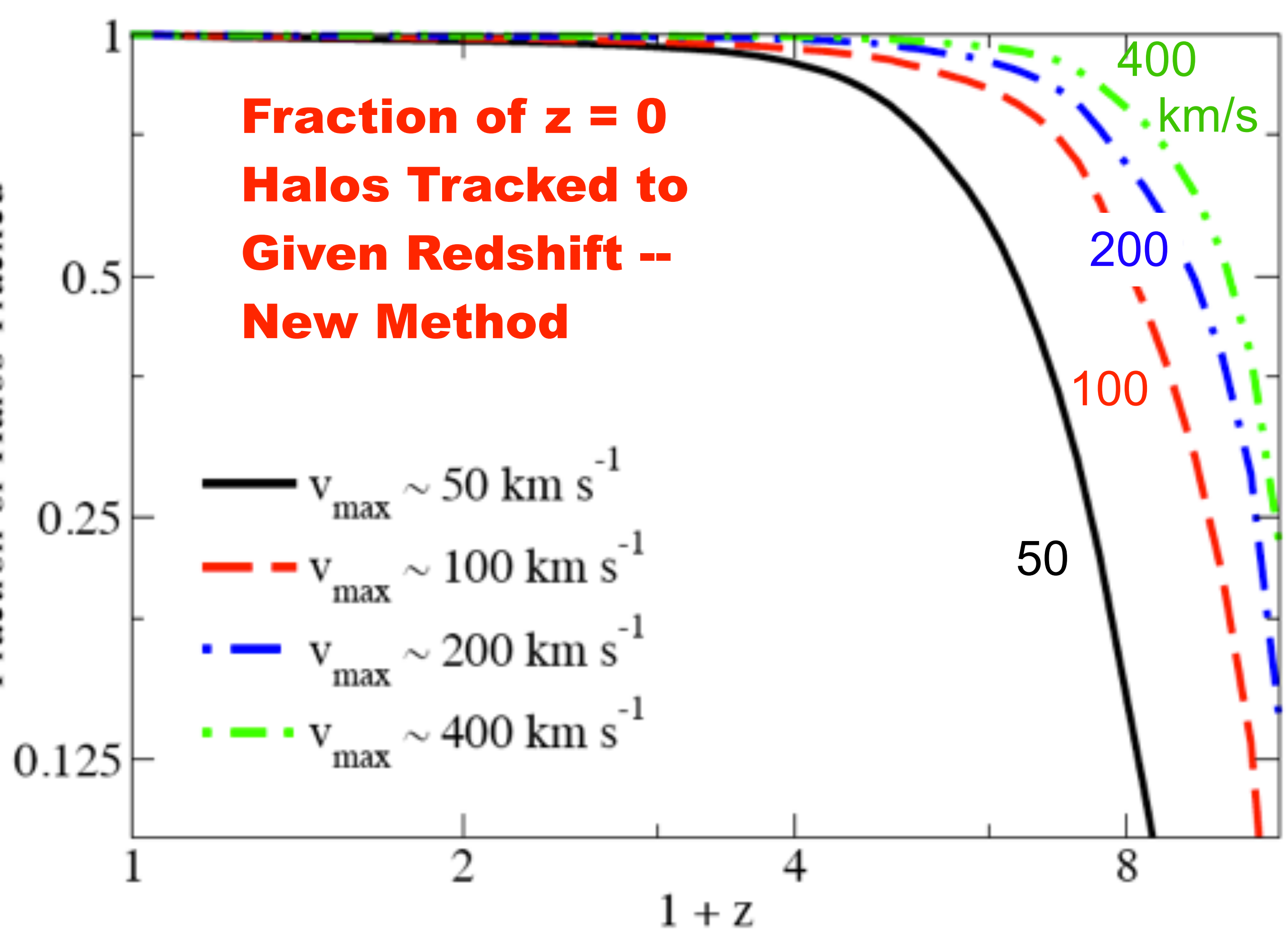

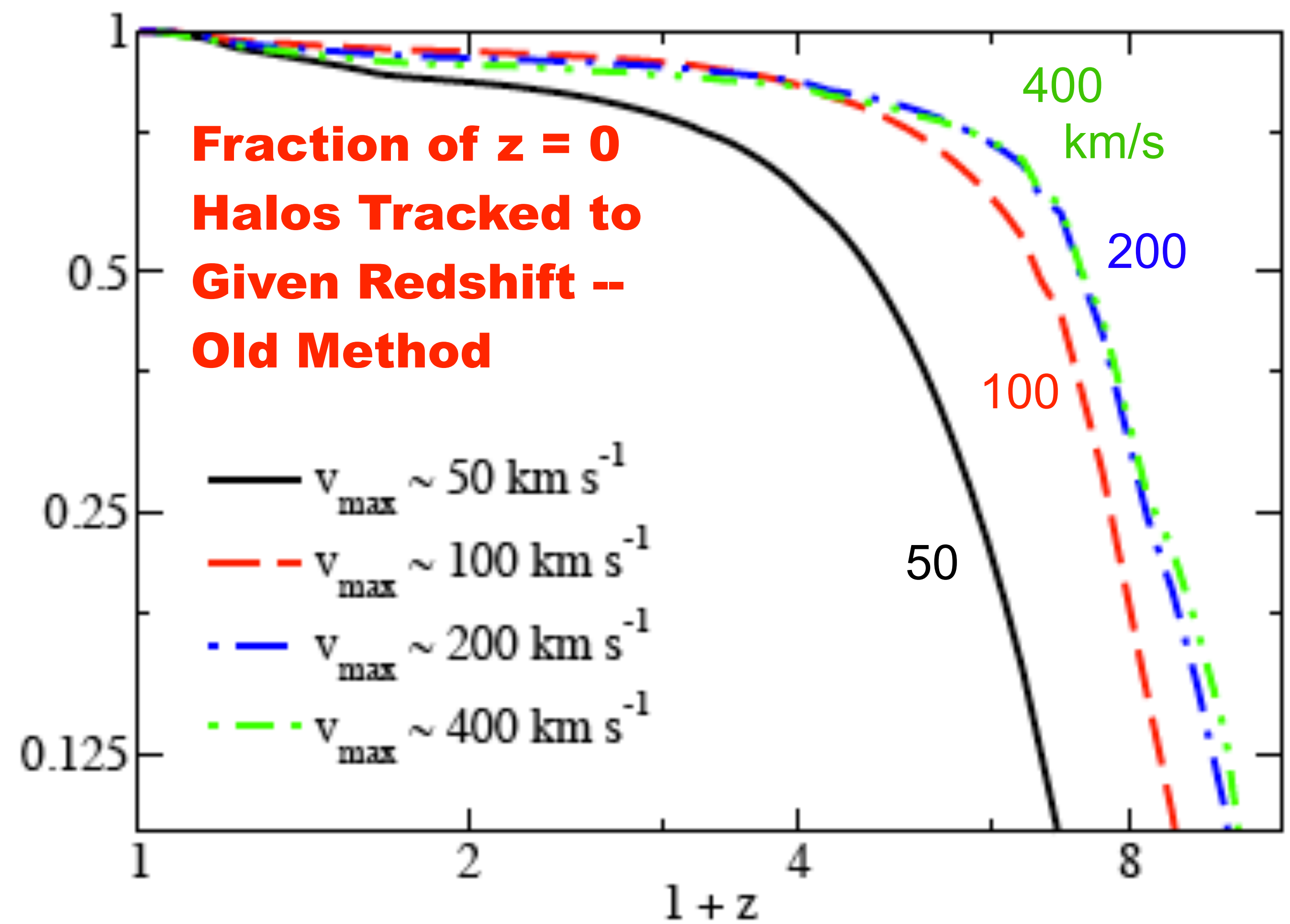

GRAVITATIONALLY CONSISTENT HALO CATALOGS AND MERGER TREES FOR PRECISION COSMOLOGY

PETER S. BEHROOZI, MICHAEL T. BUSHA, RISA H. WECHSLER
Physics Department, Stanford University; Department of Particle and Particle Astrophyiscs, SLAC National Accelerator Laboratory; Kavli Institute for Particle Astrophysics and Cosmology Stanford, CA 94305

ANATOLY KLYPIN
Astronomy Department, New Mexico State University, Las Cruces, NM, 88003

JOEL PRIMACK
Department of Physics, University of California at Santa Cruz, Santa Cruz, CA 95064

Draft version January 28, 2011

Preliminary

ABSTRACT

We present a new algorithm for generating merger trees and halo catalogs which explicitly ensures consistency of halo properties (mass, position, velocity, radius) across timesteps. We use this algorithm to generate merger trees for two large simulations (Bolshoi and Consuelo) and discuss the relative consistency of two halo finders (BDM and SUBFIND). Finally, we use the merger trees thus generated to examine the question of when satellite halos reached their peak mass. We find that the peak mass for infalling halos occurs at roughly 3 R_{vir} of the final host halo, which suggests that dark matter stripping occurs even before halos cross the virial radius of a larger halo.

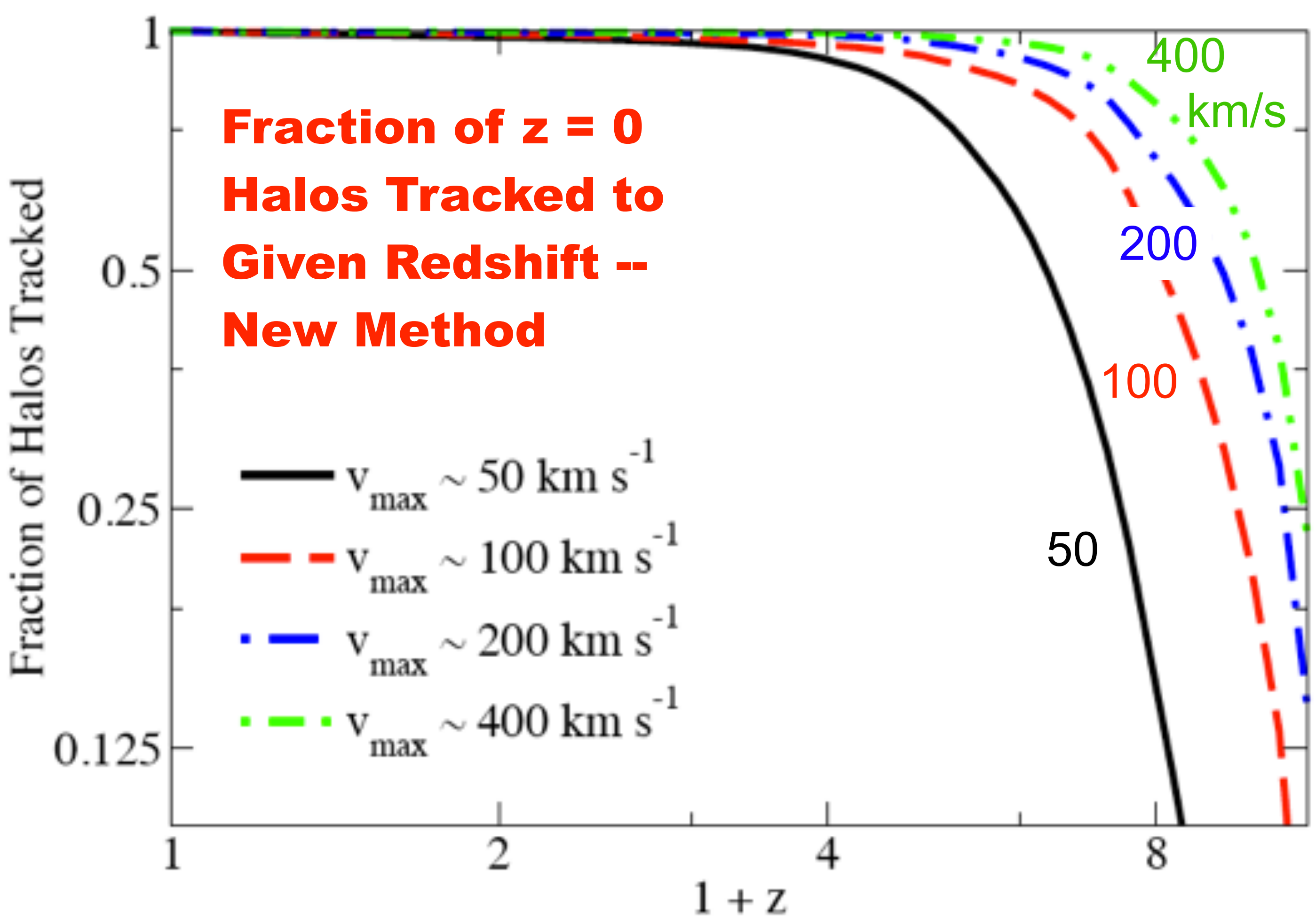

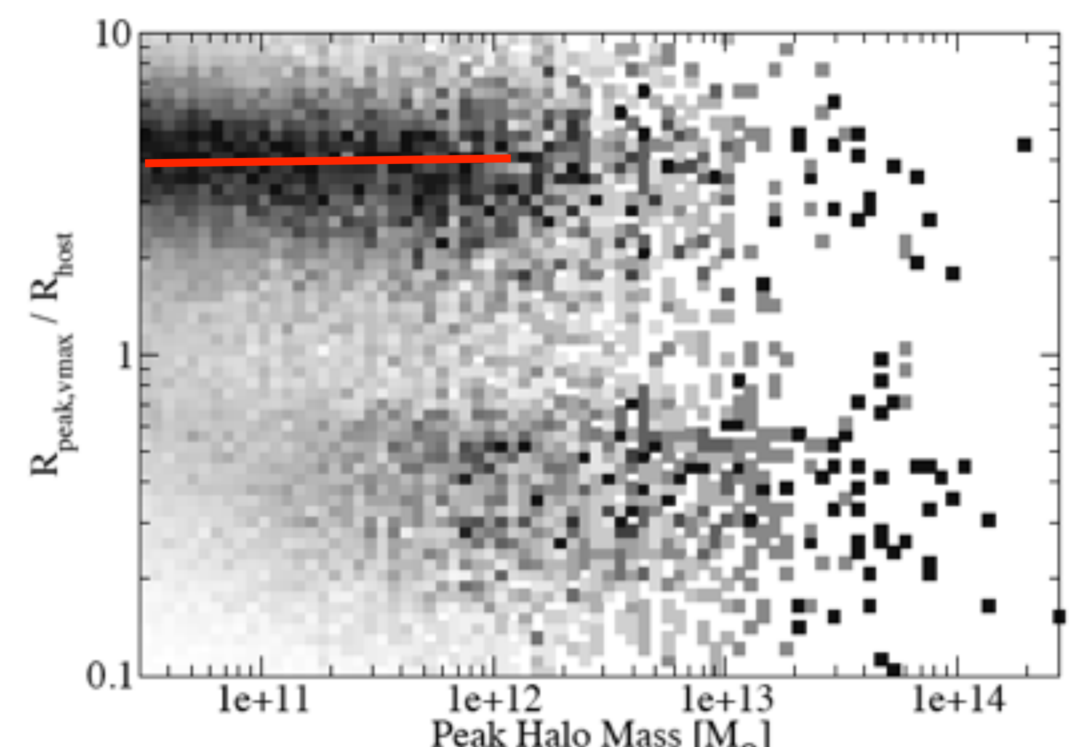

FIG. 9.— Scatter plot of R_{peak}/R_{host} as a function of subhalo mass at $z = 0$ in Bolshoi. R_{peak} is the distance from the final host at which the subhalo had its maximum v_{max}; R_{host} is the radius of the current host halo at the epoch of peak subhalo v_{max}. The region below a ratio of 1 is largely populated by subhalos which were not tracked outside of the virial radius; see Figure 7.

Bolshoi $w_p(r_p)$ by Halo Abundance Matching vs. SDSS Observations

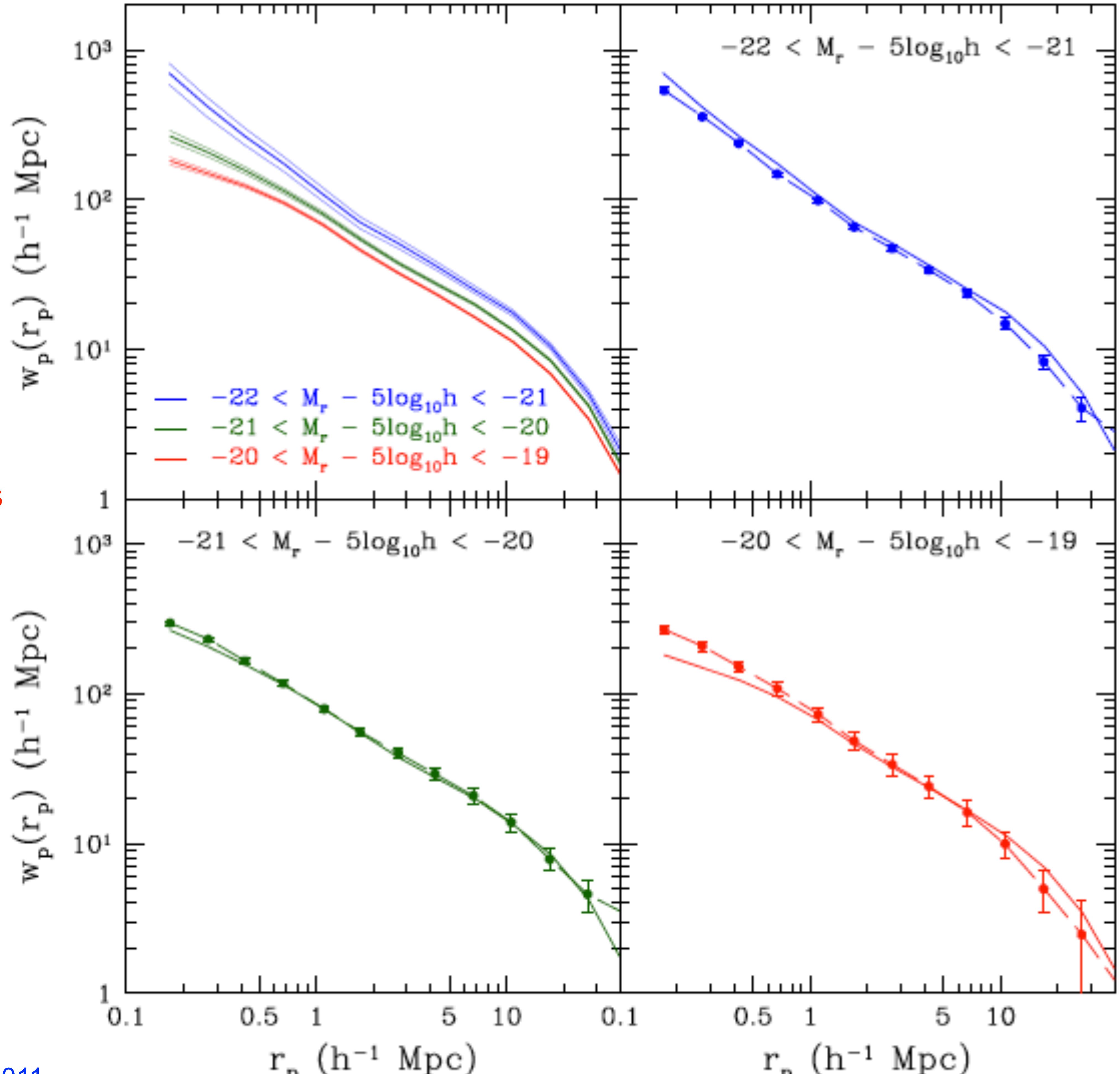

Trujillo-Gomez, Klypin, Primack, & Romanowsky 2011

Bolshoi $w_p(r_p)$ by Halo Abundance Matching vs. SDSS Observations

The correlation function of SDSS galaxies vs. Bolshoi galaxies using halo abundance matching, with scatter using our stochastic abundance matching method. This results in a better than 20% agreement with SDSS. *Top left:* correlation functinon in three magnitude bins, showing Poisson uncertainties as thin lines. *Remaining panels:* correlation function in each luminosity bin compared with SDSS galaxies (points with error bars: Zehavi et al. 2010).

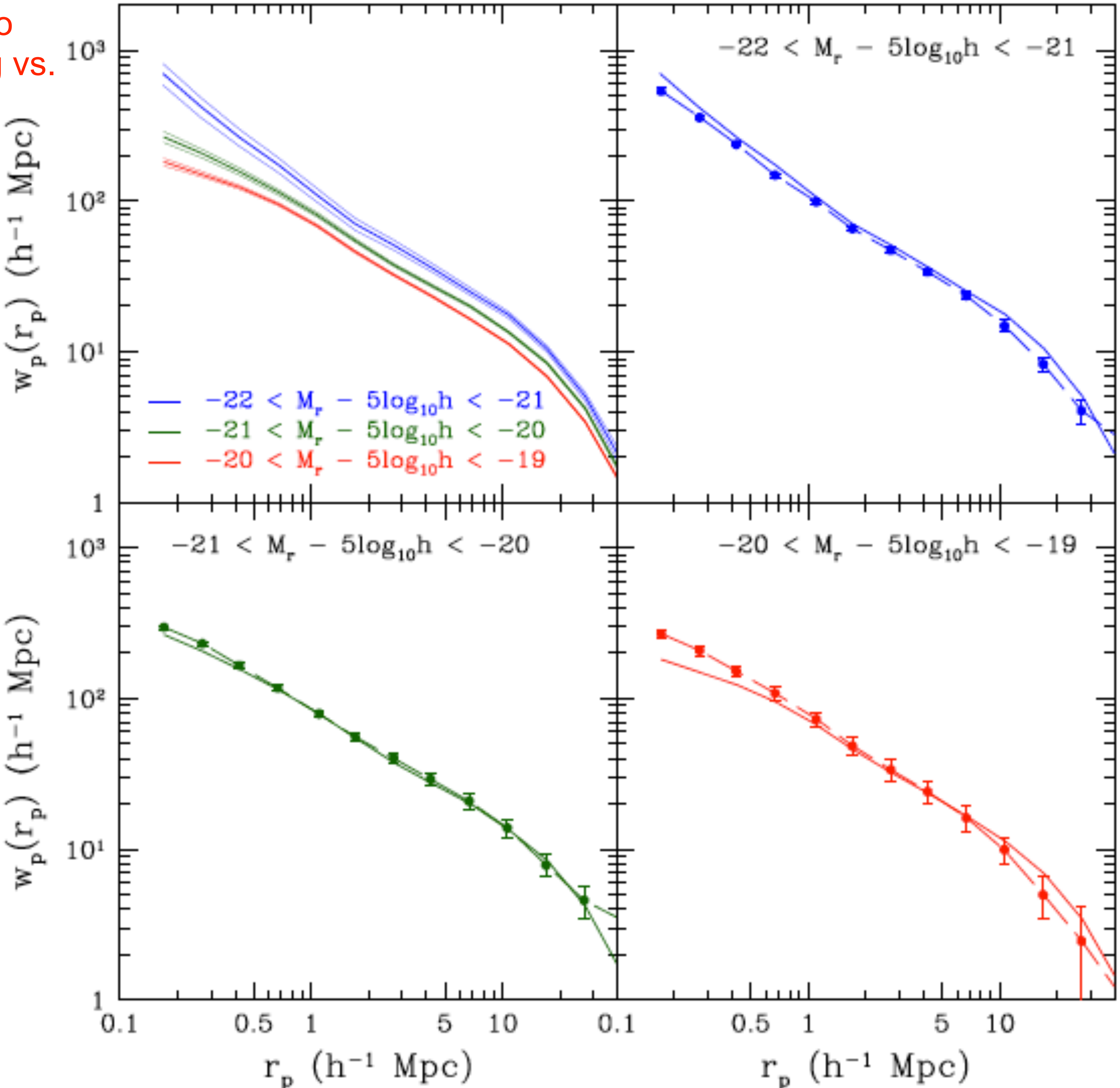

Trujillo-Gomez, Klypin, Primack, & Romanowsky 2011

Millennium-I and II $w_p(r_p)$ by SAM vs. SDSS Observations

MS

MS-II

The correlations are seriously overestimated at small separations for lower masses because the high $\sigma_8 = 0.90$ produces too many massive halos, which contain pairs of such subhalos.

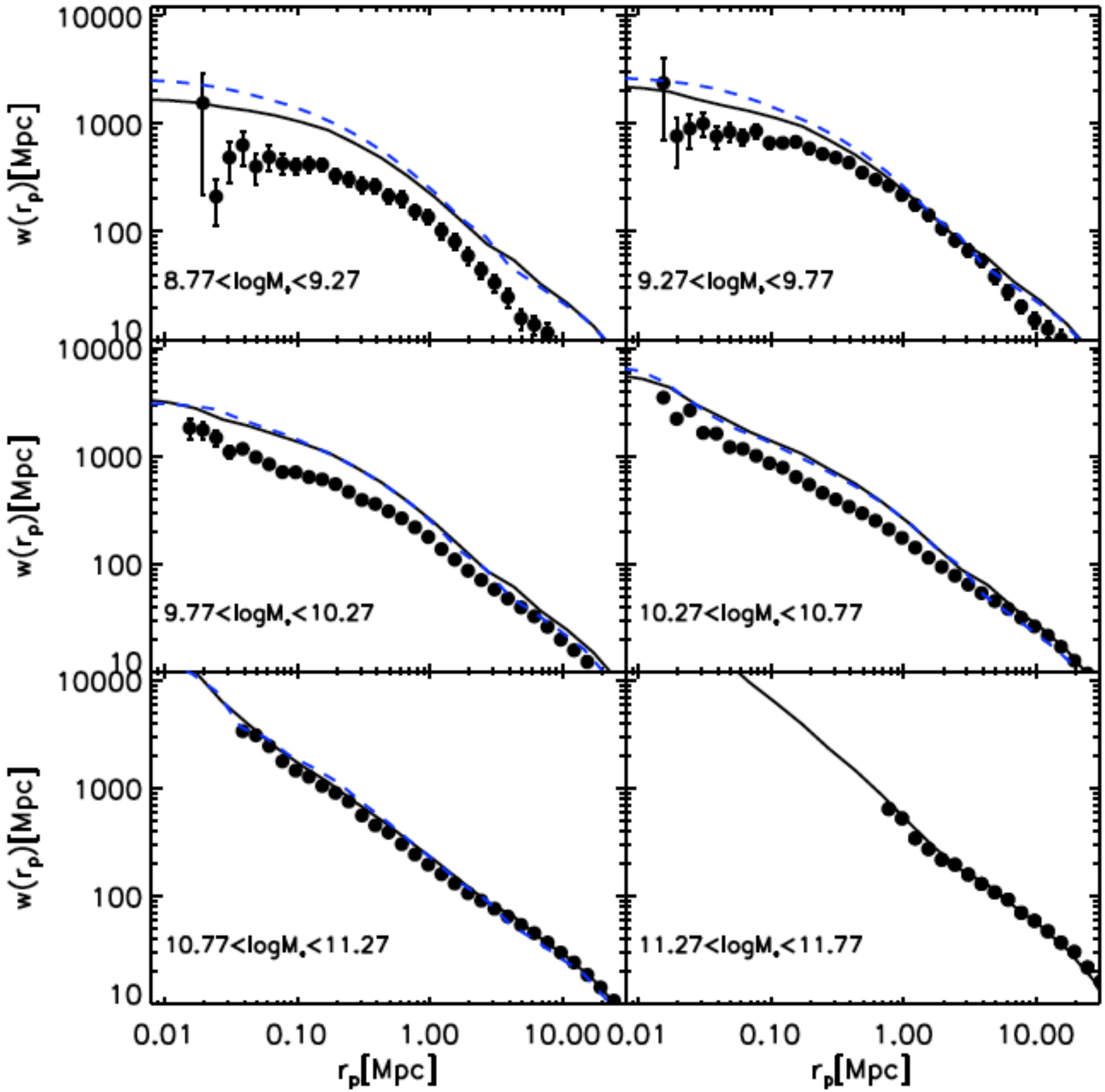

Guo, White, et al. 2011 MN in press

The Milky Way has two large satellite galaxies, the small and large Magellanic Clouds

The Bolshoi simulation predicts the likelihood of this

Statistics of MW-satellite analogs

Liu, Gerke & Wechsler

- Search SDSS DR7 Co-Add data to look for analogues of the LMC/SMC in extragalactic hosts
- SDSS Co-Add Data:
  - Stripe-82 in the SDSS was observed ~370 times, complete to observed magnitude limit $M_r = 23.6$ over ~270 sq. deg; main sample spectroscopy (mostly) complete down to $M_r = 17.77$
  - Photometric redshifts calculated for the remaining objects using a template method.
    - Training/validation set taken from CNOC2, SDSS main, and DEEP2 samples.
    - Measured scatter: $\Delta z = 0.02$
  - 23,000 spectroscopic galaxy (non-QSO) candidates in Stripe 82 with $m_r < 17.77$
- Magnitude Cuts:
  - Identify all objects with absolute $^{0.1}M_r = -20.73 \pm 0.2$ and observed $m_r < 17.6$
  - Lets us probe out to z = 0.15, a volume of roughly 500 $(\mathrm{Mpc}/h)^3$
  - leaves us with 3,200 objects.
- Isolation Criteria: exclude objects in clusters, since those are likely biased -- exclude candidates with neighbors brighter than itself within a cylinder defined by:
    - radial distance 1000 km/s -- the velocity dispersion of a typical cluster and $\Delta z \approx 0.01$ at our relevant redshifts.
    - projected angular distance $R_{iso} = 0.7$ Mpc
    - leaves us with 1,332 hosts.

- Apply the same absolute magnitude and isolation cuts to Bolshoi+SHAM galaxies as to SDSS:
  - Identify all objects with absolute $^{0.1}M_r$ = -20.73±0.2 and observed $m_r < 17.6$
  - Probe out to z = 0.15, a volume of roughly 500 (Mpc/h)^3
  - leaves us with 3,200 objects.
- Comparison of Bolshoi with SDSS observations is in close agreement, well within observed statistical error bars.

# of Subs	Prob (obs)	Prob (sim)
0	60%	61%
1	22%	25%
2	13%	8.1%
3	4%	3.2%
4	1%	1.4%
5	0%	0.58%

Statistics of MW bright satellites: SDSS data vs. Bolshoi simulation

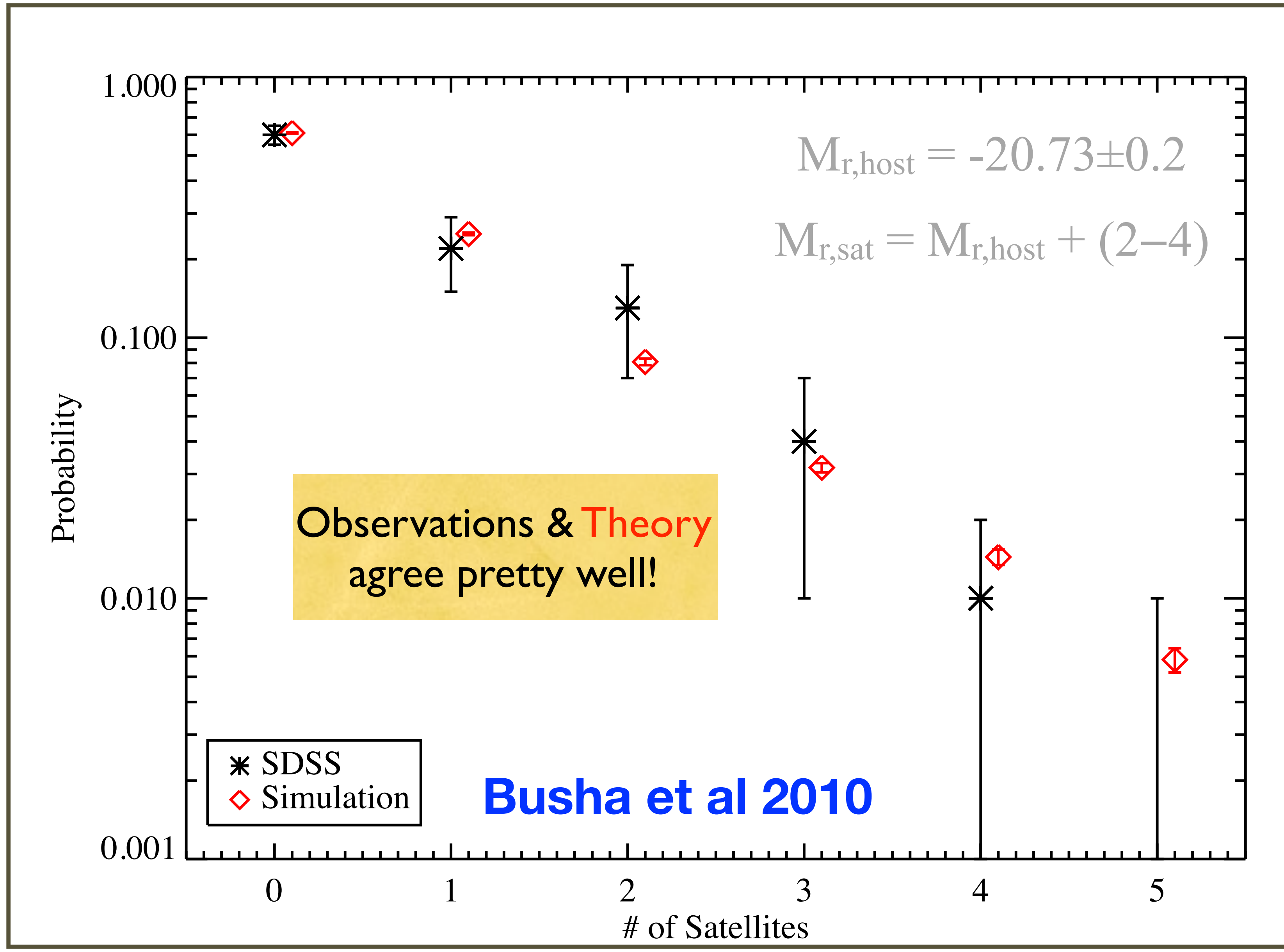

Every case agrees within observational errors!

Risa Wechsler

SMALL-SCALE STRUCTURE IN THE SDSS AND ΛCDM: ISOLATED $\sim L_*$ GALAXIES WITH BRIGHT SATELLITES

ERIK J. TOLLERUD[1], MICHAEL BOYLAN-KOLCHIN[1,2], ELIZABETH J. BARTON[1], JAMES S. BULLOCK [1], CHRISTOPHER Q. TRINH[3,1]

Draft version March 11, 2011

Similarly good agreement with SDSS for brighter satellites with spectroscopic redshifts compared with Millennium-II using abundance matching.

We use a volume-limited spectroscopic sample of isolated galaxies in the Sloan Digital Sky Survey (SDSS) to investigate the frequency and radial distribution of luminous ($M_r \lesssim -18.3$) satellites like the Large Magellanic Cloud (LMC) around $\sim L_*$ Milky Way analogs and compare our results object-by-object to ΛCDM predictions based on abundance matching in simulations. We show that 12% of Milky Way-like galaxies host an LMC-like satellite within 75 kpc (projected), and 42% within 250 kpc (projected). This implies $\sim$ 10% have a satellite within the distance of the LMC, and $\sim$ 40% of L_* galaxies host a bright satellite within the virialized extent of their dark matter halos. Remarkably, the simulation reproduces the observed frequency, radial dependence, velocity distribution, and luminosity function of observed secondaries exceptionally well, suggesting that ΛCDM provides an accurate reproduction of the observed Universe to galaxies as faint as $L \sim 10^9 L_\odot$ on $\sim$ 50 kpc scales. When stacked, the observed projected pairwise velocity dispersion of these satellites is $\sigma \simeq 160\ \mathrm{km\,s^{-1}}$, in agreement with abundance-matching expectations for their host halo masses. Finally, bright satellites around L_* primaries are significantly *redder* than typical galaxies in their luminosity range, indicating that environmental quenching is operating within galaxy-size dark matter halos that typically contain only a single bright satellite. This redness trend is in stark contrast to the Milky Way's LMC, which is unusually blue even for a field galaxy. We suggest that the LMC's discrepant color might be further evidence that it is undergoing a triggered star-formation event upon first infall.

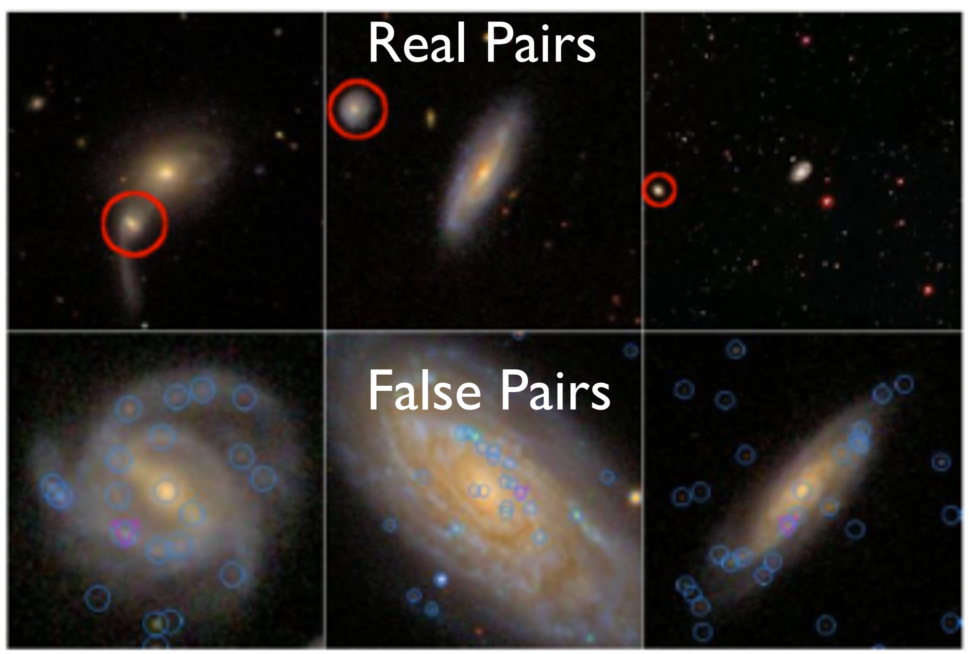

FIG. 1.— Examples of SDSS primary/secondary pairs in the clean sample (upper) and false pairs (lower). Secondaries identified by our criteria (see text) are marked with red circles (upper panels) or magenta triangles (lower panels). The upper three are all in the clean sample (have redshifts close to the primary) and span a range of projected separations. For the lower three images, blue circles are SDSS pipeline photometric objects, clearly showing the identification of HII regions as photometric objects. For these same lower three, the secondaries are clearly HII regions in the primary (or satellites that are indistinguishable from HII regions). We visually identify and remove all pairs of this kind from our sample.

Good agreement between simulated and observed pairwise velocities

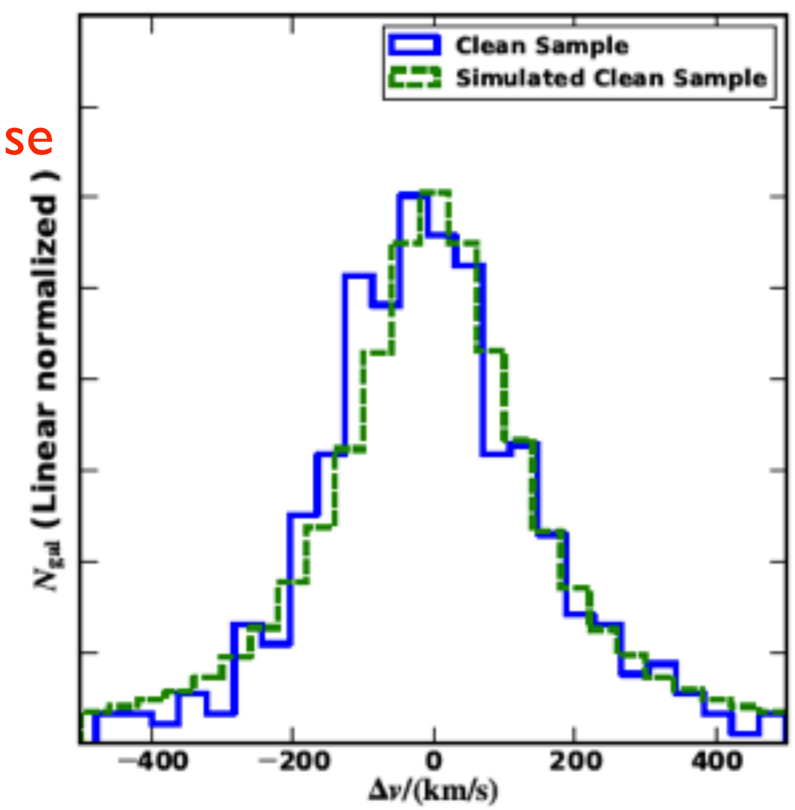

FIG. 6.— Distribution of $\Delta v \equiv c(z_{\rm pri} - z_{\rm sec})$ for the clean sample (solid blue histogram), the clean-like sample from MS-II (dashed green). The KS test yields $p_{\rm KS} = 33\%$. The pairwise velocity dispersion in the observed sample is $\sigma = 161\ \mathrm{km\,s^{-1}}$.

Halo Abundance Matching

To investigate the statistics of galaxies and their relation to host DM halos as predicted by the LCDM model, we predicted the properties of our model galaxies using the following Halo Abundance Matching (HAM) procedure:

1. Using the merger tree of each DM halo and subhalo, obtain V_{acc} = the peak value of the circular velocity over the history of the halo (this is typically the maximum circular velocity of the halo when the halo is first accreted). Perform abundance matching of the velocity function of the halos to the LF of galaxies to obtain the luminosity of each model galaxy.

2. Perform abundance matching of the velocity function to the stellar mass function of galaxies to obtain the stellar mass of each model galaxy.

3. Use the observed gas-to-stellar mass ratio as a function of stellar mass to assign cold gas masses to our model galaxies. The stellar mass added to the cold gas mass becomes the total baryonic mass.

4. Using the density profiles of the DM halos, obtain the circular velocity at 10 kpc (V_{10}) from the center of each halo. Multiply the DM mass, as it comes from simulations, by the factor $(1 - f_{bar})$, where f_{bar} is the cosmological fraction of baryons. This is the dark-matter-only contribution. Add the contribution to V_{10} of the baryon mass from step 3 assuming it is enclosed within a radius of 10 kpc.

5. Optionally implement the BFFP86 correction to V_{10} due to the adiabatic contraction of the DM halos from the infall of the baryon component to the center.

STELLAR MASS – HALO MASS RELATION

M_{star}/M_h | M_{star}/M_{bar}

3% | 20%

1% | 7%

0.3% | 2%

0.1% | 0.7%

| 0.2%

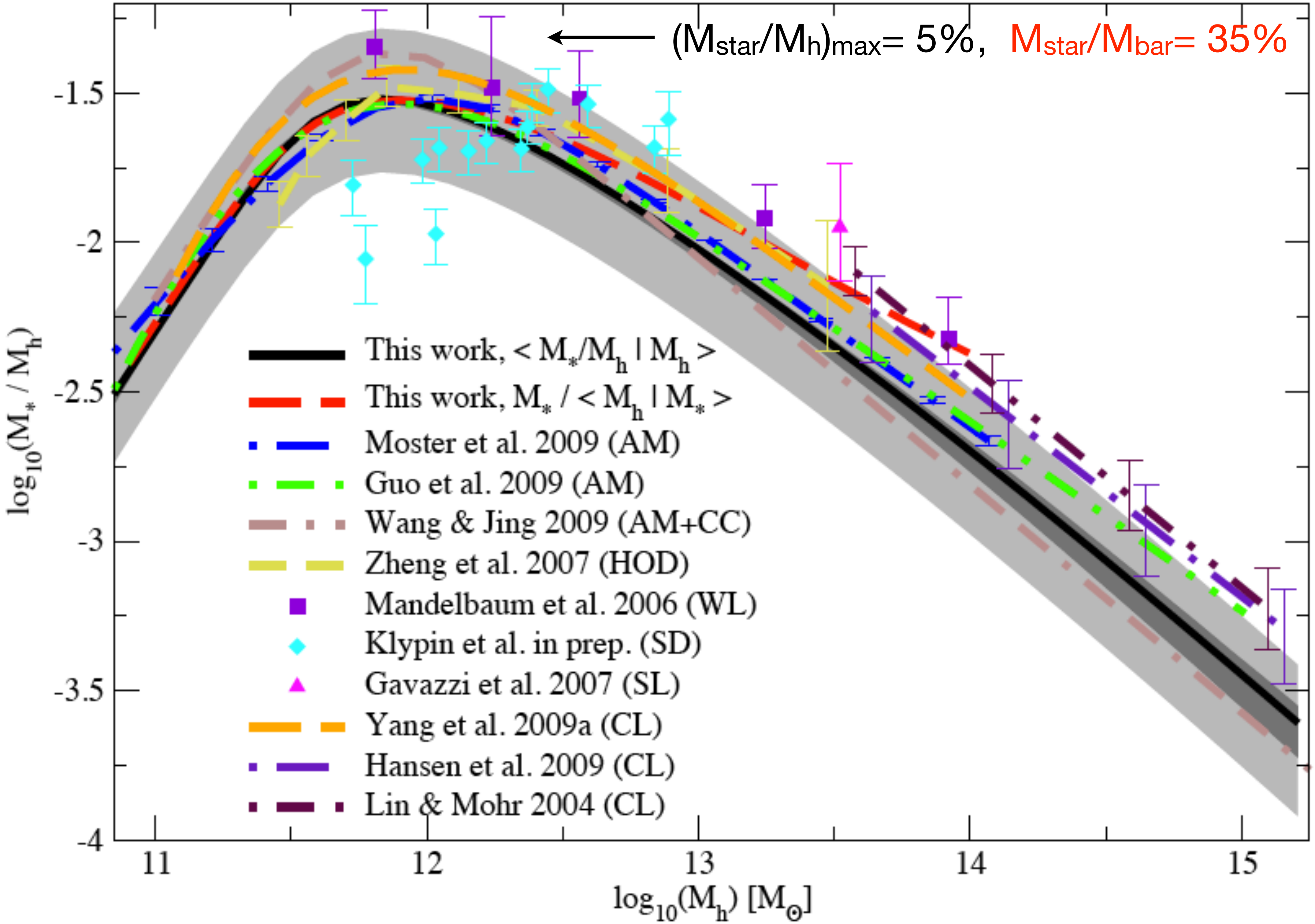

Comparison of best-fit model of Behroozi, Conroy, Wechsler (2010) at *z* = 0.1 to previously published results.

Bolshoi Sub-Halo Abundance Matching

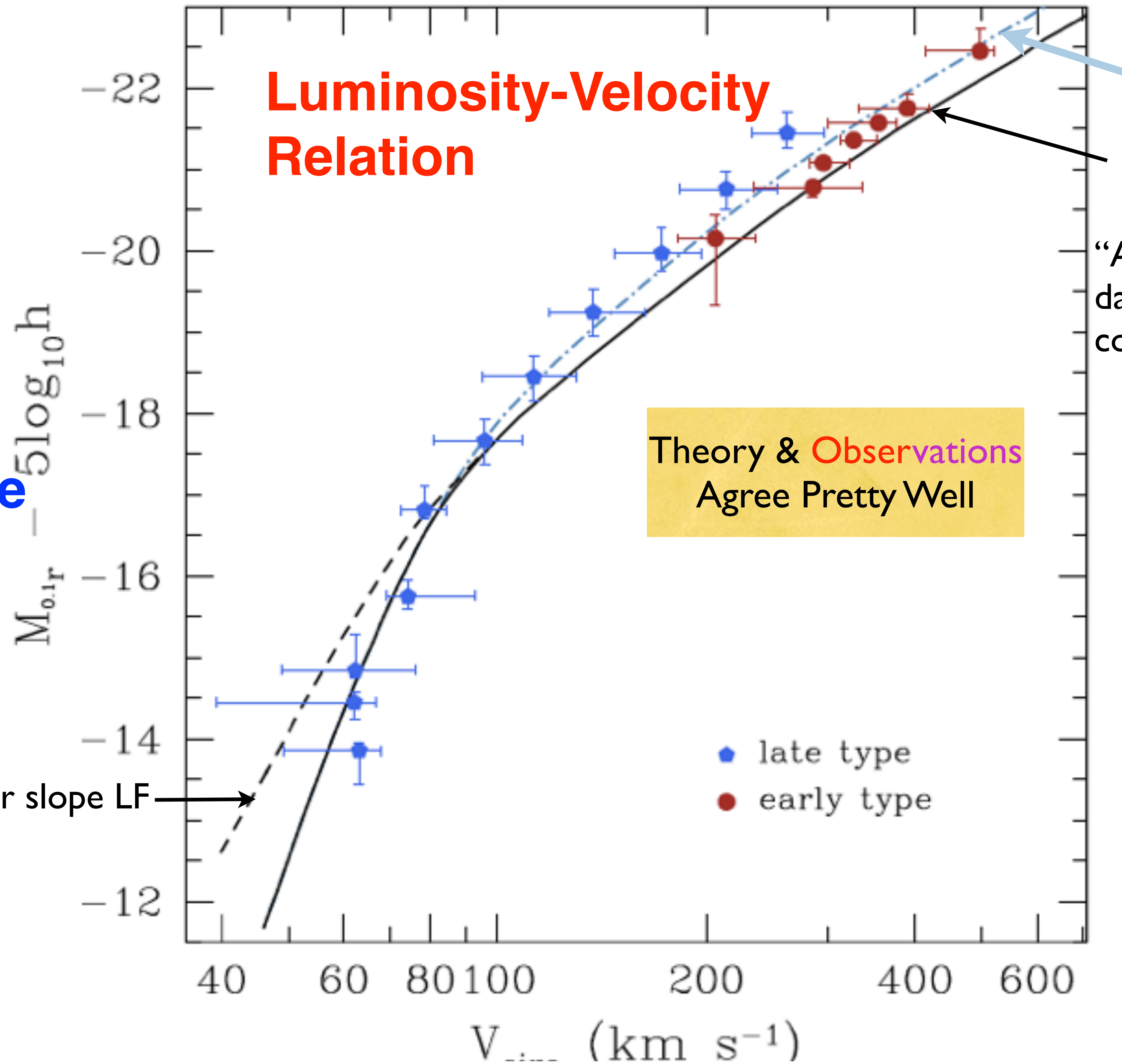

"AC" = Adiabatic Contraction of dark matter halos when baryons cool & condense to halo centers, following Blumenthal, Faber, Flores, & Primack 1986

Trujillo-Gomez, Klypin, Primack, & Romanowsky arXiv: 1005.1289 ApJ in press

Fig. 4.— Comparison of the observed Luminosity Velocity relation with the predictions of the ΛCDM model. The solid curve shows the median values of $^{0.1}r$-band luminosity vs. circular velocity for the model galaxy sample. The circular velocity for each model galaxy is based on the peak circular velocity of its host halo over its entire history, measured at a distance of 10 kpc from the center including the cold baryonic mass and the standard correction due to adiabatic halo contraction. The dashed curve show results for a steeper ($\alpha = -1.34$) slope of the LF. The dot-dashed curve shows predictions after adding the baryon mass but without adiabatic contraction. Points show representative observational samples.

Baryonic Mass - Velocity Relation

Bolshoi Sub-Halo Abundance Matching

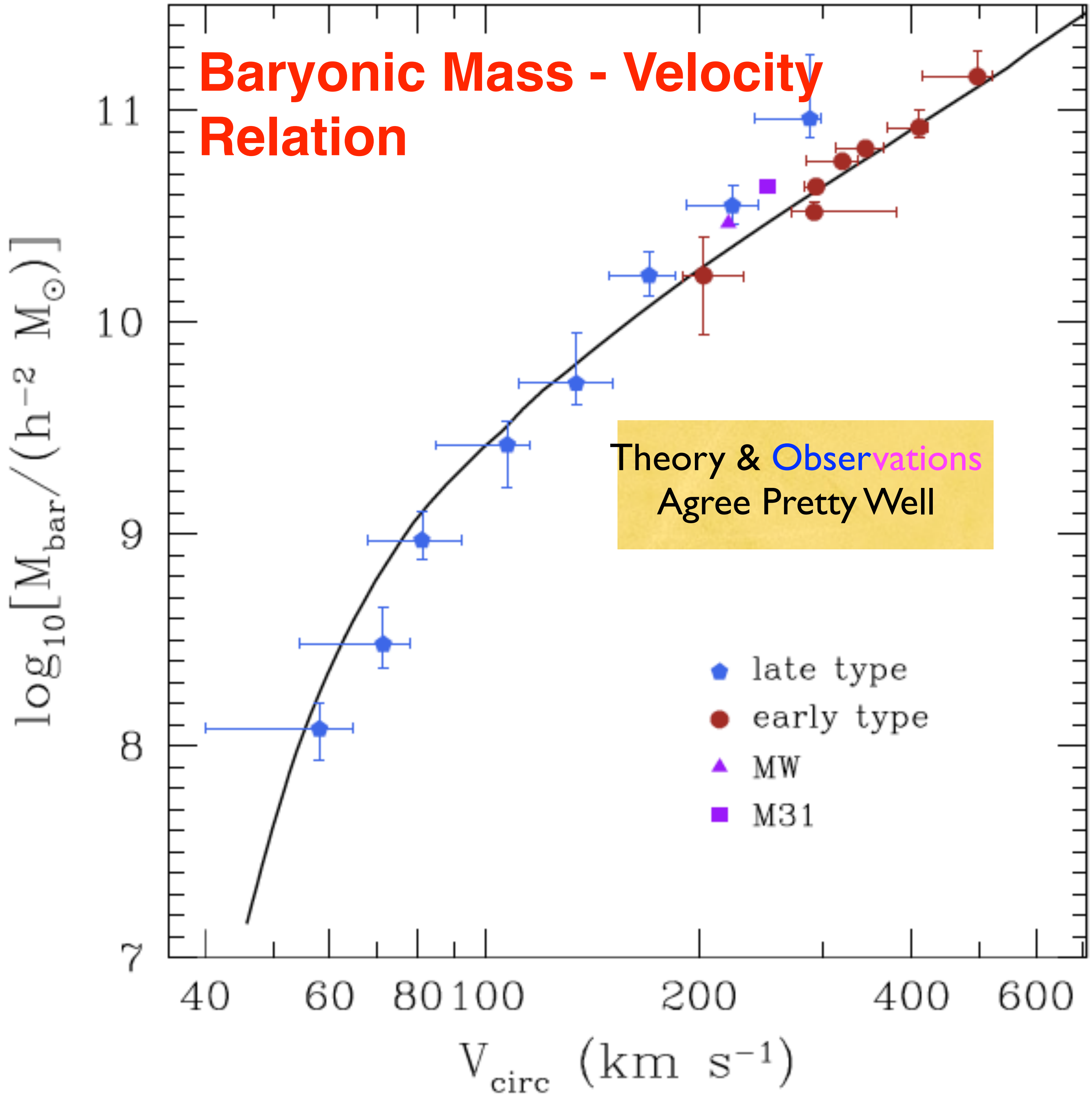

Trujillo-Gomez, Klypin, Primack, & Romanowsky arXiv: 1005.1289 ApJ in press

Fig. 10.— Mass in cold baryons as a function of circular velocity. The solid curve shows the median values for the ΛCDM model using halo abundance matching. The cold baryonic mass includes stars and cold gas and the circular velocity is measured at 10 kpc from the center while including the effect of adiabatic contraction. For comparison we show the individual galaxies of several galaxy samples. Intermediate mass galaxies such as the Milky Way and M31 lie very close to our model results.

Bolshoi Sub-Halo Abundance Matching

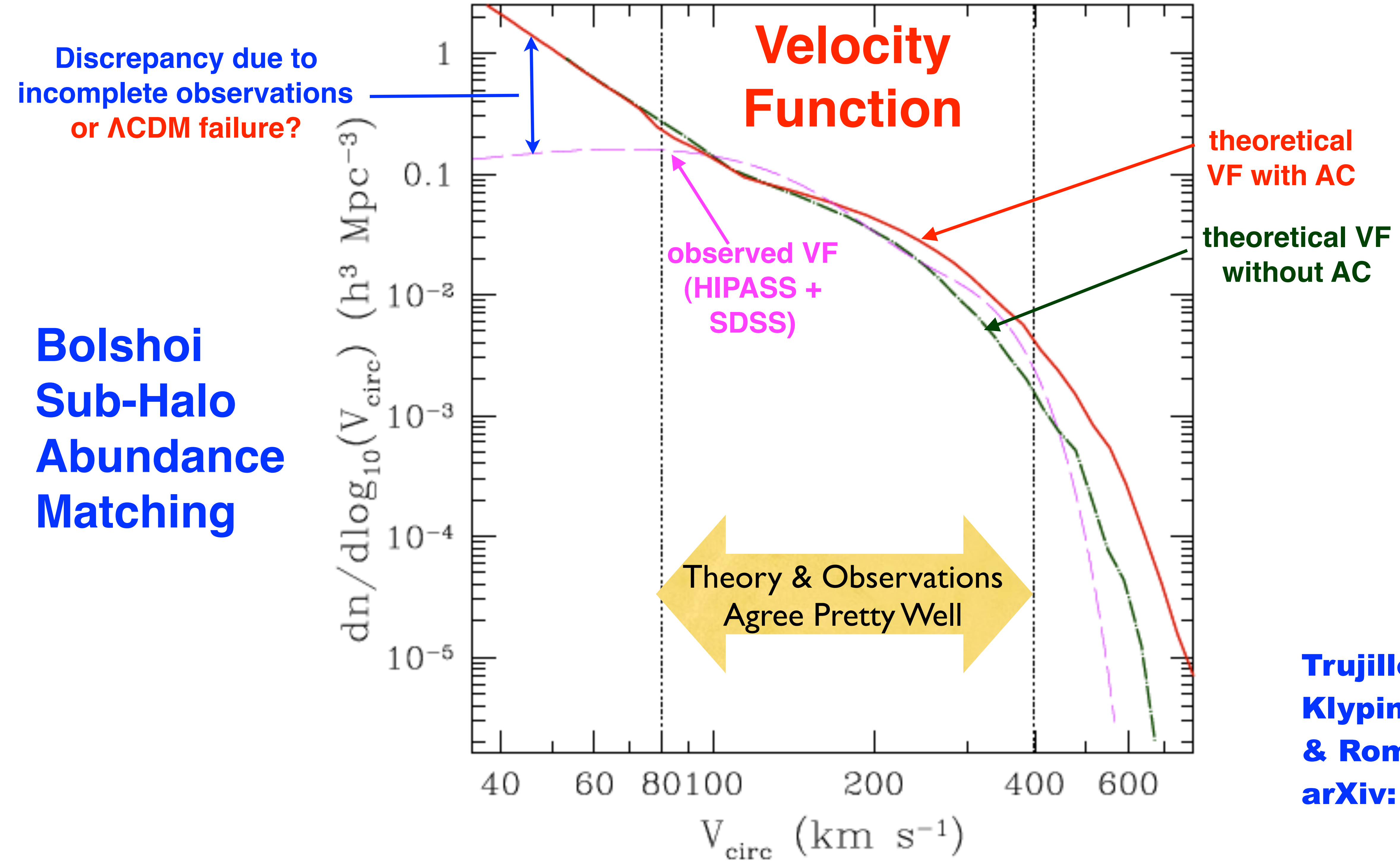

Trujillo-Gomez, Klypin, Primack, & Romanowsky arXiv: 1005.1289

Fig. 11.— Comparison of theoretical (dot-dashed and thick solid curves) and observational (dashed curve) circular velocity functions. The dot-dashed line shows the effect of adding the baryons (stellar and cold gas components) to the central region of each DM halo and measuring the circular velocity at 10 kpc. The thick solid line is the distribution obtained when the adiabatic contraction of the DM halos is considered. Because of uncertainties in the AC models, realistic theoretical predictions should lie between the dot-dashed and solid curves. Both the theory and observations are highly uncertain for rare galaxies with $V_{circ} > 400$ km s^{-1}. Two vertical dotted lines divide the VF into three domains: $V_{circ} > 400$ km s^{-1} with large observational and theoretical uncertainties; < 80 km $s^{-1} < V_{circ} < 400$ km s^{-1} with a reasonable agreement, and $V_{circ} < 80$ km s^{-1}, where the theory significantly overpredicts the number of dwarfs.

Bolshoi simulations - recent progress

- Anatoly Klypin has improved his BDM halofinder. It now finds the spin parameter, concentration, and shape and orientation of all halos. It also produces catalogs for both "virial" and overdensity-200 halo definitions. Results on all 180 stored timesteps of the Bolshoi simulation will be finished in a week or so. Peter Behroozi has written a new phase-space halofinder that finds subhalos better in the central regions of larger halos.
- All catalogs are finished for BigBolshoi-1(MultiDark), which has the same cosmology as Bolshoi in a volume 64x larger. It has 7 kpc/h resolution, and is complete to Vcirc > 170 km/s (so all MWy-size halos are found). BigBolshoi simulations can now be run and analyzed in one week; two more are planned to get statistics for BOSS. Merger trees are coming soon.
- A new miniBolshoi simulation is runing now. It will have a force resolution of about 100 pc and a mass resolution of about 10^6 M_{sun} and it will be complete to 15 km/s or better. We will have complete merger histories and substructure for hundreds of MWy-size halos.
- All catalogs will be available at Astrophysicalishes Institut Potsdam: http://www.multidark.org/MultiDark/ (You have to get an account there.) We hope to have them up soon also on the VAO and perhaps elsewhere.

Dependence of Halo Concentration on Mass and Redshift

Profiles of dark haloes: evolution, scatter, and environment

J. S. Bullock[1,2], T. S. Kolatt[1,3], Y. Sigad[3], R.S. Somerville[3,4], A. V. Kravtsov[2,5★], A. A. Klypin[5], J. R. Primack[1], and A. Dekel[3] 2001 MNRAS 321, 559

ABSTRACT

We study dark-matter halo density profiles in a high-resolution N-body simulation of a ΛCDM cosmology. Our statistical sample contains ∼5000 haloes in the range $10^{11} - 10^{14} h^{-1} M_\odot$ and the resolution allows a study of subhaloes inside host haloes. The profiles are parameterized by an NFW form with two parameters, an inner radius r_s and a virial radius R_{vir}, and we define the halo concentration $c_{vir} \equiv R_{vir}/r_s$. We find that, for a given halo mass, the redshift dependence of the median concentration is $c_{vir} \propto (1+z)^{-1}$. This corresponds to $r_s(z) \sim$ constant, and is contrary to earlier suspicions that c_{vir} does not vary much with redshift. The implications are that high-redshift galaxies are predicted to be more extended and dimmer than expected before. Second, we find that the scatter in halo profiles is large, with a 1σ $\Delta(\log c_{vir}) = 0.18$ at a given mass, corresponding to a scatter in maximum rotation velocities of $\Delta V_{max}/V_{max} = 0.12$. We discuss implications for modelling the Tully-Fisher relation, which has a smaller reported intrinsic scatter. Third, subhaloes and haloes in dense environments tend to be more concentrated than isolated haloes, and show a larger scatter. These results suggest that c_{vir} is an essential parameter for the theory of galaxy modelling, and we briefly discuss implications for the universality of the Tully-Fisher relation, the formation of low surface brightness galaxies, and the origin of the Hubble sequence. We present an improved analytic treatment of halo formation that fits the measured relations between halo parameters and their redshift dependence, and can thus serve semi-analytic studies of galaxy formation.

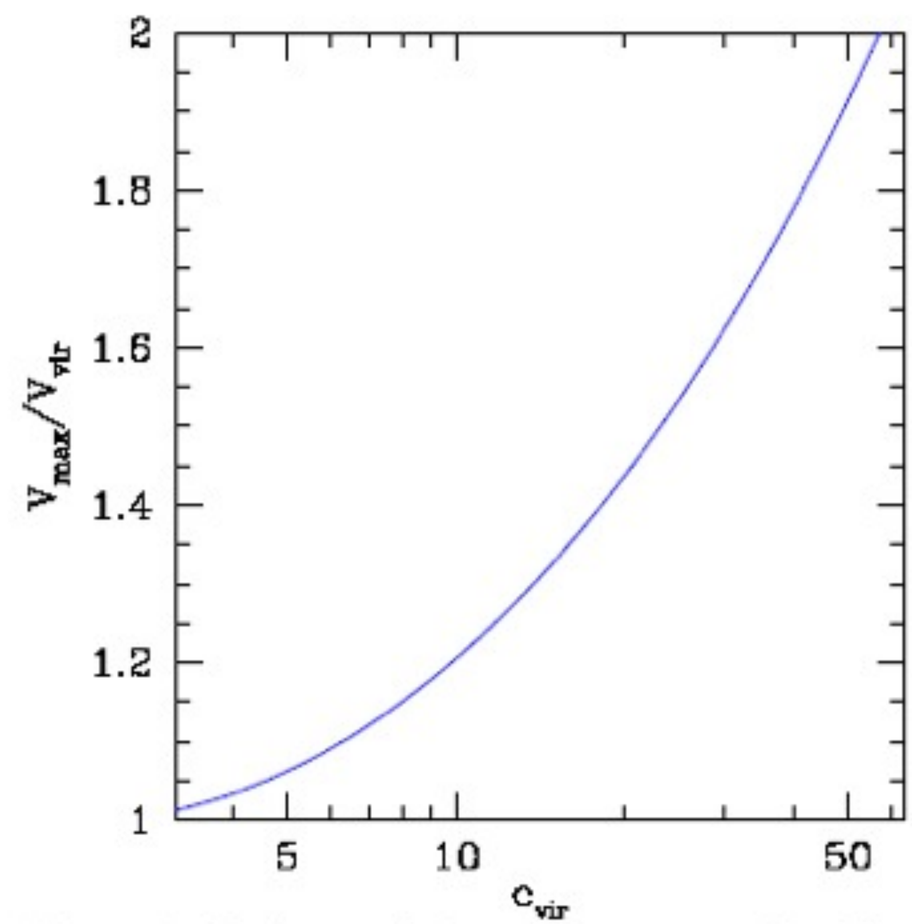

Figure 1. Maximum velocity versus concentration. The maximum rotation velocity for an NFW halo in units of the rotation velocity at its virial radius as a function of halo concentration.

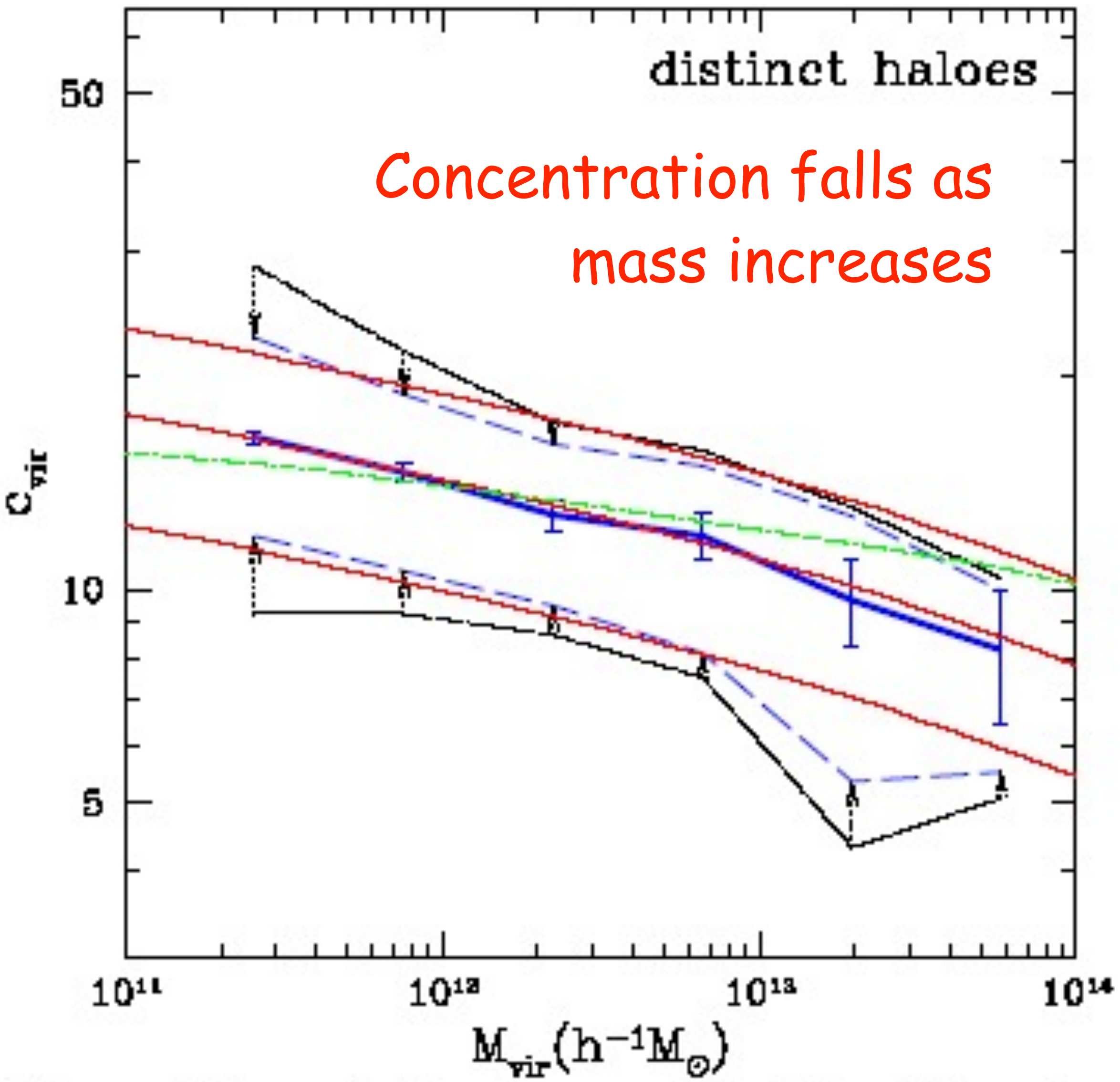

Figure 4. Concentration versus mass for distinct haloes at $z = 0$. The thick solid curve is the median at a given M_{vir}. The error bars represent Poisson errors of the mean due to the sampling of a finite number of haloes per mass bin. The outer dot-dashed curves encompass 68% of the c_{vir} values as measured in the simulations. The inner dashed curves represent only the true, intrinsic scatter in c_{vir}, after eliminating both the Poisson scatter and the scatter due to errors in the individual profile fits due, for example, to the finite number of particles per halo. The central and outer thin solid curves are the predictions for the median and 68% values by the toy model outlined in the text, for $F = 0.01$ and three different values of K. The thin dot-dashed line shows the prediction of the toy model of NFW97 for $f = 0.01$ and $k = 3.4 \times 10^3$.

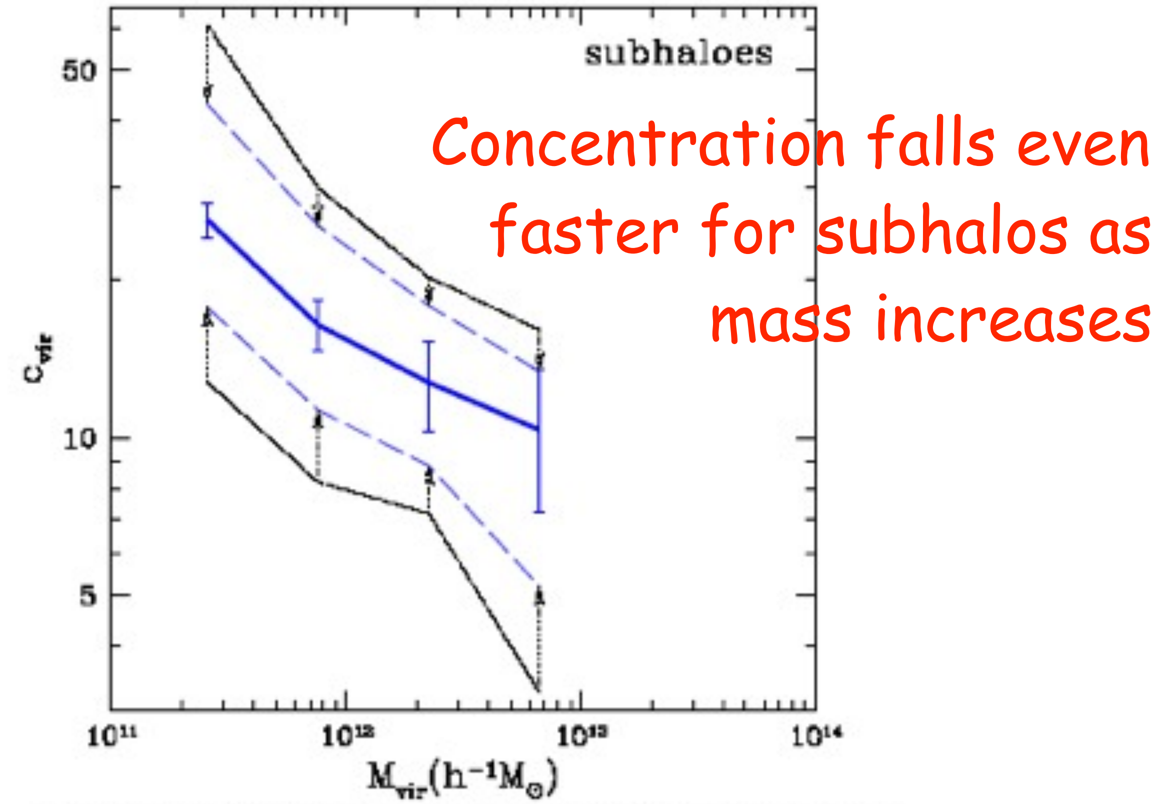

Figure 5. Concentration versus mass for subhaloes at $z = 0$. The curves and errors are the same as in Figure 4.

Bullock et al. 2001

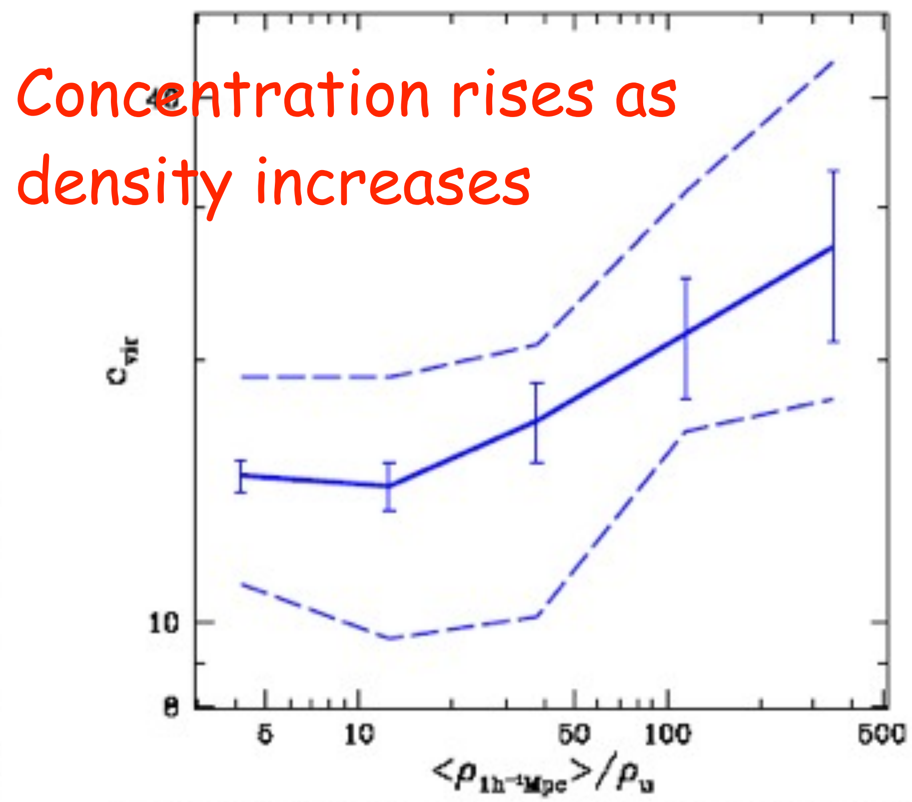

Figure 6. Concentrations versus environment. The concentration at $z = 0$ of all haloes in the mass range $0.5 - 1.0 \times 10^{12} h^{-1} M_{\odot}$ as a function of local density in units of the average density of the universe. The local density was determined within spheres of radius $1h^{-1}$Mpc. The solid line represents the median c_{vir} value, the error bars are Poisson based on the number of haloes, and the dashed line indicates our best estimate of the intrinsic scatter.

Spread of Halo Concentrations

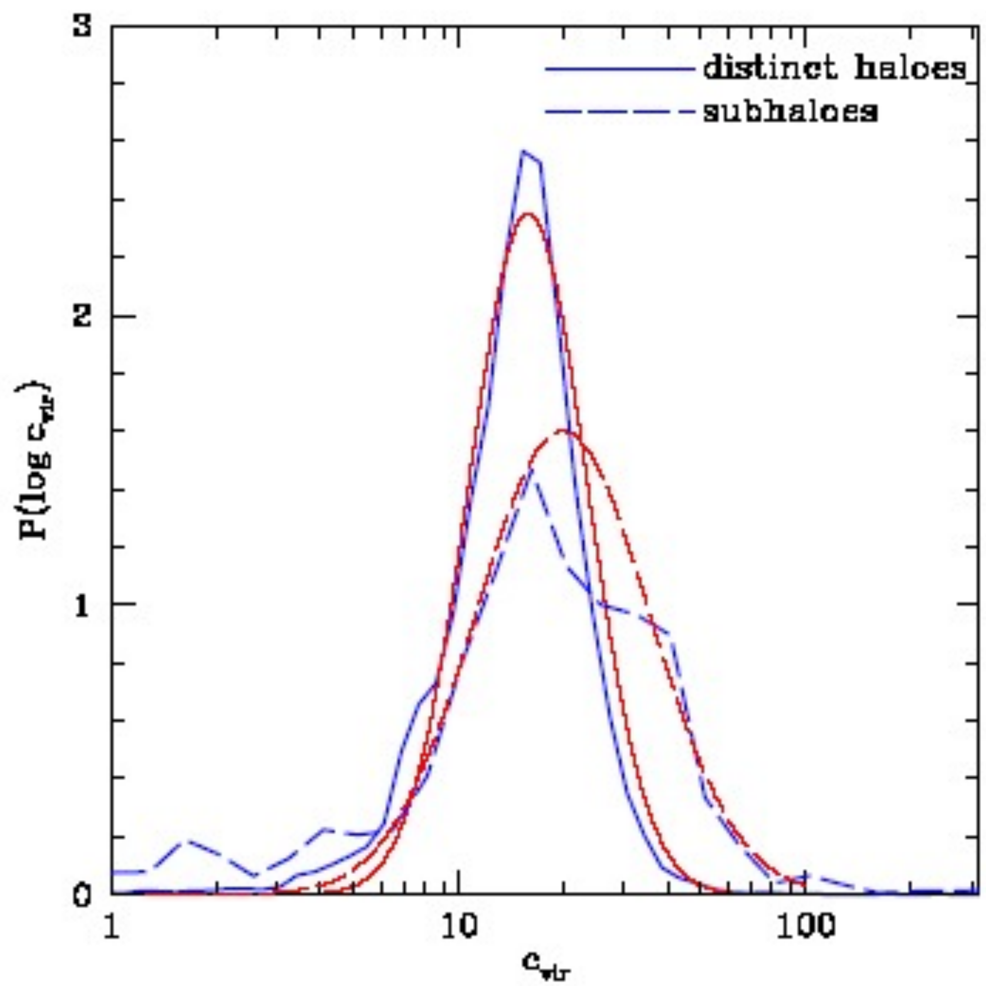

Figure 7. The probability distributions of distinct haloes (solid line) and subhaloes (dashed line) at $z = 0$ within the mass range $(0.5 - 1.0) \times 10^{12} h^{-1} M_{\odot}$. The simulated distributions (thick lines) include, the $\sim 2,000$ distinct haloes and ~ 200 subhaloes within this mass range. Log-normal distributions with the same median and standard deviation as the measured distributions are shown (thin lines). Subhaloes are, on average, more concentrated than distinct haloes and they show a larger spread.

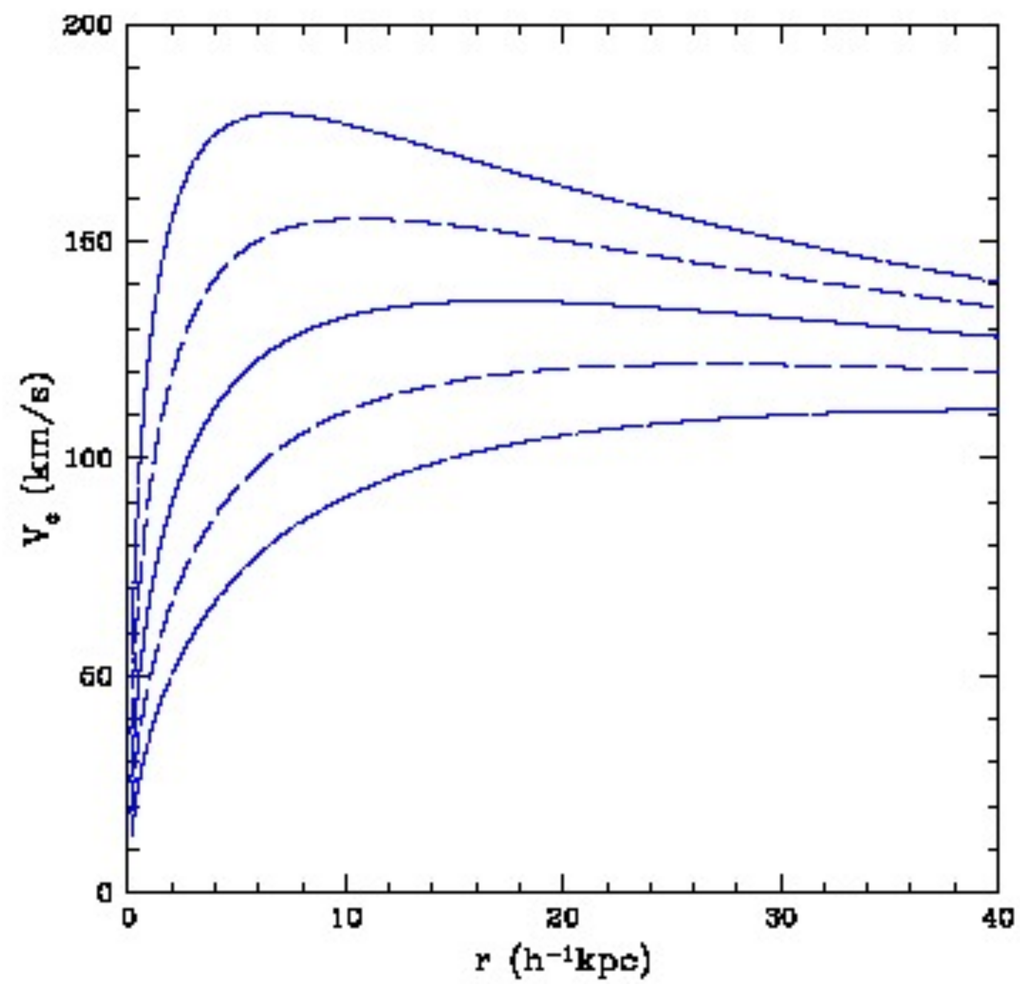

Figure 8. The spread in NFW rotation curves corresponding to the spread in concentration parameters for distinct haloes of $3 \times 10^{11} h^{-1} M_{\odot}$ at $z = 0$. Shown are the median (solid), $\pm 1\sigma$ (long dashed), and $\pm 2\sigma$ (dot-dashed) curves. The corresponding median rotation curve for subhaloes is comparable to the upper 1σ curve of distinct haloes.

Bullock et al. 2001

Evolution of Halo Concentration with Redshift

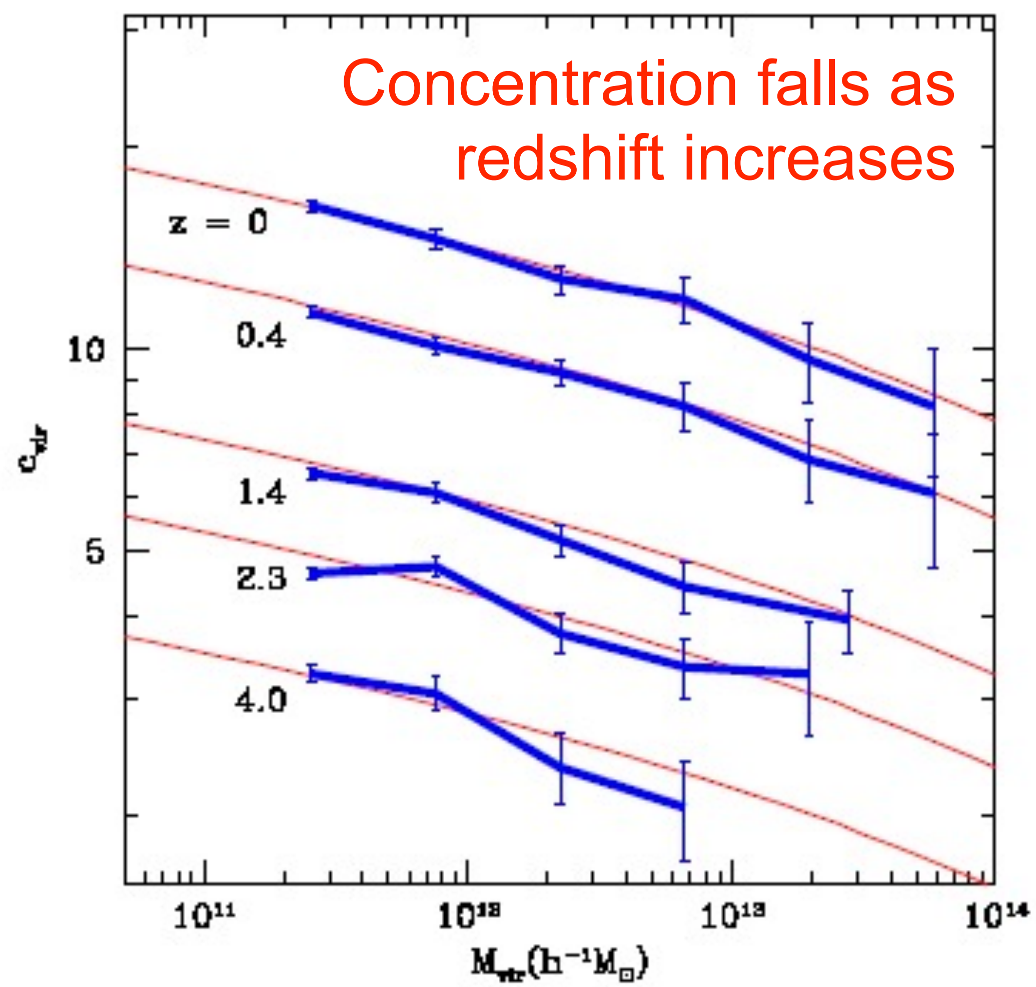

Figure 10. Median $c_{\rm vir}$ values as a function of $M_{\rm vir}$ for distinct haloes at various redshifts. The error bars are the Poisson errors due to the finite number of haloes in each mass bin. The thin solid lines show our toy model predictions.

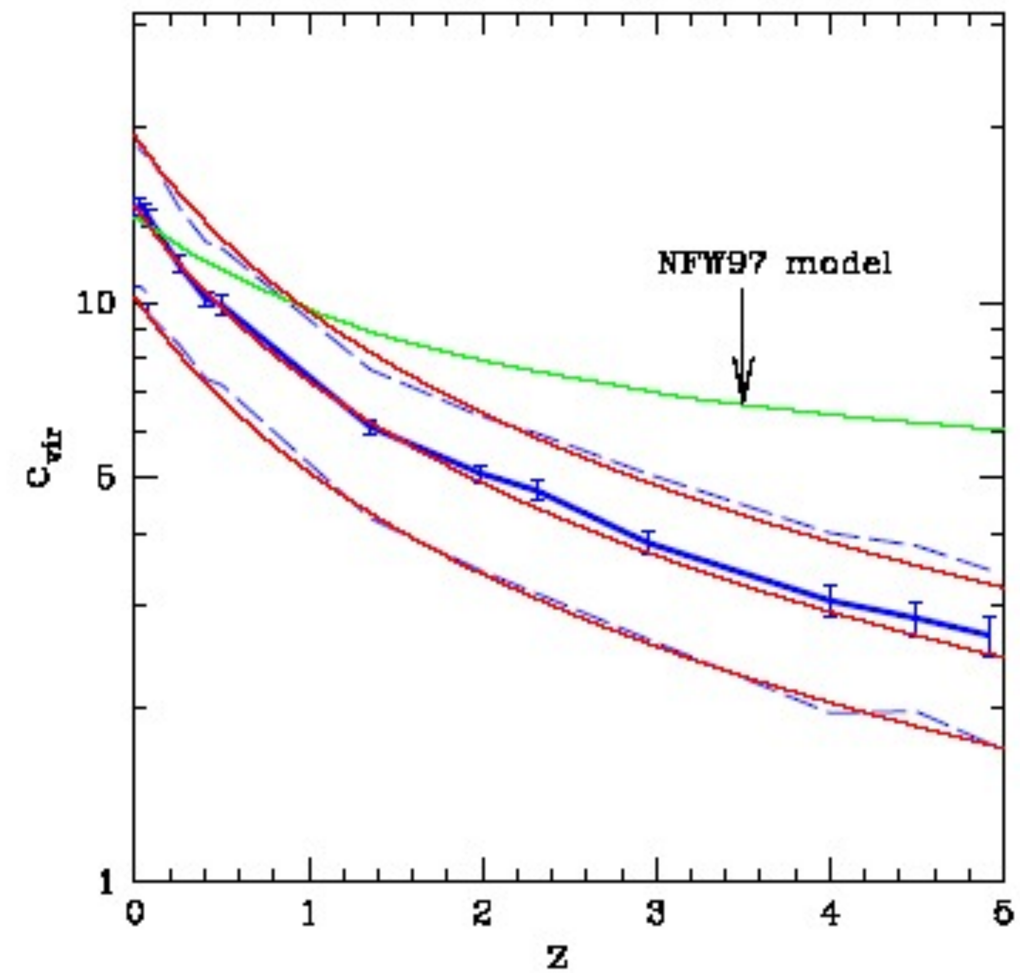

Figure 11. Concentration as a function of redshift for distinct haloes of a fixed mass, $M_{\rm vir} = 0.5 - 1.0 \times 10^{12} h^{-1} M_\odot$. The median (heavy solid line) and intrinsic 68% spread (dashed line) are shown. The behavior predicted by the NFW97 toy model is marked. Our revised toy model for the median and spread for $8 \times 10^{11} h^{-1} M_\odot$ haloes (thin solid lines) reproduces the observed behavior rather well.

$C_{vir} \propto 1/(1+z)$
at fixed mass

Bullock et al. 2001

Halo concentrations in the standard ΛCDM cosmology

Francisco Prada, Anatoly A. Klypin, Antonio J. Cuesta, Juan E. Betancort-Rijo, and Joel Primack

We study the concentration of dark matter halos and its evolution in N-body sim- ulations of the standard ΛCDM cosmology. The results presented in this paper are based on 4 large N-body simulations with ~ 10 billion particles each: the Millennium-I and II, Bolshoi, and MultiDark simulations. The MultiDark (or BigBolshoi) simula- tion is introduced in this paper. This suite of simulations with high mass resolution over a large volume allows us to compute with unprecedented accuracy the concen- tration over a large range of scales (about six orders of magnitude in mass), which constitutes the state-of-the-art of our current knowledge on this basic property of dark matter halos in the ΛCDM cosmology. We find that there is consistency among the different simulation data sets, despite the different codes, numerical algorithms, and halo/subhalo finders used in our analysis. We confirm a novel feature for halo concentrations at high redshifts: a flattening and upturn with increasing mass.

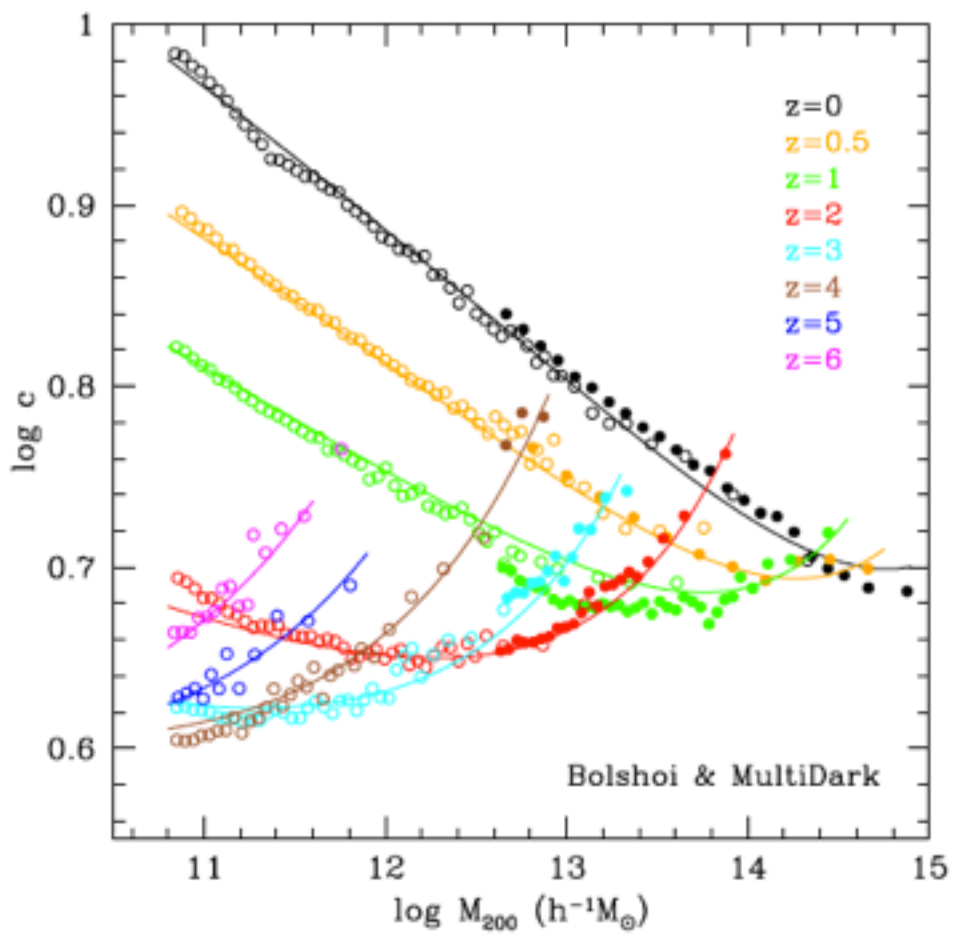

Halo mass–concentration relation of distinct halos atdifferent redshifts in the Bolshoi (open symbols) and MultiDark (filled symbols) simulations is compared with analytical approximation (curves). The errors of the approximation are less than a few percent.

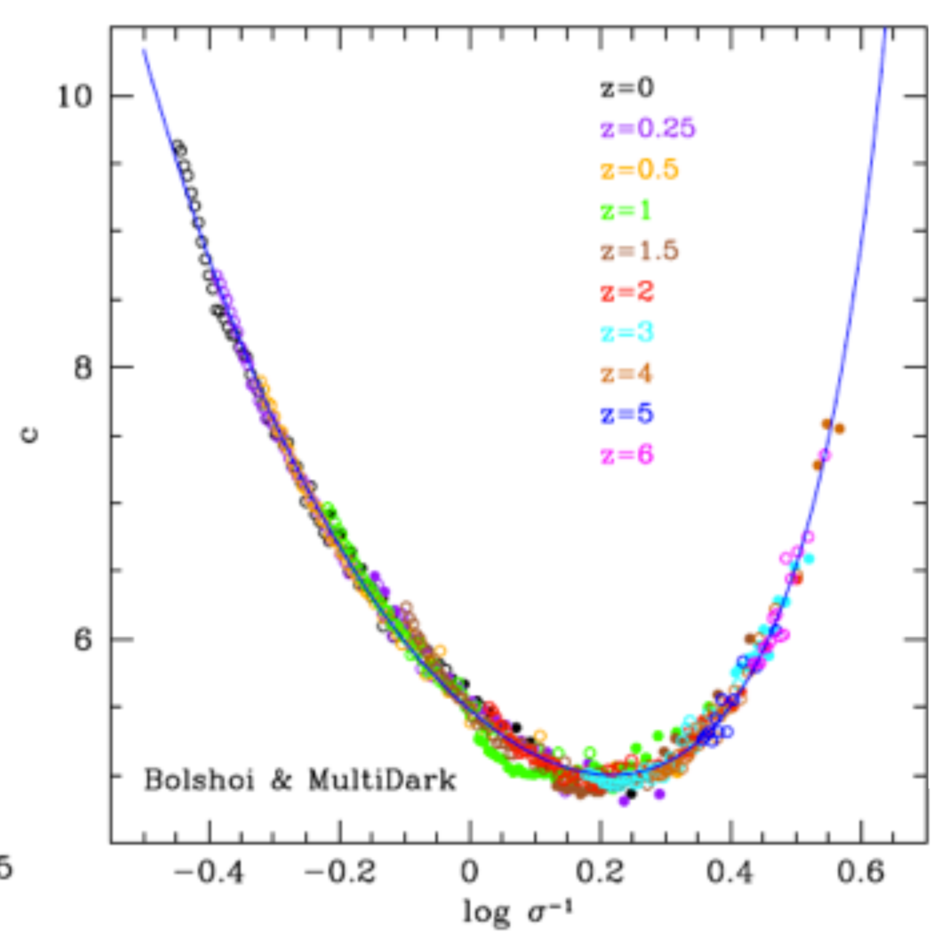

Dependence of halo concentration c on log σ^{-1} after rescaling all the results of Bolshoi and MultiDark simulations to z = 0. The plot shows a tight intrinsic correlation of c on σ′.

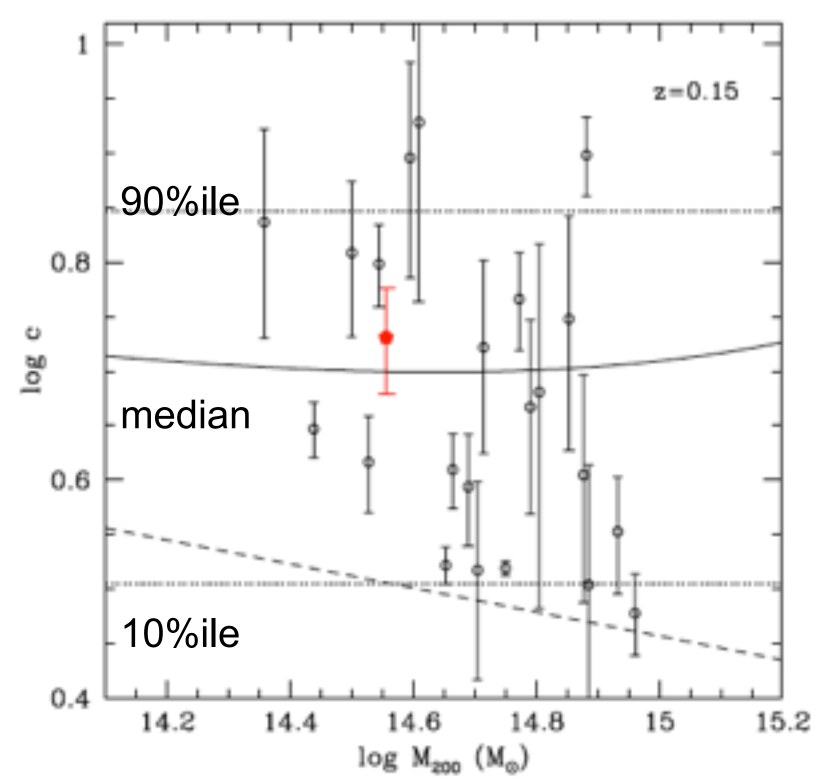

Comparison of observed cluster concentrations (data points with error bars) with median halo concentration of cluster-size halos (full curve). Open circles show results for X-ray luminous galaxy clusters in the redshift range 0.1-0.3 (Ettori et al. 2010). The pentagon presents galaxy kinematic estimate for relaxed clusters by Wojtak & Lokas (2010). The dashed curve shows prediction by Maccio, Dutton, & van den Bosch (2008), which significantly under- estimates the concentrations of clusters.

Merger Trees

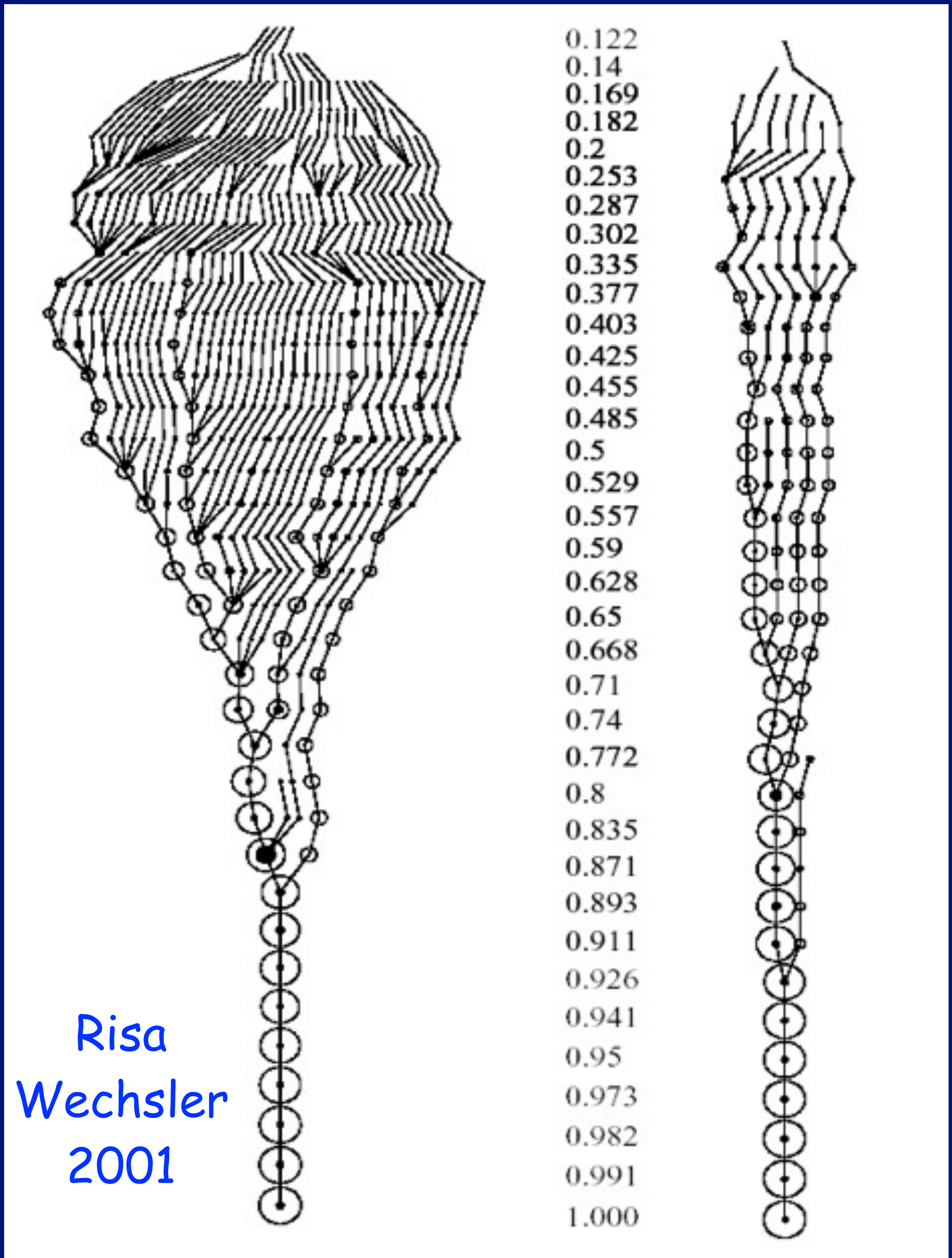

Based on our ART simulations, Wechsler created the first structural merger trees tracing the merging history of thousands of halos with structural information on their higher-redshift progenitors, including their radial profiles and spins. This led to the discovery that a halo's merging history can be characterized by a single parameter a_c which describes the scale factor at which the halo's mass accretion slows, and that this parameter correlates very well with the halo concentration, thus showing that the distribution of dark matter halo concentrations reflects mostly the distribution of their mass accretion rates. We found that the radius of the inner part of the halo, where the density profile is roughly 1/r, is established during the early, rapid-accretion phase of halo growth (a result subsequently confirmed and extended by other groups, e.g., Zhao et al. 2003, Reed et al. 2004).

CONCENTRATIONS OF DARK HALOS FROM THEIR ASSEMBLY HISTORIES

RISA H. WECHSLER[1], JAMES S. BULLOCK[2], JOEL R. PRIMACK[1], ANDREY V. KRAVTSOV[2,3], AVISHAI DEKEL[4], ApJ 568 (2002) 52-70

$$\rho_{\rm NFW}(r) = \frac{\rho_{\rm s}}{(r/R_{\rm s})\,(1+r/R_{\rm s})^2}, \qquad (1)$$

where $R_{\rm s}$ is a characteristic "inner" radius, and $\rho_{\rm s}$ a corresponding inner density. One of the inner parameters can be replaced by a "virial" parameter, either the virial radius ($R_{\rm vir}$), mass ($M_{\rm vir}$), or velocity ($V_{\rm vir}$), defined such that the mean density inside the virial radius is $\Delta_{\rm vir}$ times the mean universal density ρ_u at that redshift:

$$M_{\rm vir} \equiv \frac{4\pi}{3}\Delta_{\rm vir}\rho_u {R_{\rm vir}}^3. \qquad (2)$$

The critical overdensity at virialization, $\Delta_{\rm vir}$, is motivated by the spherical collapse model; it has a value $\simeq 180$ for the Einstein-deSitter cosmology, and $\simeq 340$ for the ΛCDM cosmology assumed here. A useful alternative parameter for describing the shape of the profile is the concentration parameter $c_{\rm vir}$, defined as $c_{\rm vir} \equiv R_{\rm vir}/R_{\rm s}$.

(Bryan & Norman 1998) $\Delta_{\rm vir} \simeq (18\pi^2 + 82x - 39x^2)/\Omega(z)$ where $x \equiv \Omega(z) - 1$

By examining a range of full mass assembly histories for our sample of halos, we have found a useful parameterized form that captures many essential aspects of halo growth over time. Remarkably, we find that both average mass accretion histories and mass accretion histories for individual halos, as observed at $z = 0$, can be characterized by a simple function:

$$M(a) = M_{\rm o} e^{-\alpha z}, \quad a = (1+z)^{-1}. \qquad (3)$$

The single free parameter in the model, α, can be related to a characteristic epoch for formation, a_c, defined as the expansion scale factor a when the logarithmic slope of the accretion rate, $d\log M/d\log a$, falls below some specified value, S. The functional form defined in Eq. 3 implies $a_c = \alpha/S$. In what follows we have chosen $S = 2$.

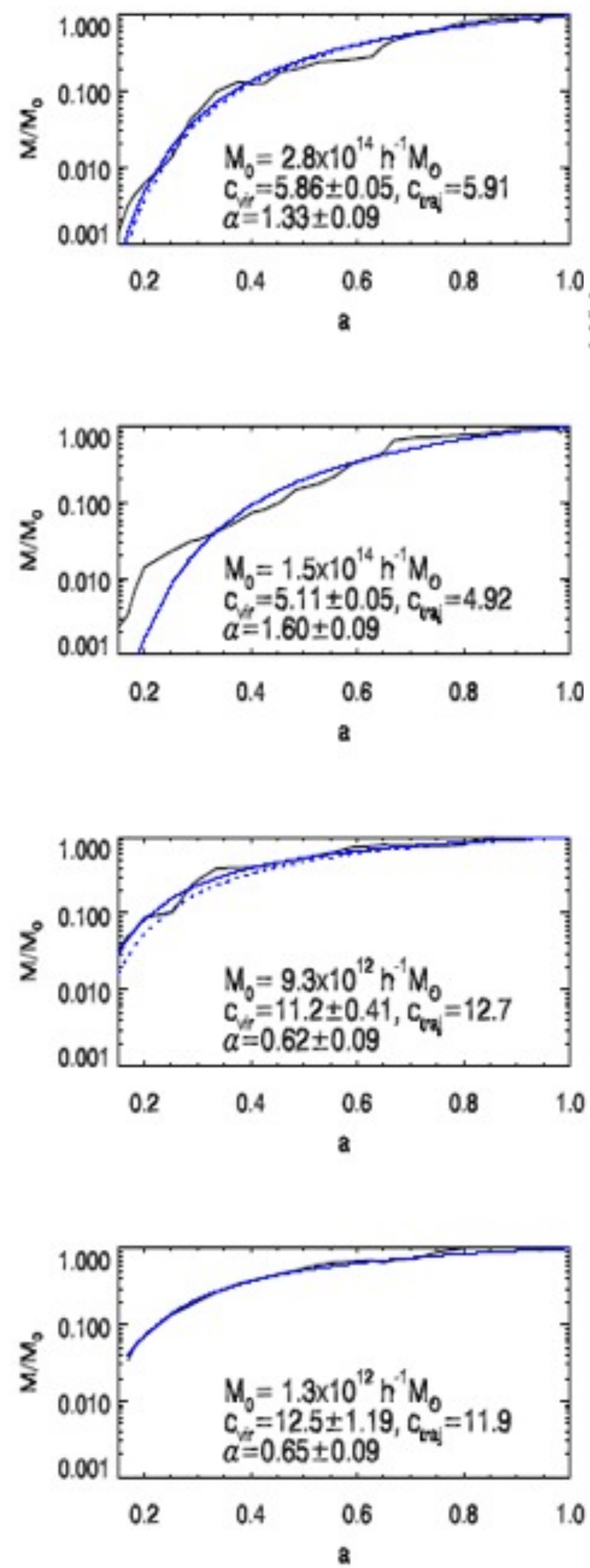

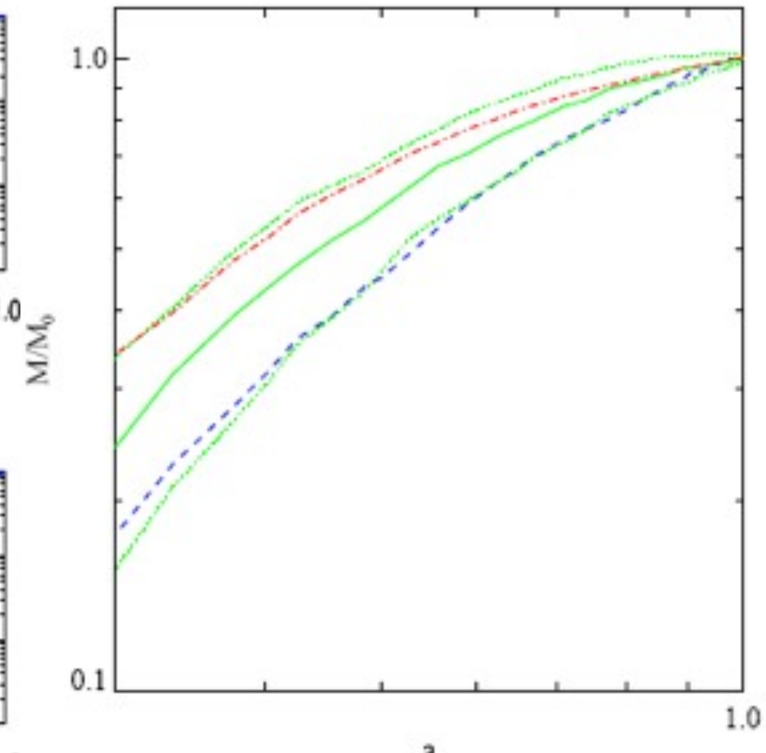

Average mass accretion histories, normalized at a = 1. The three green curves connect the averages of $M(a)/M_0$ at each output time. The pair of dotted lines shows the 68% spread about the middle case. Red dot-dashed lines correspond to early formers (typically low mass halos), blue dashed lines to late formers (typically higher mass halos). We see that massive halos tend to form later than lower mass halos, whose mass accretion rate peaks at an earlier time.

Structural merger trees for two halos. The radii of the outer and inner (filled) circles are proportional to the virial and inner NFW radii, Rvir and Rs, respectively, scaled such that the two halos have equal sizes at a = 1. Lines connect halos with their progenitor halos.

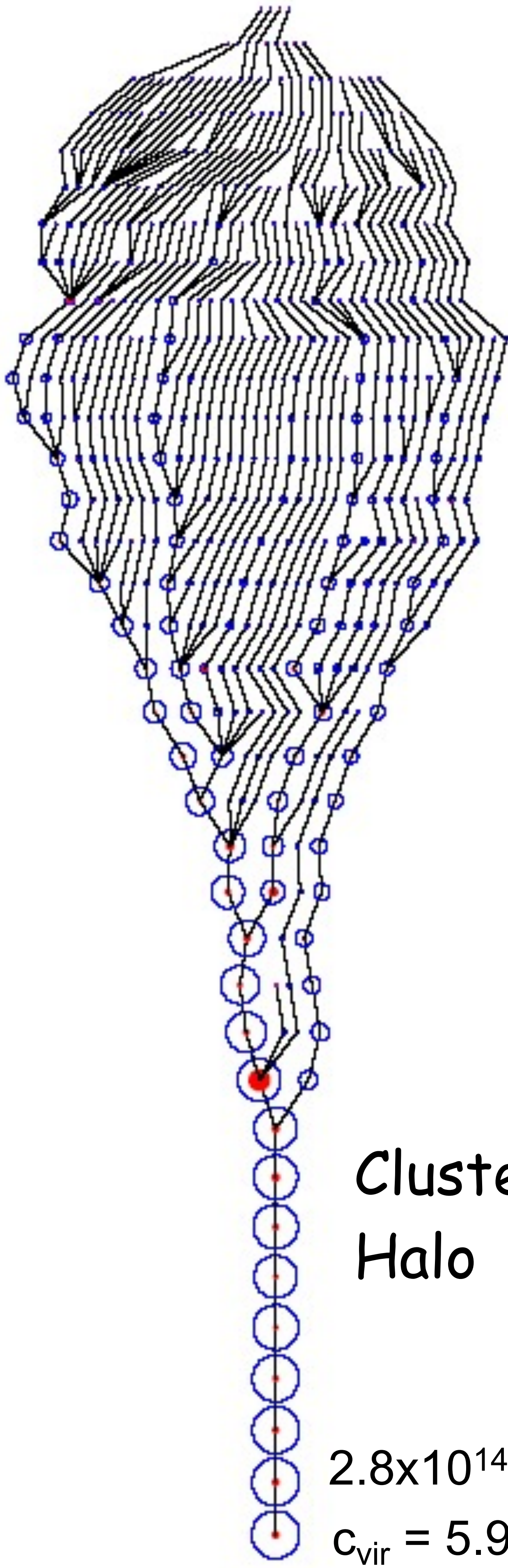

Cluster Halo

$2.8 \times 10^{14}\ M_{sun}/h$

$c_{vir} = 5.9$

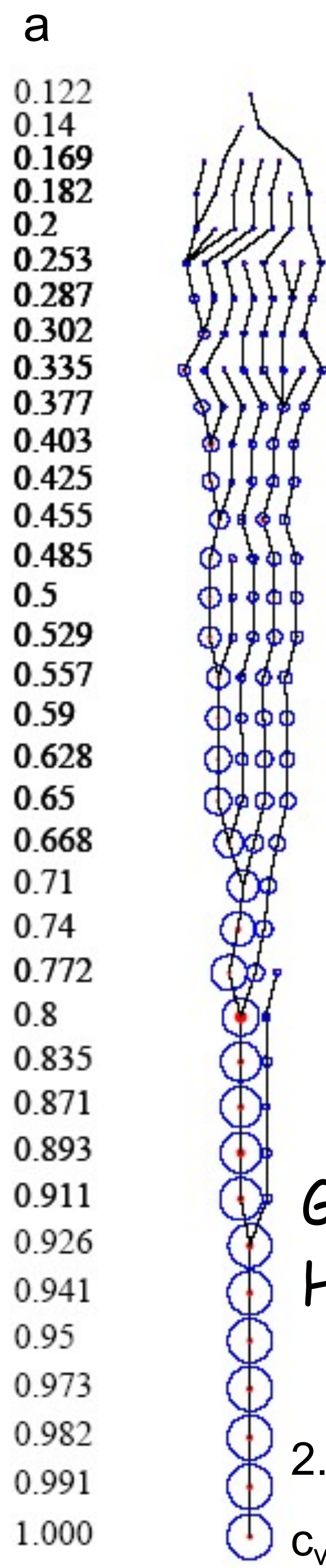

Galaxy Halo

$2.9 \times 10^{12}\ M_{sun}/h$

$c_{vir} = 12.5$

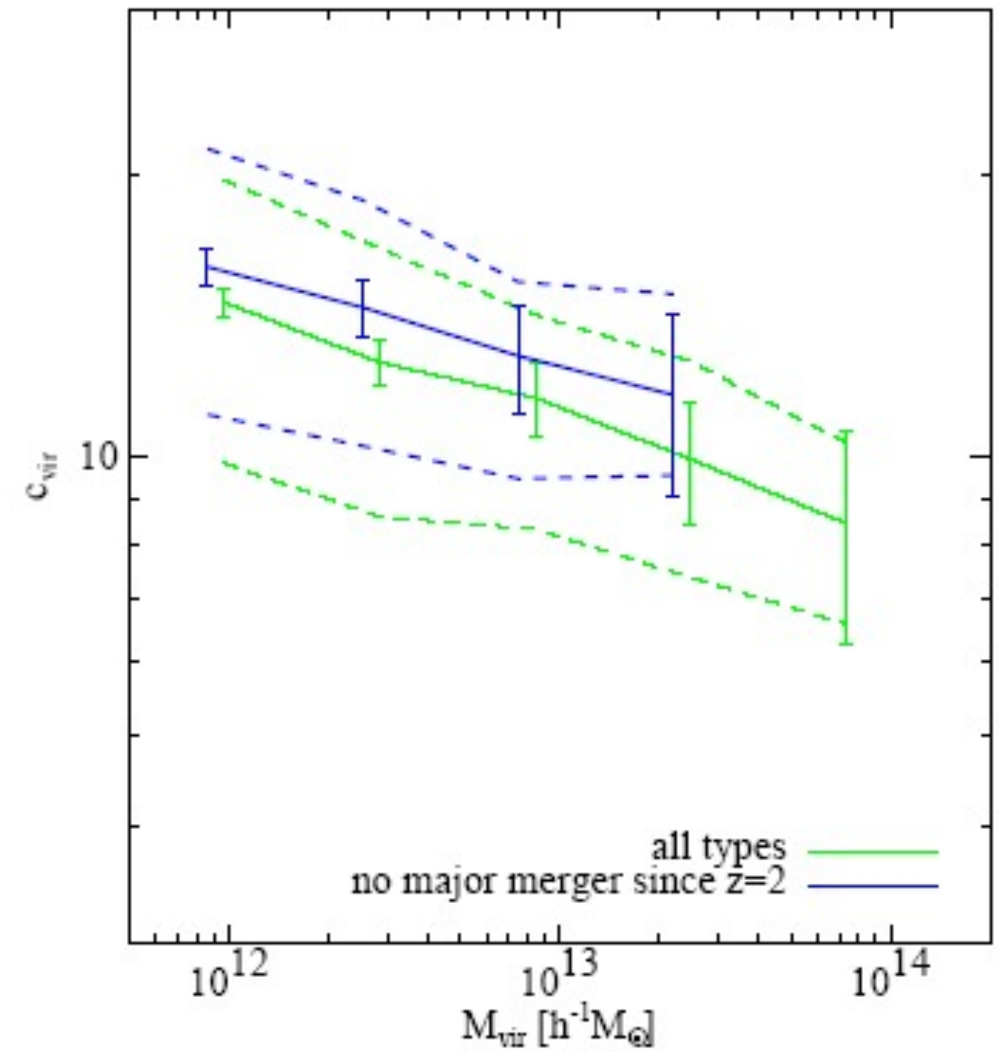

For halos without recent mergers, c_{vir} is higher and the scatter is reduced to log c_{vir} ≈ 0.10.

Wechsler et al. 2002

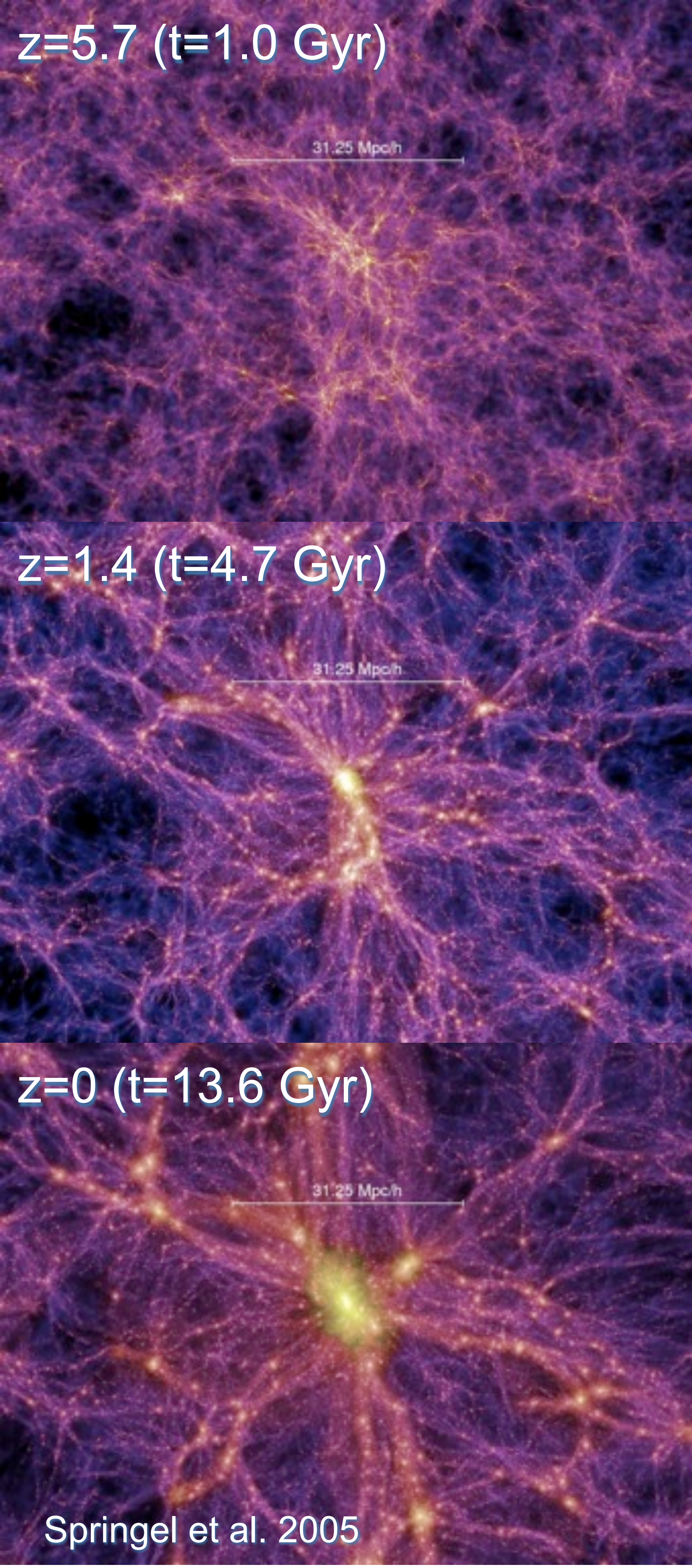

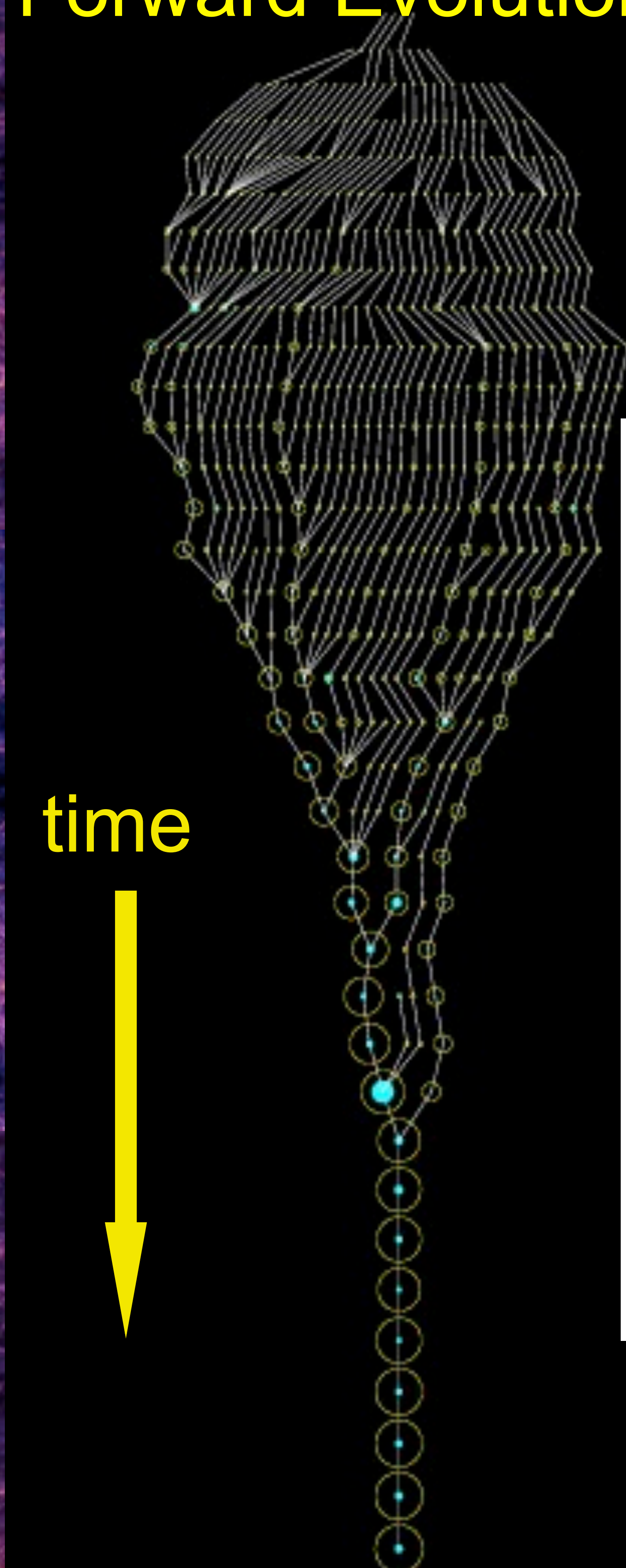

Present status of ΛCDM "Double Dark" theory:

- cosmological parameters are now well constrained by observations

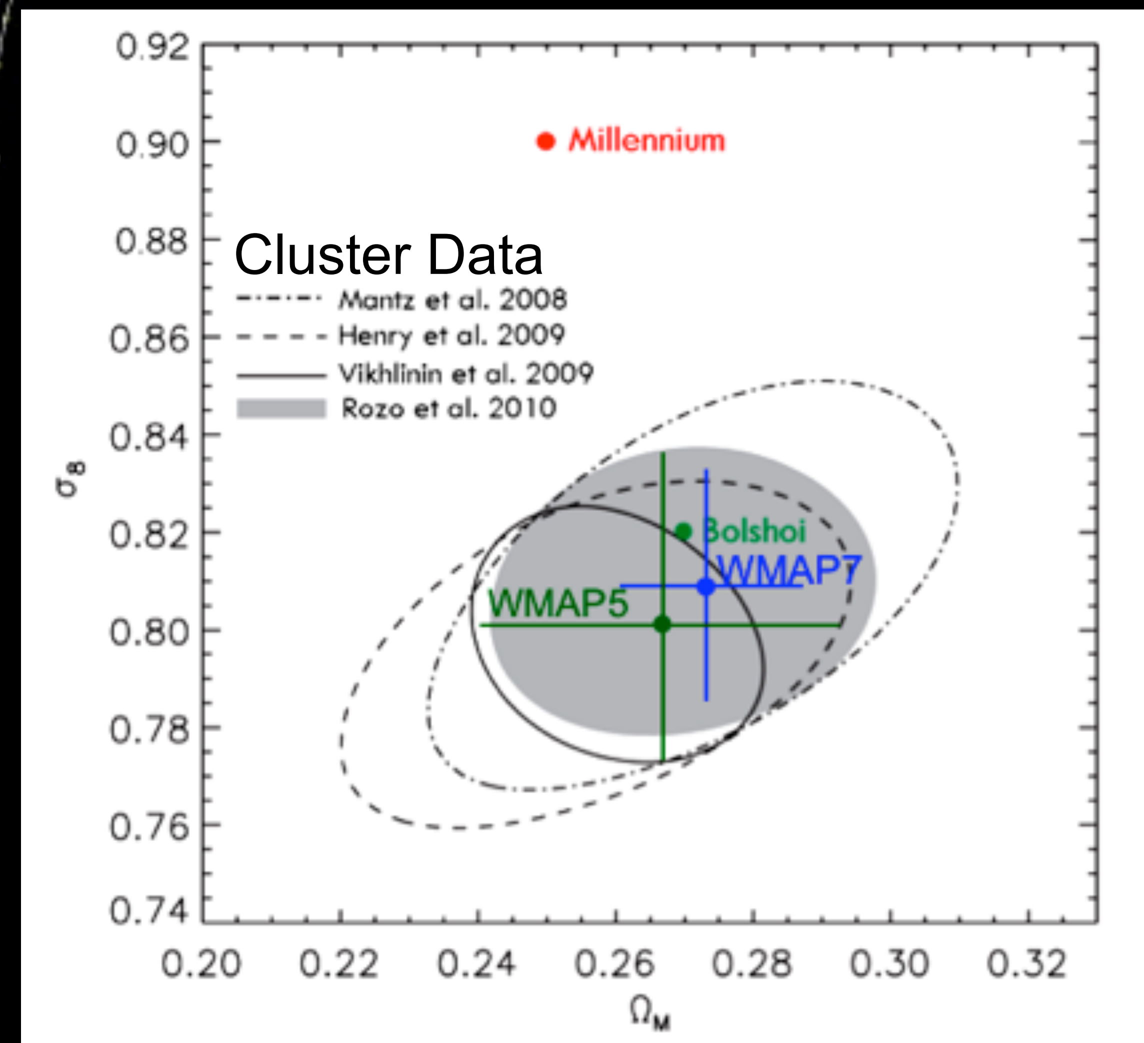

- mass accretion history of dark matter halos is represented by 'merger trees' like the one at left

Semi-Analytic Models of Galaxy Formation

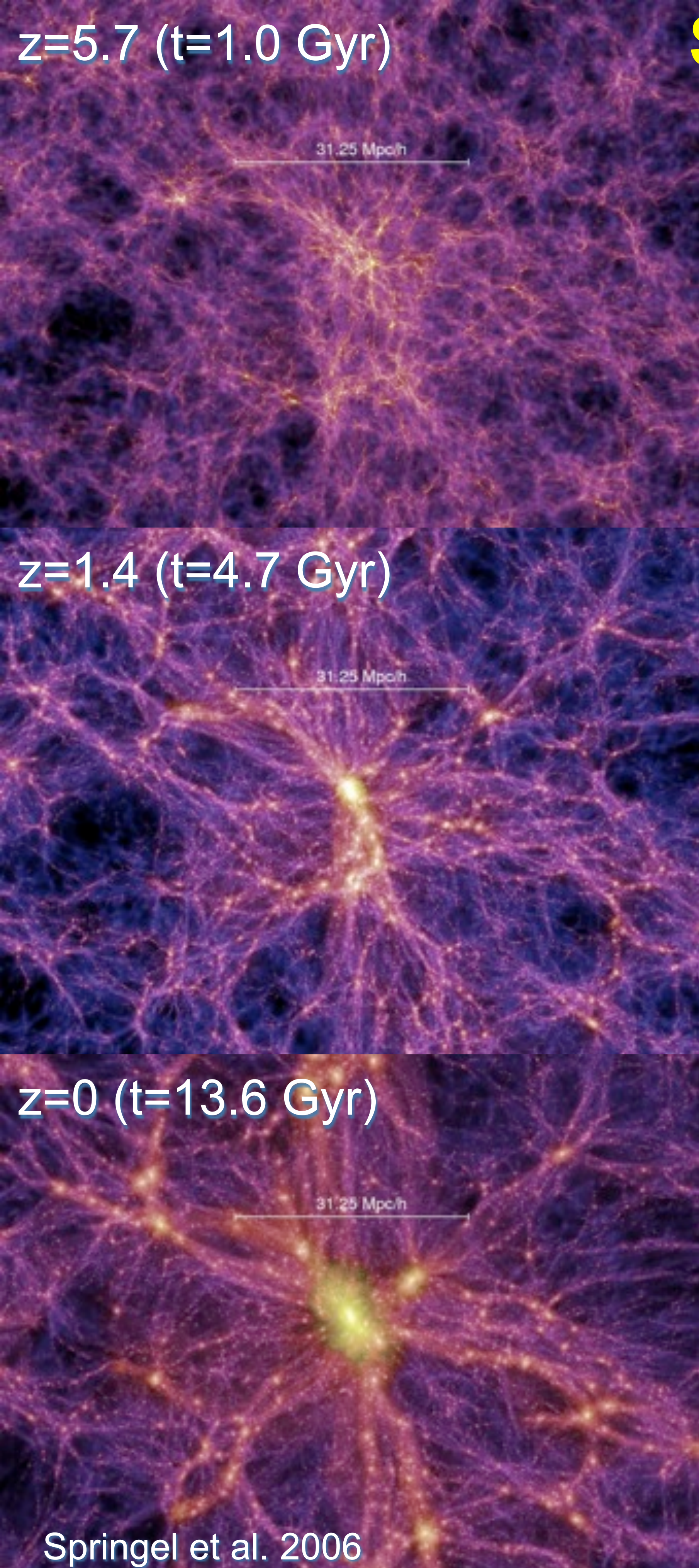

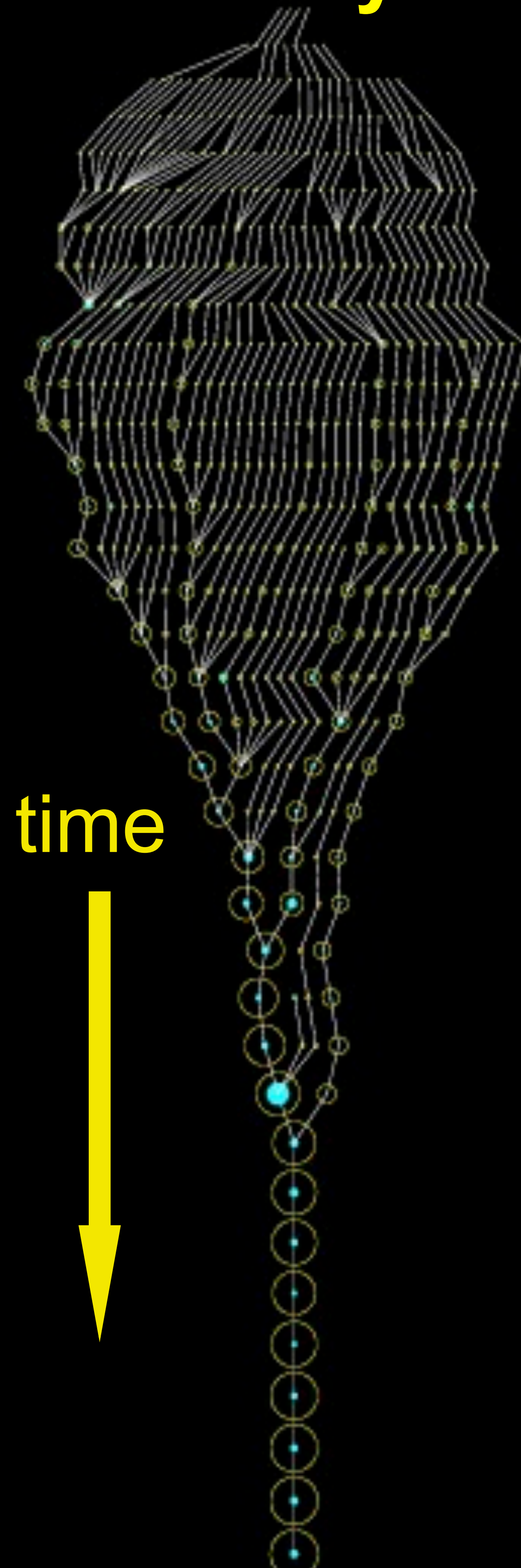

Astrophysical processes modeled:

- shock heating & radiative cooling
- photoionization squelching
- merging
- star formation (quiescent & burst)
- SN heating & SN-driven winds
- AGN accretion and feedback
- chemical evolution
- stellar populations & dust

Galaxy Formation in ΛCDM

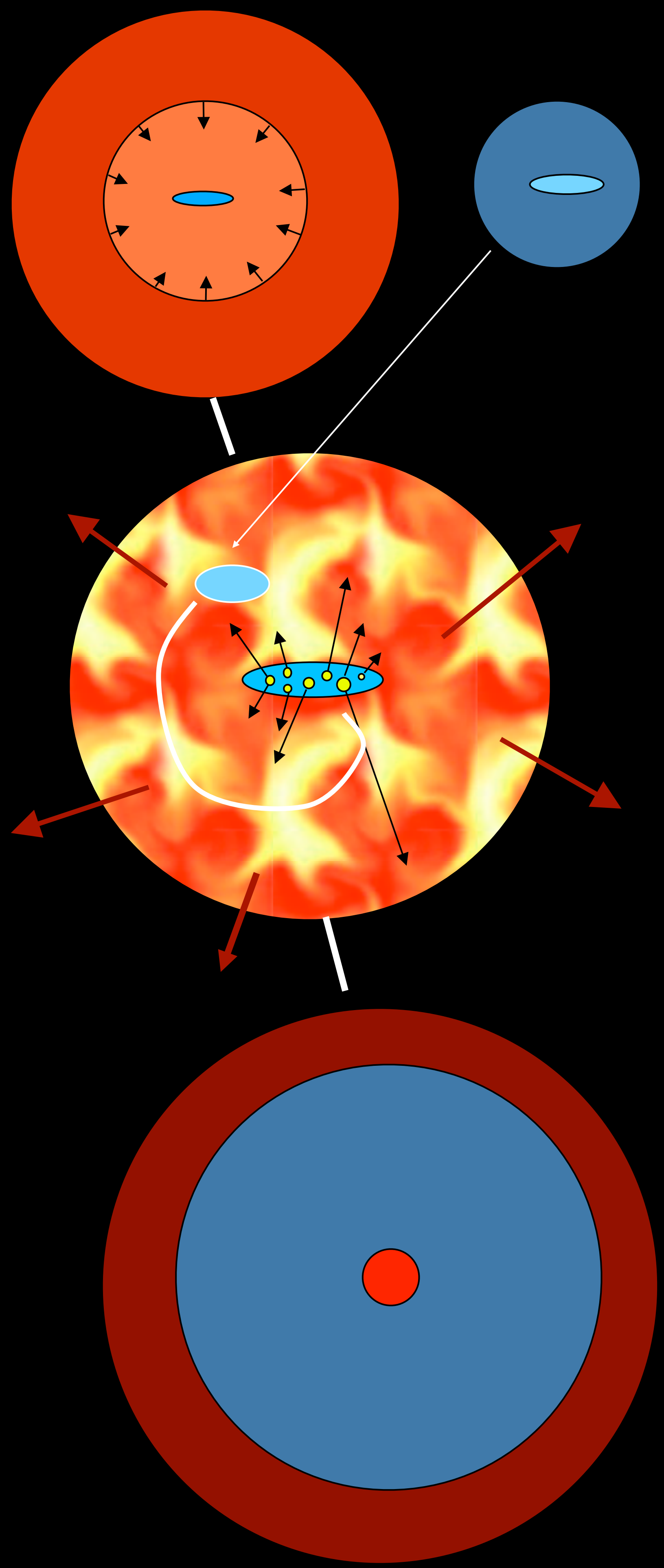

- gas is collisionally heated when perturbations 'turn around' and collapse to form gravitationally bound structures
- gas in halos cools via atomic line transitions (depends on density, temperature, and metallicity)
- cooled gas collapses to form a rotationally supported disk
- cold gas forms stars, with efficiency a function of gas density (e.g. Schmidt-Kennicutt Law)
- massive stars and SNae reheat (and in small halos expel) cold gas and some metals
- galaxy mergers trigger bursts of star formation; 'major' mergers transform disks into spheroids and fuel AGN
- AGN feedback cuts off star formation

White & Frenk 91; Kauffmann+93; Cole+94; Somerville & Primack 99; Cole+00; Somerville, Primack, & Faber 01; Croton et al. 2006; Somerville +08; Fanidakis+09; Somerville, Gilmore, Primack, & Dominguez 11

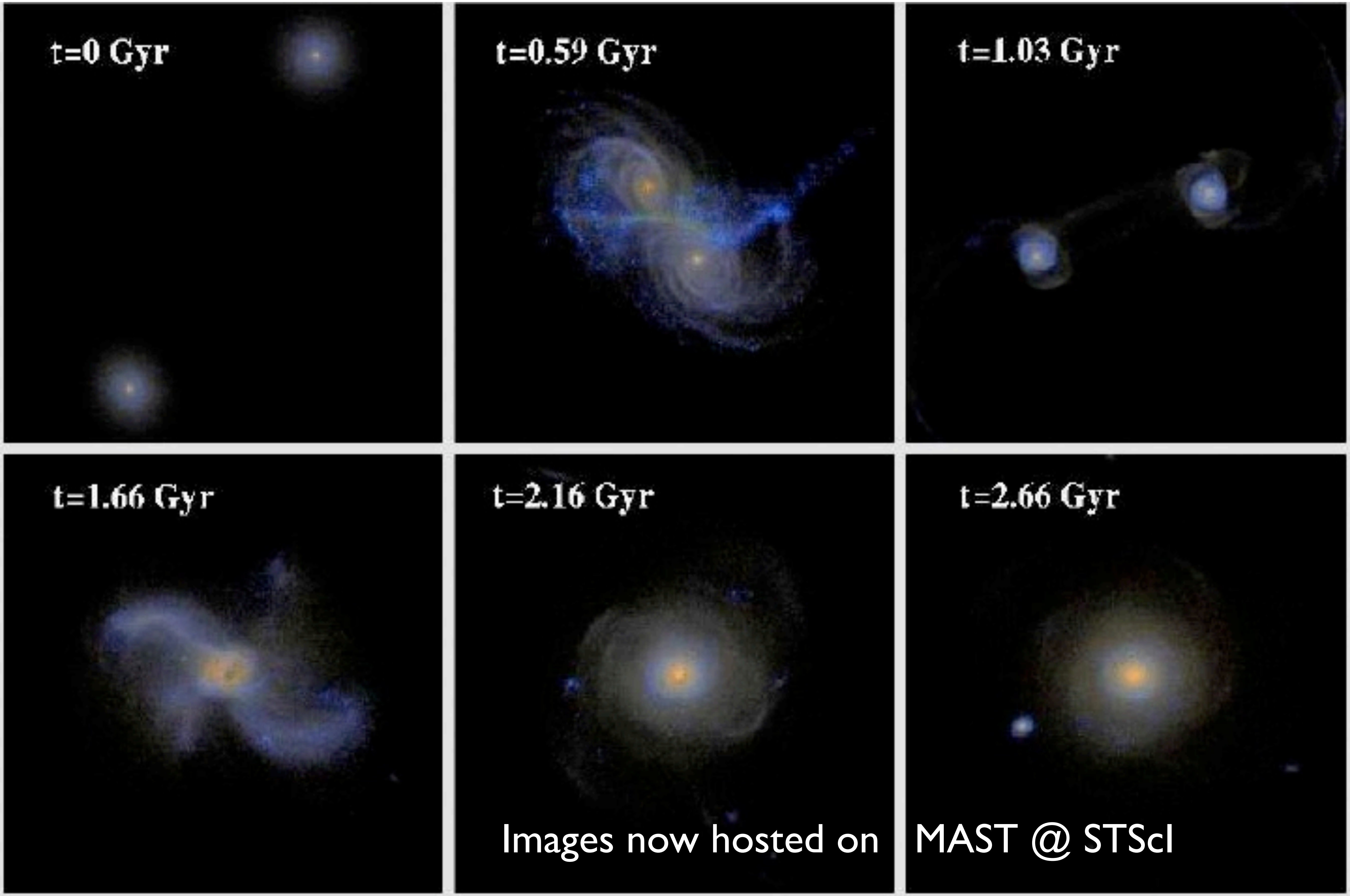

Lotz, Jonsson, Cox, Primack 2008 Galaxy Merger Morphologies and Time-Scales from Simulations analyzed to determine observability timescales using CAS, G-M_{20}, pairs → merger rates

Baryons in Dark Matter Halos

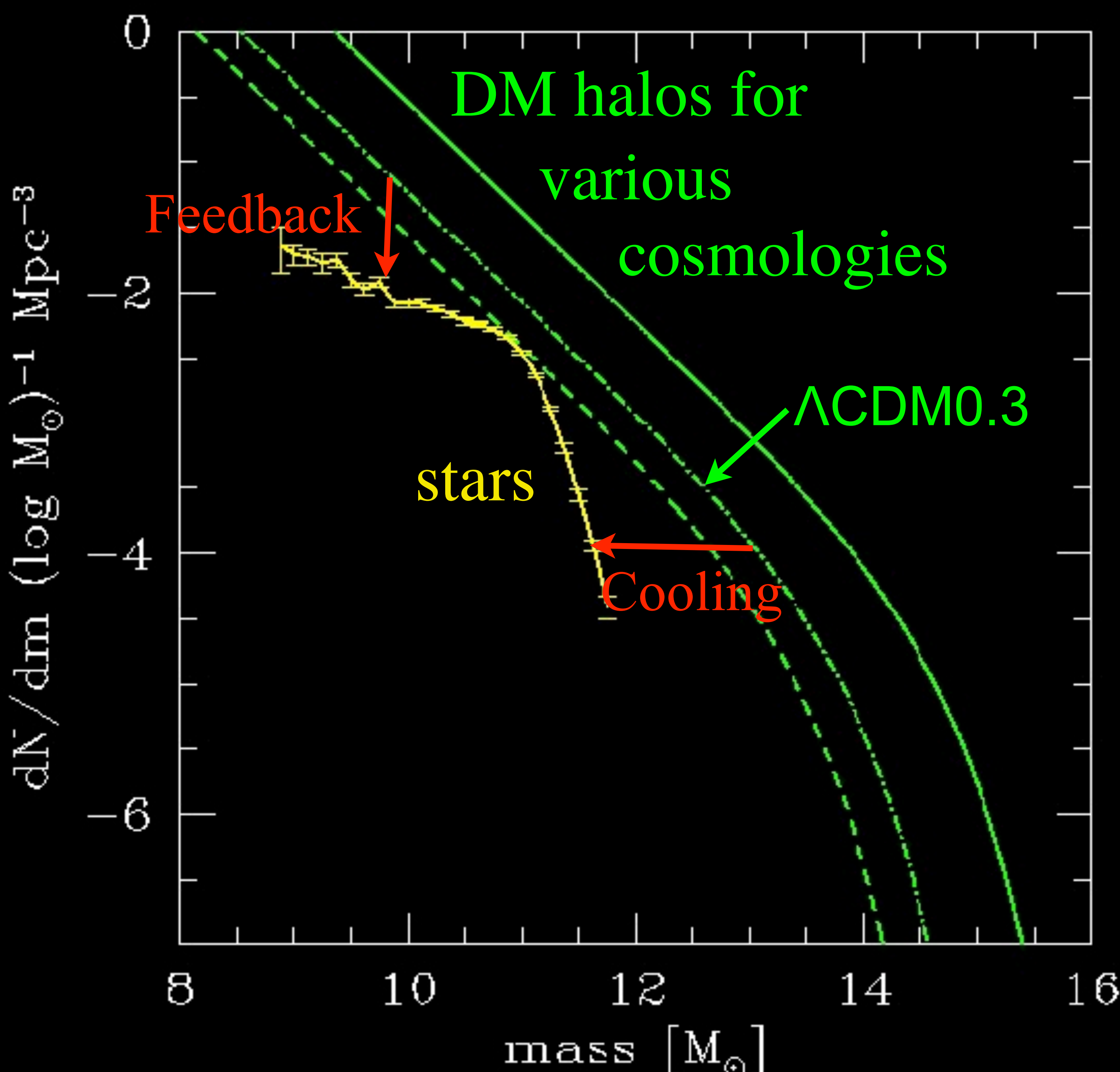

- in order to reconcile CDM (sub)halo mass function with galaxy LF or stellar MF, cooling/star formation must be inefficient overall, most efficient at $M_{halo} \sim 10^{11}$ M_{sun}
- baryon/DM ratio must be a strongly non-linear (& non-monotonic) function of halo mass

Somerville & Primack 1999; cf. Benson et al. 2003

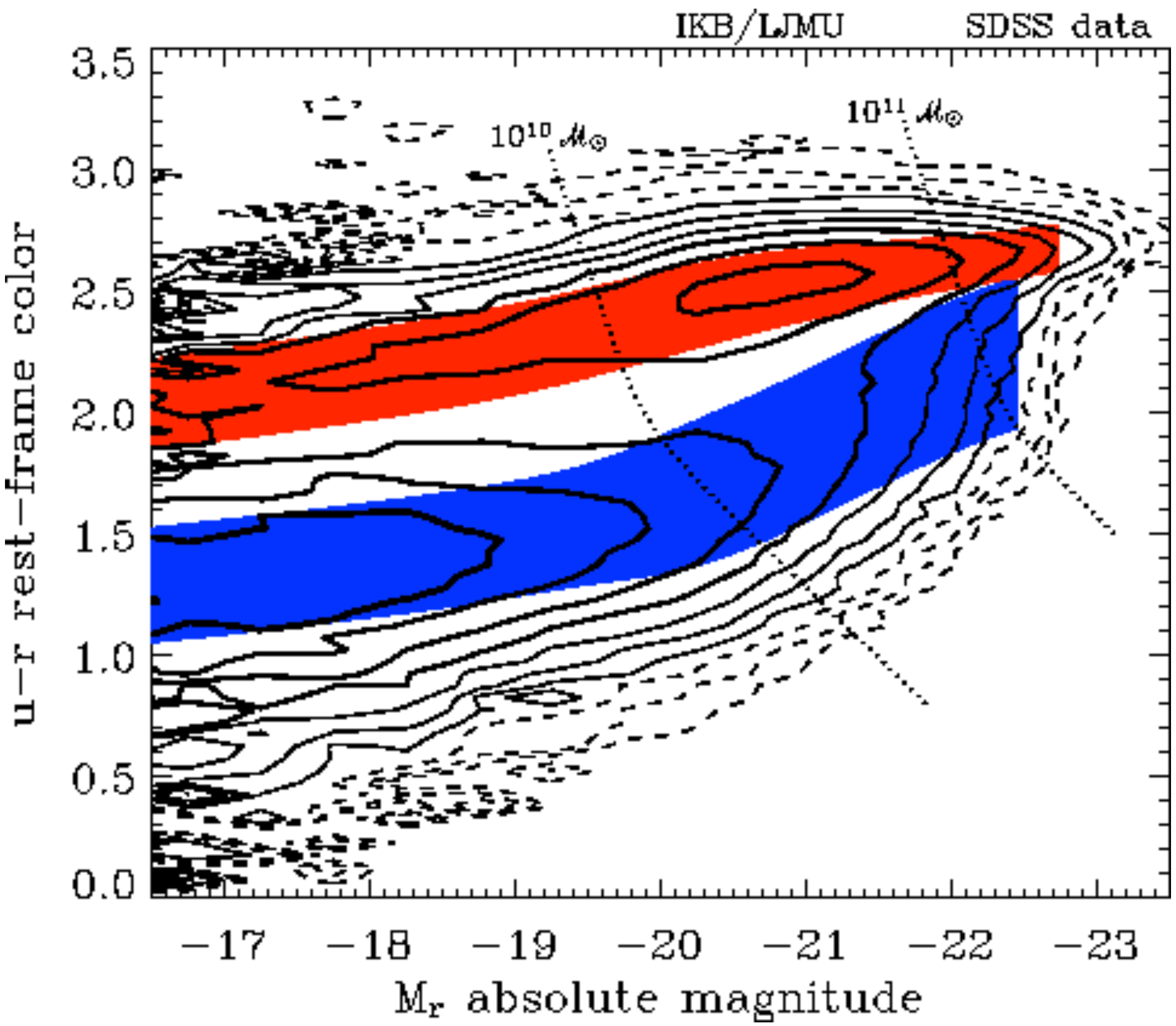

Color bimodality of galaxies on color-magnitude plot from [Baldry et al. (2004)](). The black solid and dashed contours represent the number density of galaxies: logarithmically spaced with four contours per factor of ten. The distribution is bimodal: there are two peaks corresponding to a red sequence (generally early types) and a blue sequence (late types).

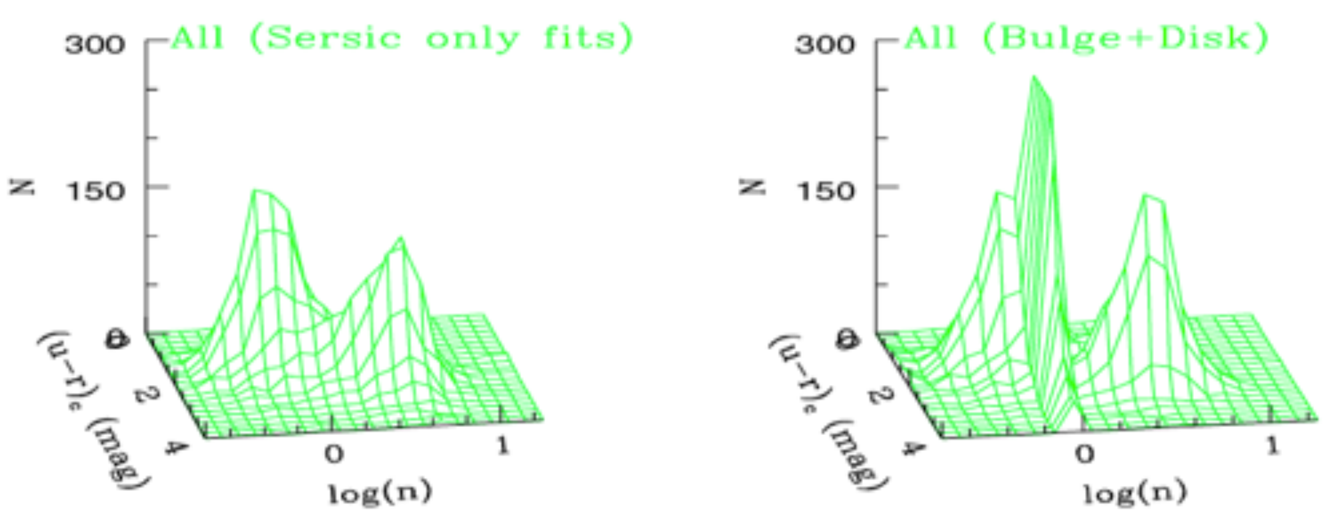

Galaxy bimodality in the color-structure plane (S. Driver et al. 2006)

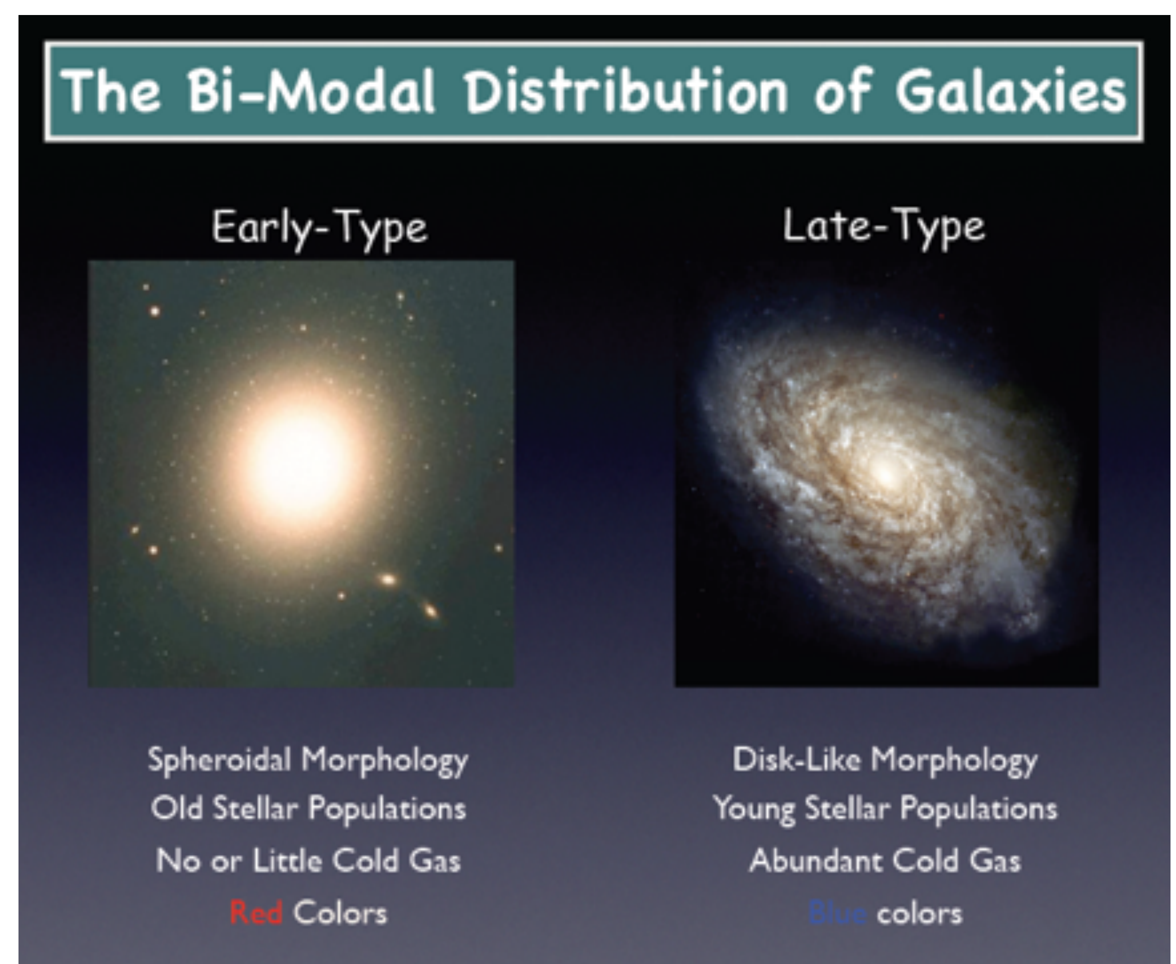

Flow through the color-mass diagram for "central" galaxies

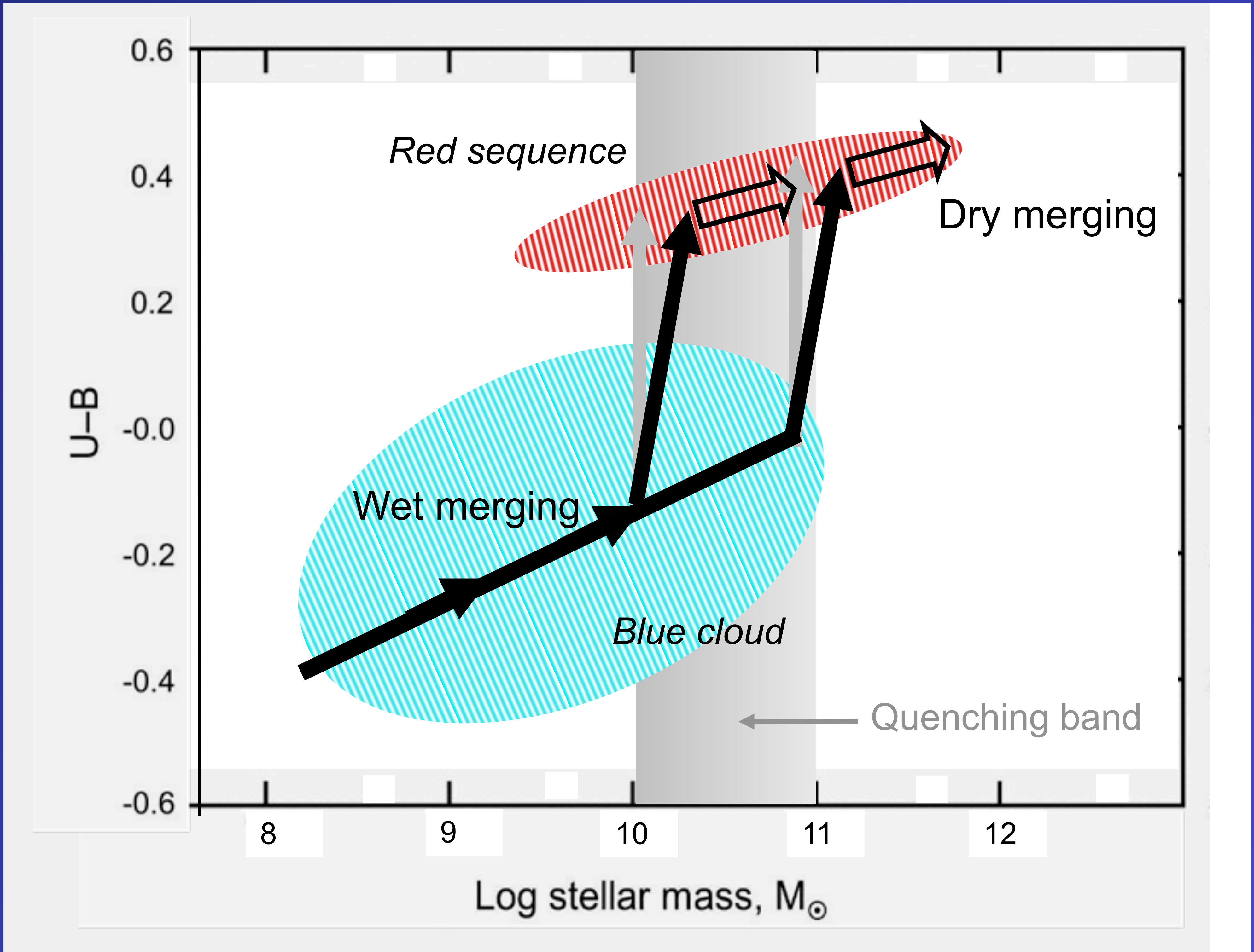

Sandra Faber

Flow through the color-mass diagram for “satellite” galaxies

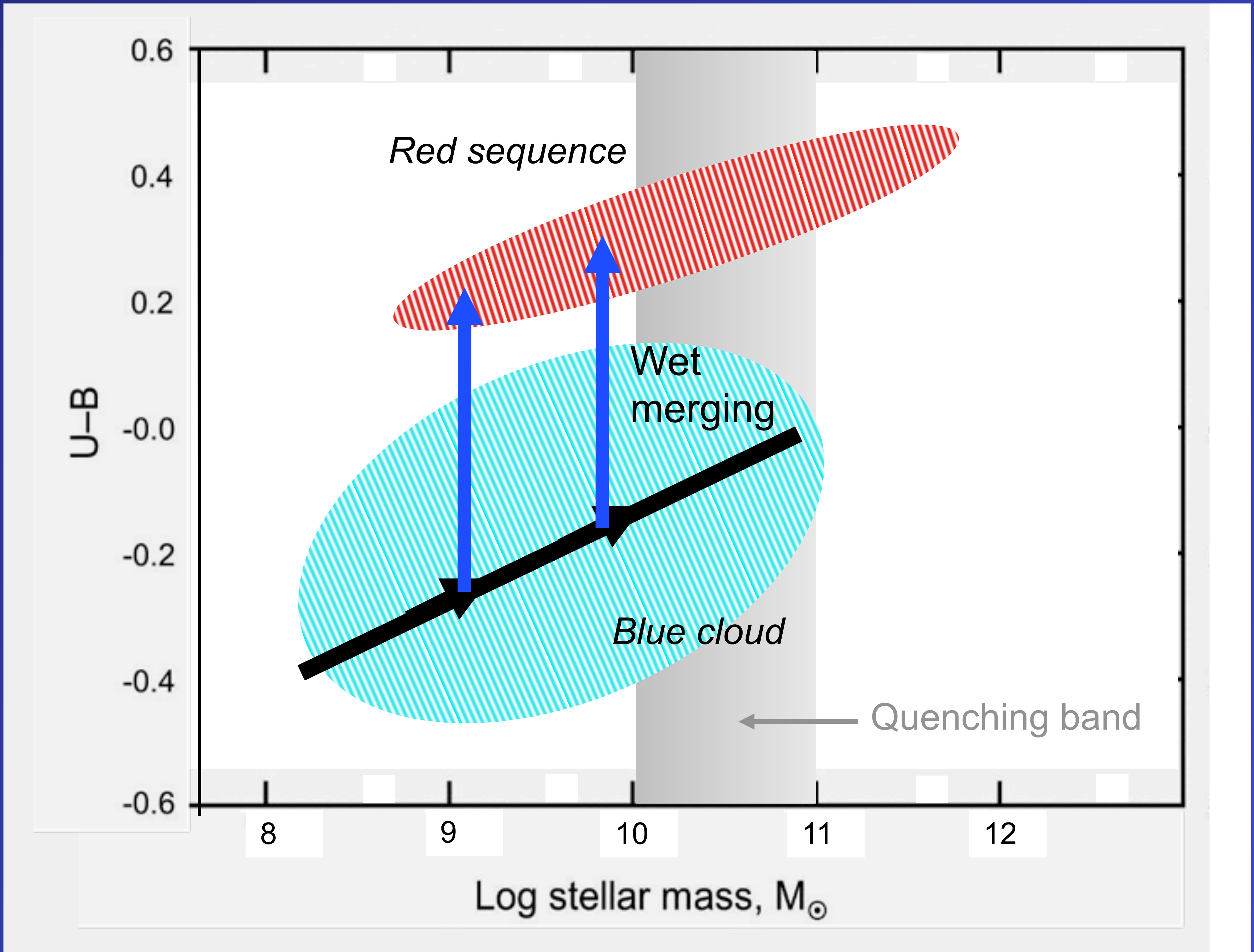

Sandra Faber

Flow through the CM diagram versus environment

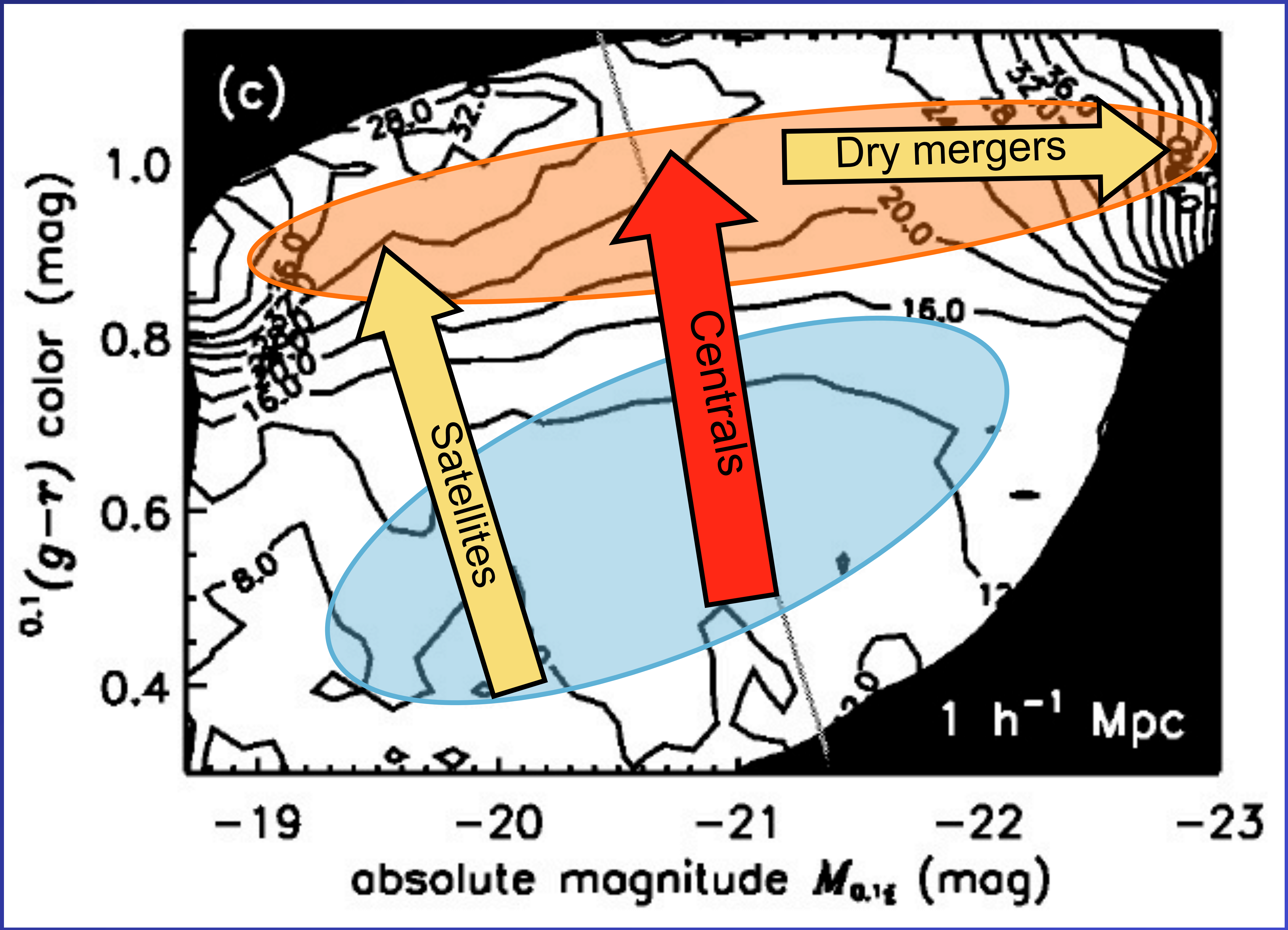

Hogg et al. 2003: Sloan Survey

All formed by environment

BH not avail?

$M_i^{0.1} = -19.3$

Transition mass
$3 \times 10^{10}\ M_\odot$

$M_i^{0.1} \sim -21.0$

Satellite/Central wet/dry transition

$M_i^{0.1} > -22.1$

All boxy/dry

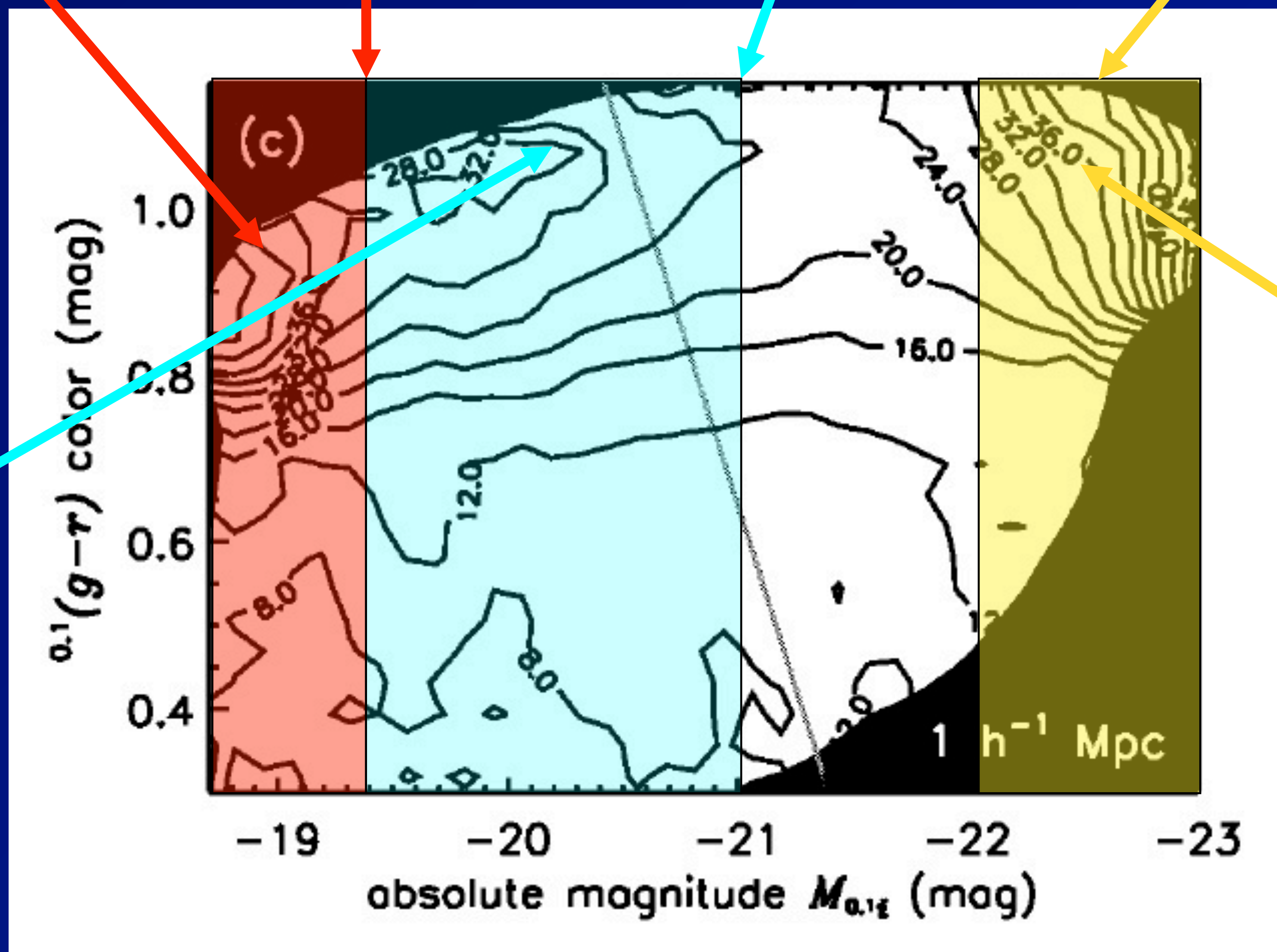

Some by env, some by wet mergers

All by dry mergers

Sandra Faber

New Improved Semi-Analytic Models Work!

- Earlier CDM-based galaxy formation models suffered from a set of interlinked problems
  - overcooling/cooling flow problems in galaxies and clusters
  - failure to produce observed color bimodality
- ‘Bright mode’ AGN feedback may regulate BH formation & temporarily quench star formation, but is not a viable ‘maintenance’ mechanism
- Low-accretion rate ‘radio mode’ feedback is a promising mechanism for counteracting cooling flows over long time scales
- New self-consistent ‘hybrid’ models based on physical scaling from numerical simulations and calibrated against empirical constraints now enable us to predict/interpret the relationship between galaxies, BH, and AGN across cosmic history

-- Rachel Somerville

Dark halo mass growth vs. time: 4 clusters

GALics DM halos by Cattaneo et al. 2006

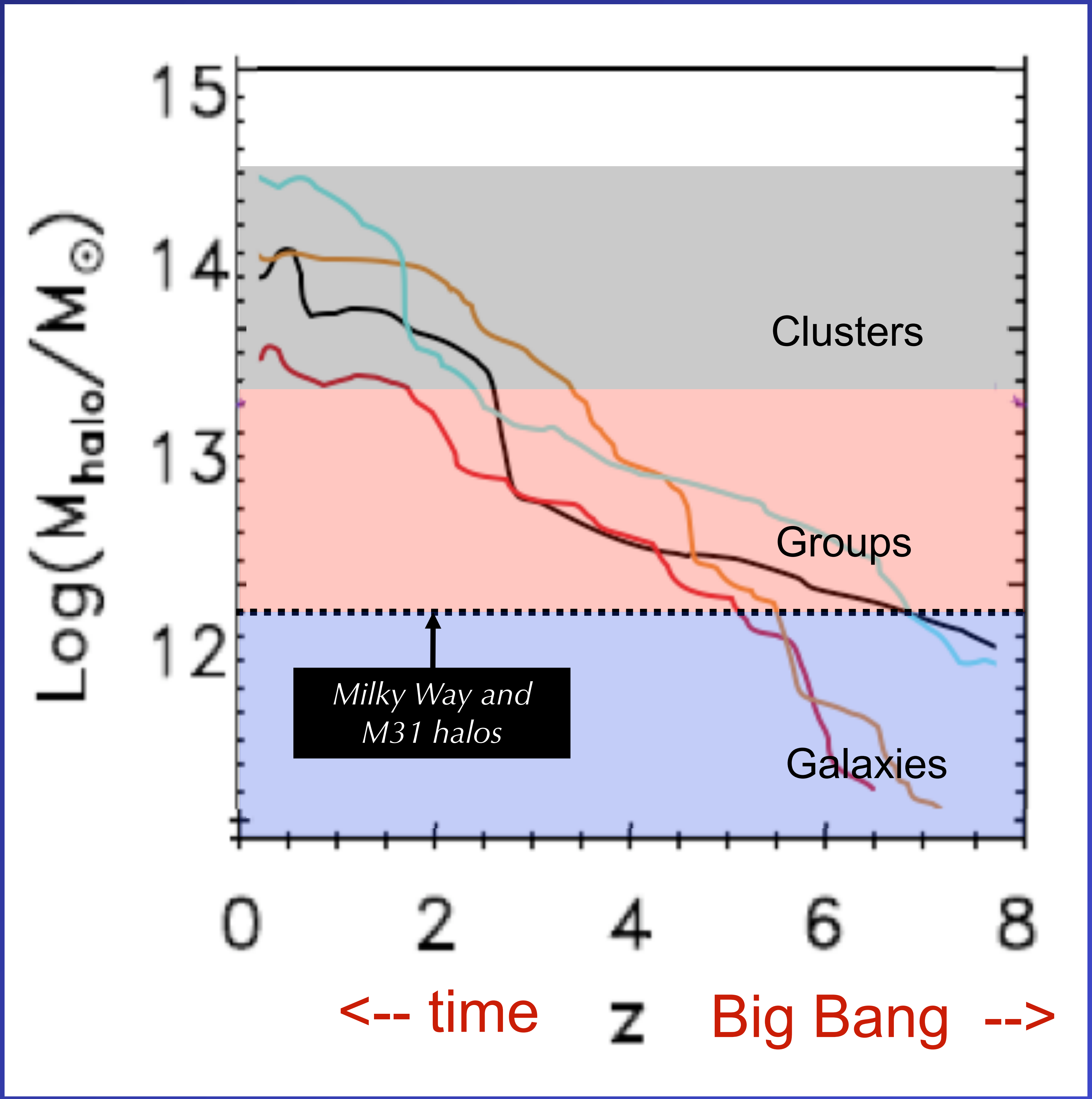

Sandra Faber

Dark halos of progressively smaller mass

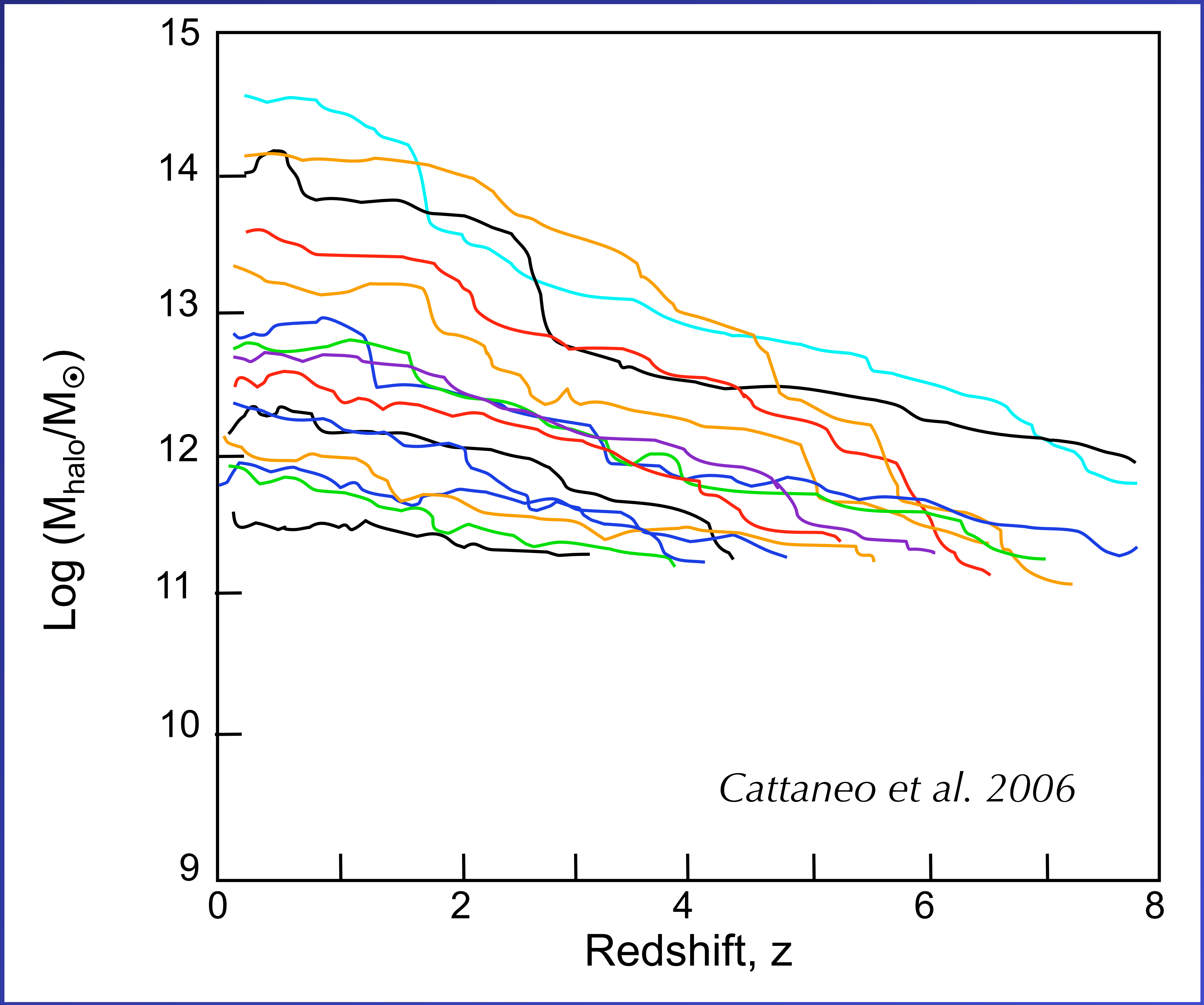

A schematic model of average halo mass growth

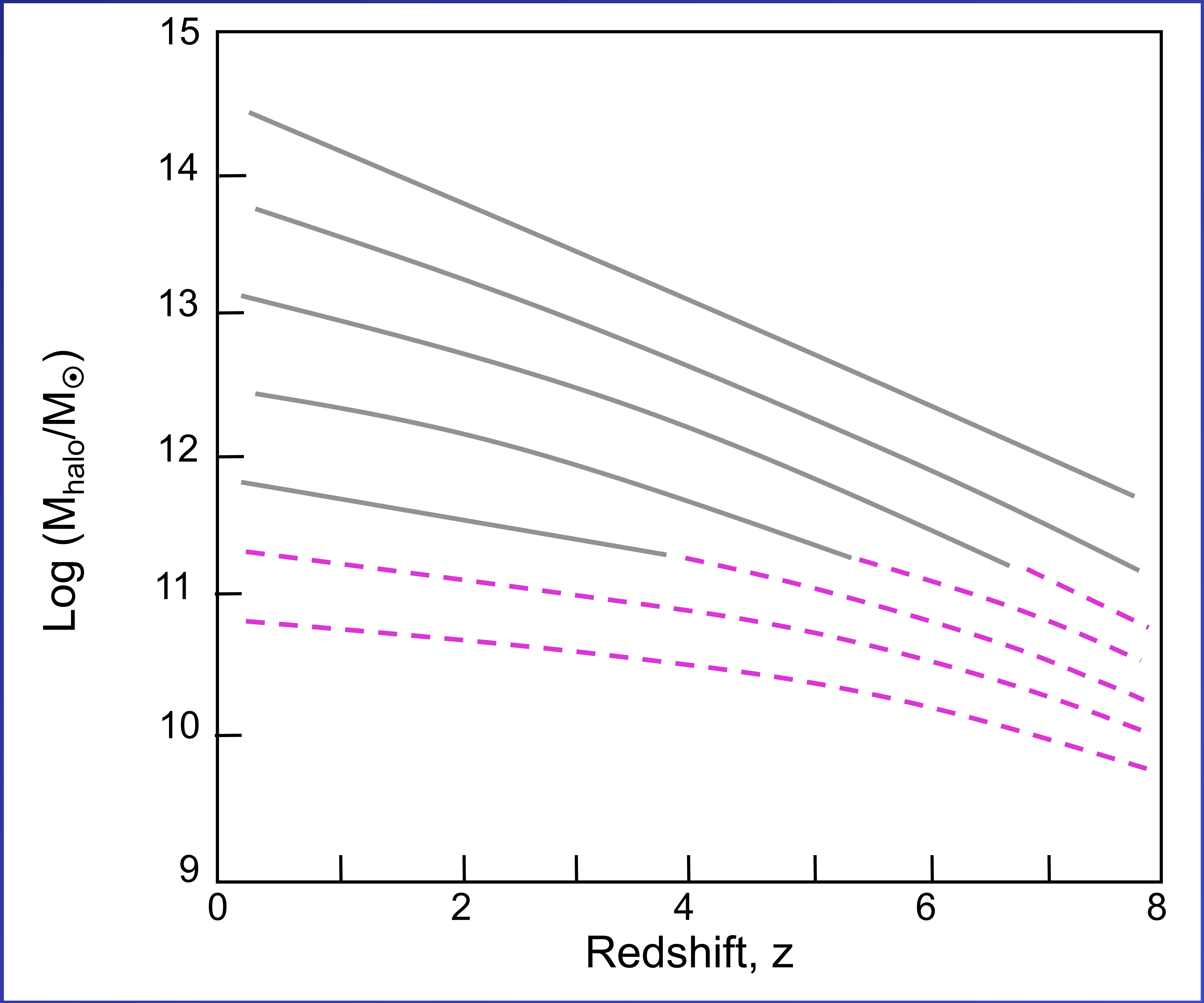

Key assumption: *star-forming band* in dark-halo mass

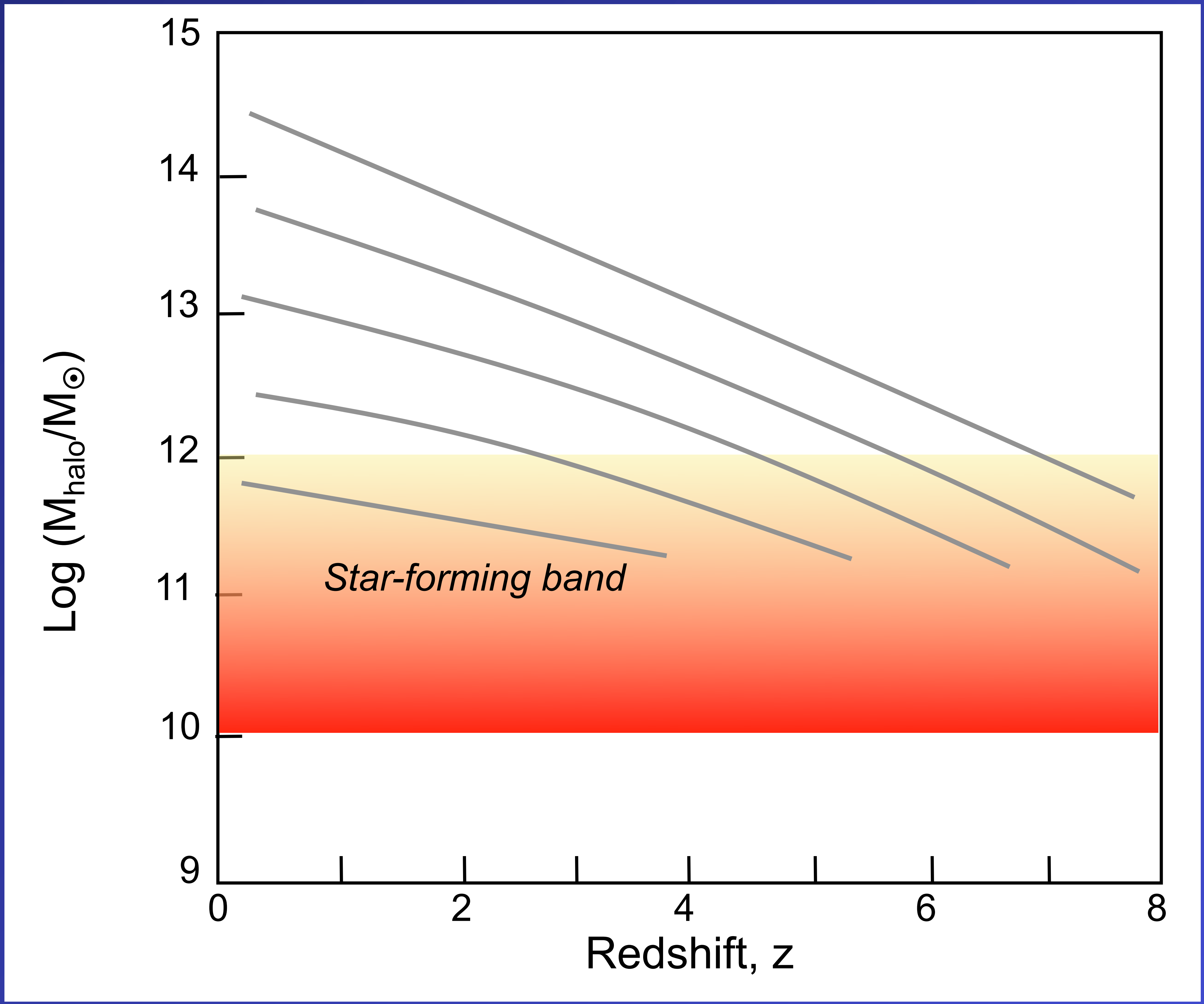

Key assumption: *star-forming band* in dark-halo mass

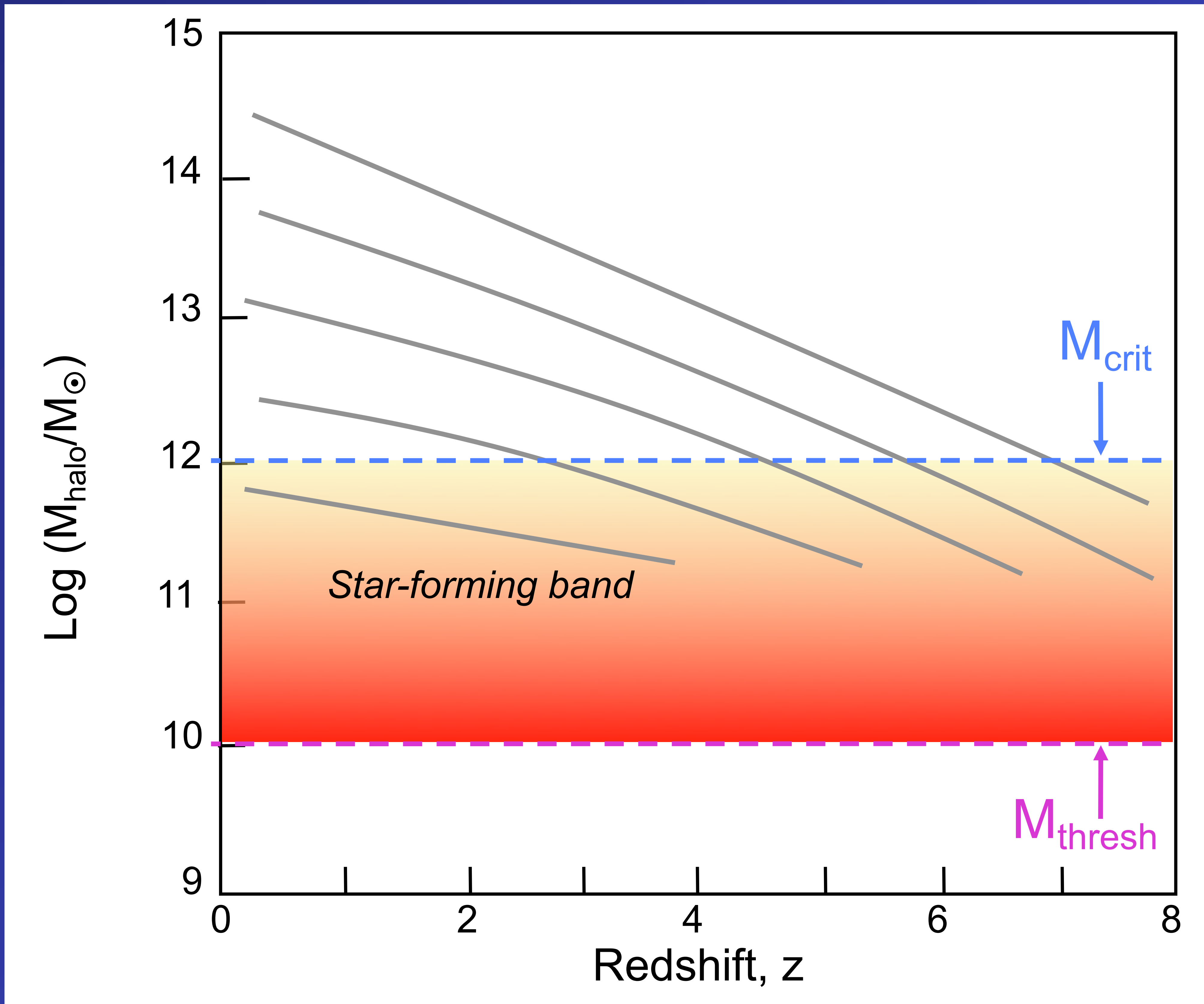

Key assumption: *star-forming band* in dark-halo mass

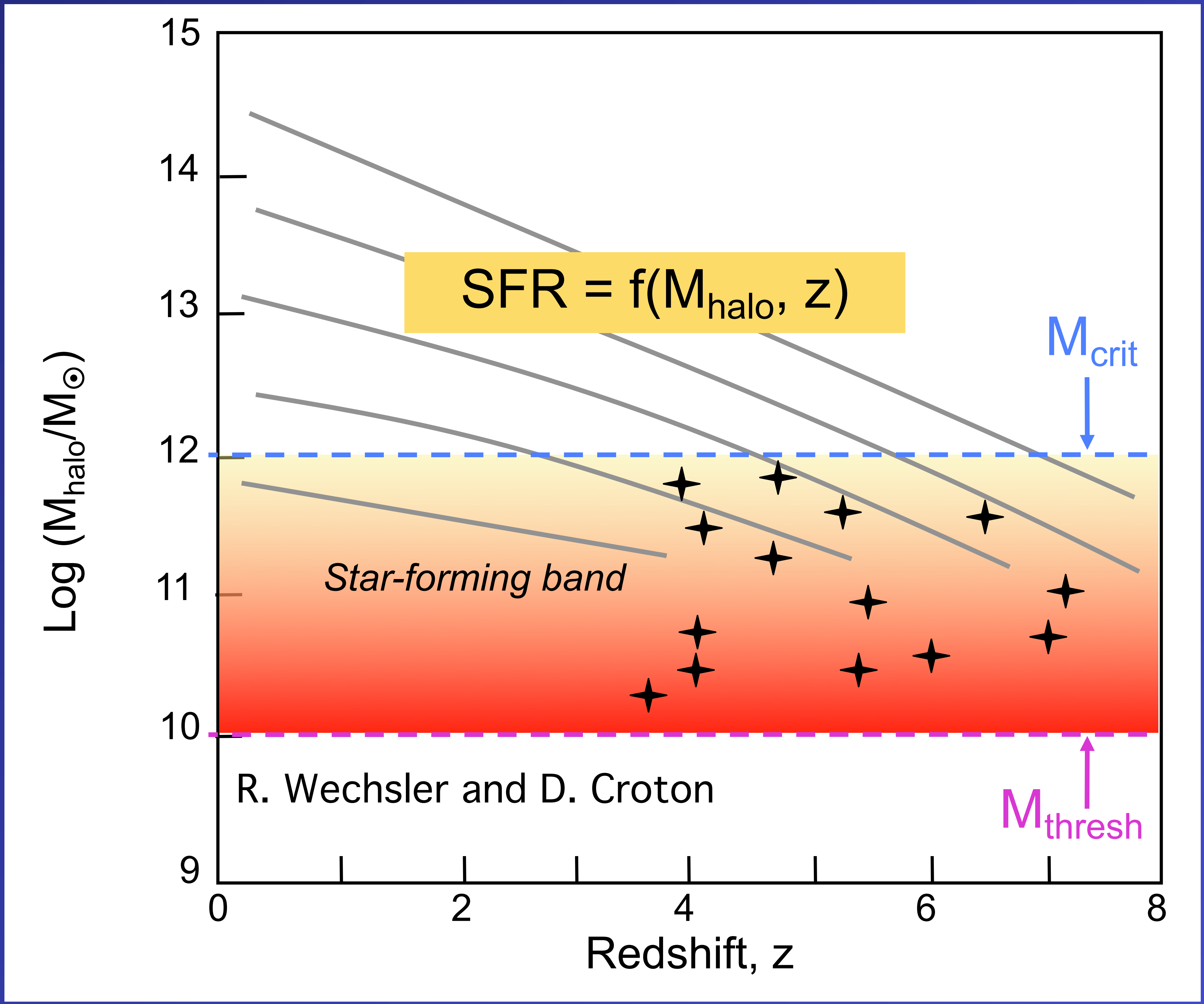

Implications and Predictions of the Model

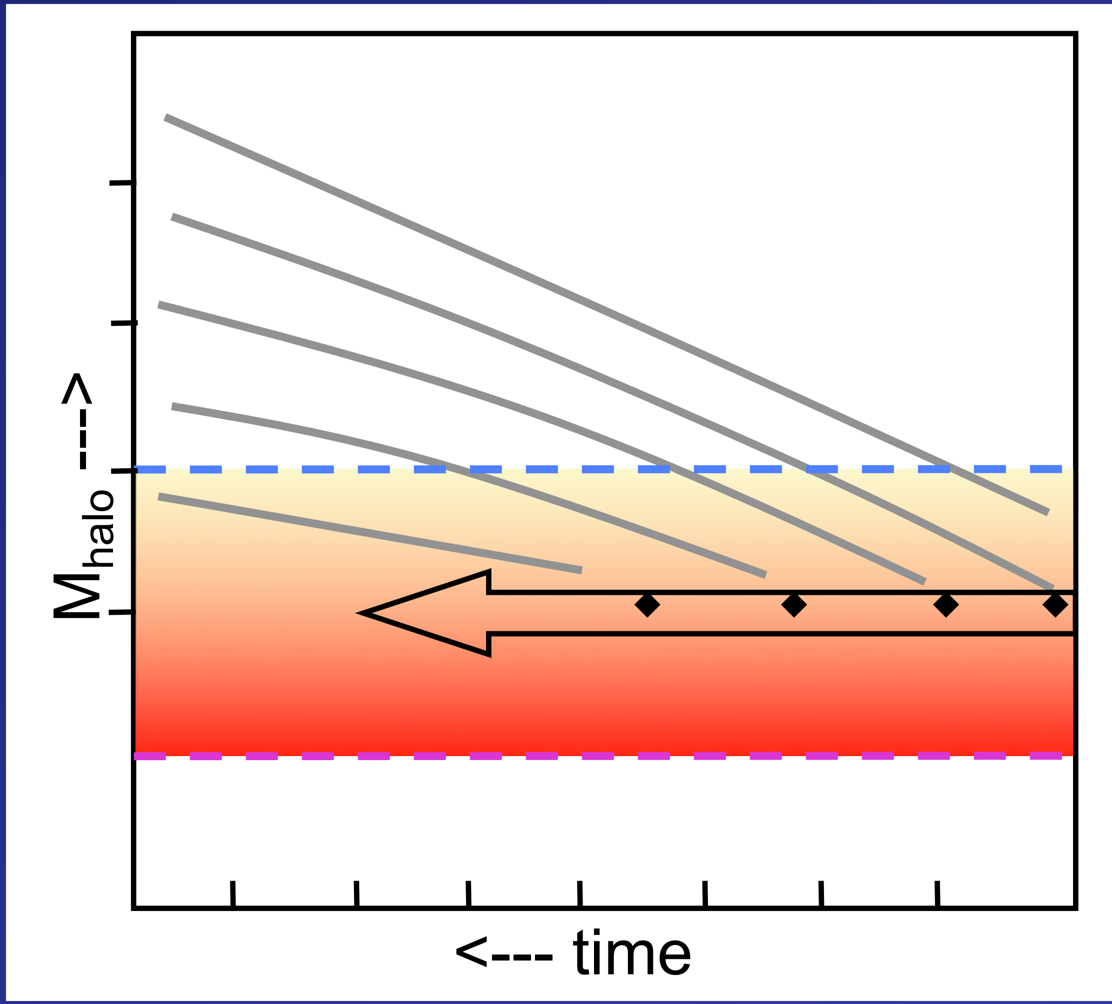

1) Each halo has a unique dark-matter growth path and associated stellar mass growth path.

2) Stellar mass follows halo mass until M_{halo} crosses M_{crit}.

SAMs: $M_{star} < 0.05\ M_{halo}$

3) A *mass sequence* comes from the fact that different halo masses enter the star-forming band at different times. A galaxy's position is determined by its *entry redshift* into the band. More massive galaxies enter earlier. Thus:

z_{entry} <--> M_{halo} <--> M_{star}

Sandra Faber

Implications and Predictions of the Model

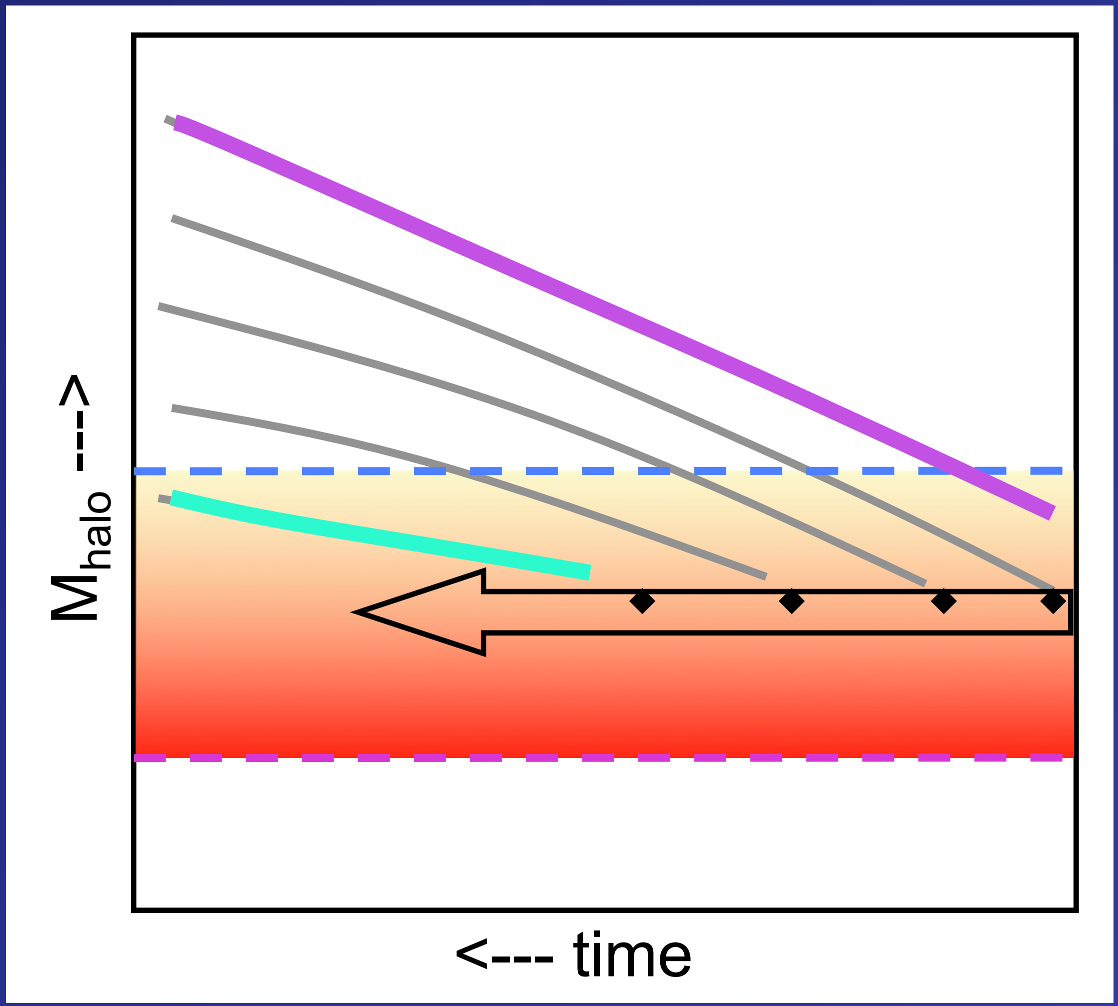

Massive galaxies:

- Started forming stars early.
- Shut down early.
- Are red today.
- Populate dark halos that are much more massive than their stellar mass.

Small galaxies:

- Started forming stars late.
- Are still making stars today.
- Are blue today.
- Populate dark halos that match their stellar mass.

"Downsizing"

Star formation is a wave that started in the largest galaxies and swept down to smaller masses later (Cowie et al. 1996).

Sandra Faber

Theories for the *lower* halo star-formation boundary

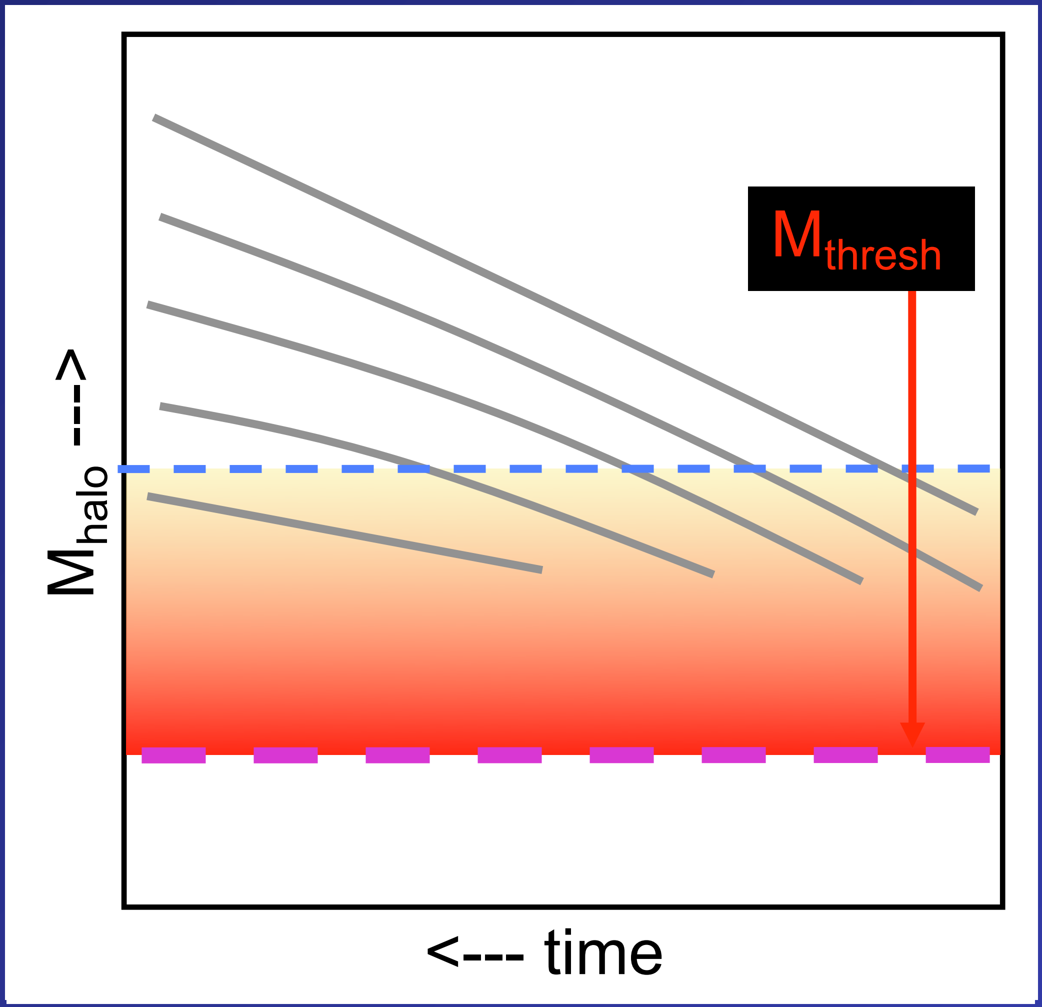

M_{thresh} is the halo mass at the LOWER edge of the star-formation band, roughly 10^{10} $M_{\odot}$.

Not yet well understood

1. Supernova feedback (Dekel & Silk 1985):

   $v_{lim} < 100$ km/sec

2. Early Universe reionization (e.g., Somerville 2002):

   $v_{lim} < 30$ km/sec

3. Plus tidal destruction!

Theories for the *upper* halo star-formation boundary

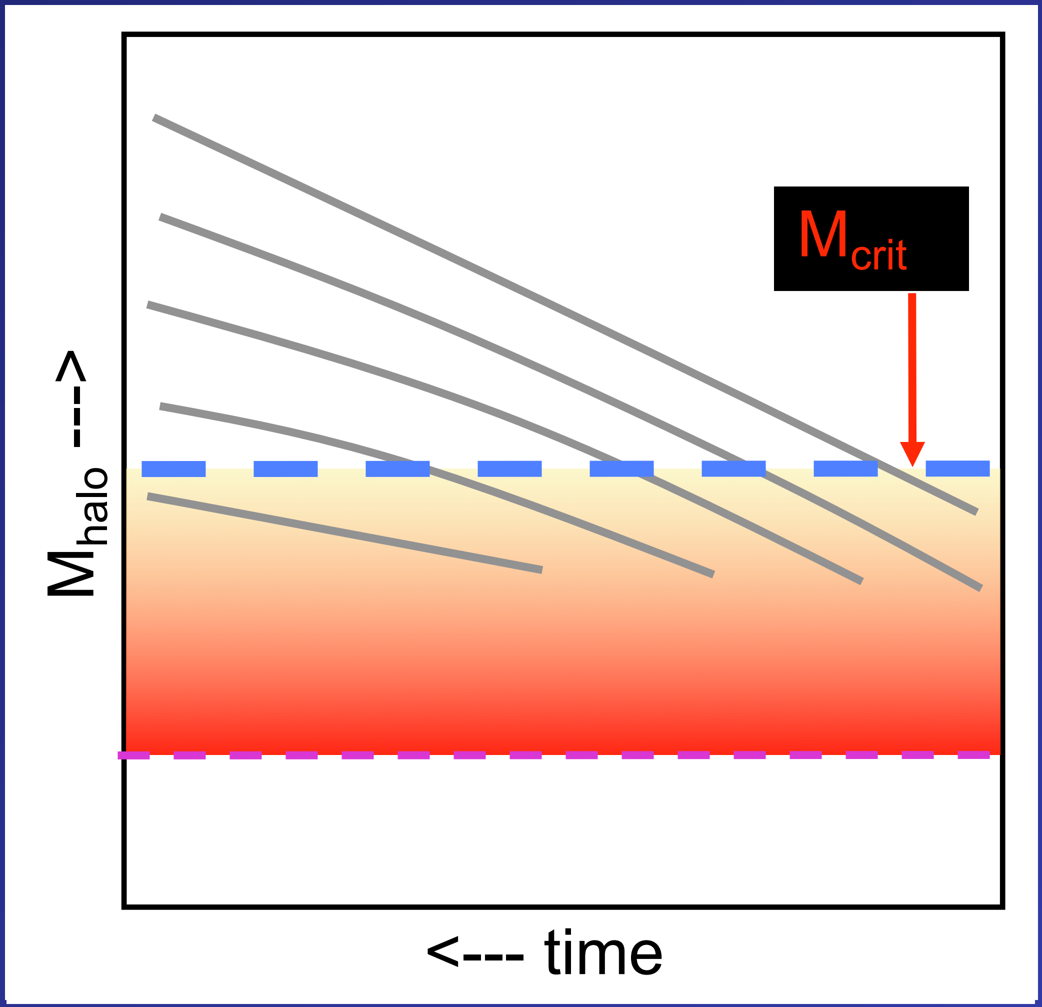

M_{crit} is the halo mass at the UPPER edge of the star-formation band, roughly 10^{12} M¤.

1. Gas in halos above the critical halo mass $M_{crit} \sim 10^{12}\ M_{\odot}$ cannot cool (Ostriker & Rees 1978, Blumenthal et al. 1984, Dekel & Birnboim 2007).